UNIVERSITY OF CALIFORNIA,

IRVINE

Acoustically Enhanced Nonaqueous Phase Liquid Remediation

In Porous Media

DISSERTATION

submitted in partial satisfaction of the requirements for the degree of

DOCTOR OF PHILOSOPHY

in Civil Engineering

by

Eric Todd Vogler

Dissertation Committee:

Professor Constantinos V. Chrysikopoulos, Chair

Professor Brett F. Sanders

Professor John C. LaRue

Professor Jan S. Scherfig

2003

The dissertation of Eric Todd Vogler is approved:

Committee Chair

University of California, Irvine

2003

Dedication

In loving memory of my Grandfather Walter “Bugs” Bunko.

Contents

List of Tables

List of Figures

Nomenclature

$A_1, ..., A_4$	Laplace domain constants.
A_c	cross sectional area of porous medium, (L^2).
A_p	pore conduit cross sectional area, (L^2)
B	Bond number, (-)
C	dissolved phase DNAPL concentration (solute mass/ liquid volume), (M/L^3).
Ca	Capillary number, (-)
C_f	effluent flux concentration, (M/L^3).
C_p^w	equilibrium aqueous solubility concentration of component p, (M/L^3).
C_s	pure component saturation aqueous solubility, (M/L^3).
$\overline{C}_{\mathrm{a}}$	mean concentration in presence of acoustic waves, (M/L^3).
$\overline{C}_{\mathrm{b}}$	mean base case concentration, (M/L^3).
ΔC	percent change in concentration, (%).
d	mean grain size diameter of the porous medium, (L).
D	hydrodynamic dispersion coefficient, (L^2/t).
D_e	effective hydrodynamic dispersion coefficient, (L^2/t).
D^*	hydrodynamic dispersion coefficient component due to acoustic waves, (L^2/t).
$\mathcal{D}$	molecular diffusion coefficient, (L^2/t).
$\mathcal{D}_e$	effective molecular diffusion coefficient, (L^2/t).
$f(t)$	time dependent source function, (F/L^2).
$G_{i,j}$	conductance of pore conduit, (L^5/Ft).
g	acceleration due to gravity, (L/t^2).
H	Heaviside unit step function, ($-$).
h_w	hydraulic head of water, (L).
I_0	modified Bessel function of zero order, ($-$).
J_i	mass flux across DNAPL-water interface per unit interfacial area, (M/L^2t).

K	hydraulic conductivity, (L/t).
K_e	effective mass transfer coefficient, (1/t).
k	intrinsic porous media permeability, (L^2).
k_i	local mass transfer coefficient at pore i, (L/t).
ΔL	ganglia length, (L).
l	pore separation distance, (L).
l_p	pore conduit perimeter, (L).
l_i	stagnant aqueous layer thickness in pore i, (L).
M	injected mass, (M).
M_0	injected mass/cross sectional column pore space area, (M/L^2).
$\mathbf{m}$	vector of Laplace transformed dependent variables.
$\mathbf{m}_0$	function of transformed variable ν.
N_x	number of network pores in the direction of flow, (-).
N_y	number of network pores normal to the direction of flow, (-).
P_c	capillary pressure, (F/L^2).
P_o	nonaqueous phase fluid pressure, (F/L^2).
P_w	fluid pressure, (F/L^2).
p	fluid pressure, (F/L^2).
p_e	column effluent fluid pressure, (F/L^2).
p_s	acoustic source fluid pressure, (F/L^2).
$\Delta p_{i,j}$	difference in pore fluid pressure between pores i and j, (F/L^2).
$\mathbf{q}_1, ..., \mathbf{q}_4$	eigenvectors, defined in (4.26)-(4.28).
Re_a	acoustic Reynolds number defined in (4.41), $(-)$.
r_H	hydraulic radius, (L).
$r_{1,2}$	principle radii of interface curvature, (L).
S	fluid–solid interaction function, (L/t).
t	time, (t).
U	steady state, background interstitial fluid velocity, (L/t).
U_e	effective interstitial fluid velocity, (L/t).
U_r	relative pore water velocity, (L/t).

U_{r_a}	oscillatory pore water velocity amplitude, (L/t).
U^*	interstitial fluid velocity component due to acoustic waves, (L/t).
u	dynamic fluid viscosity, (M/Lt).
X_p	mole fraction of component p in the nonaqueous phase, (-).
x	longitudinal spatial coordinate, (L).
z	vertical spatial coordinate, (L).
Greek Letters	
$\alpha_1, ..., \alpha_4$	eigenvalues, defined in (4.21)-(4.23), $(-)$.
α_L	longitudinal dispersivity, (L).
β	interfacial contact angle, $(^\circ)$.
γ	specific fluid weight, (F/L^3).
γ_{ow}	interfacial tension, (F/L).
γ_p	activity coefficient of component p in the nonaqueous phase, (-).
δ	Dirac delta function, (1/t).
η	kinematic fluid viscosity, (L^2/t).
θ	porosity (liquid volume/aquifer volume), (L^3/L^3).
κ	dummy variable.
λ	solid matrix Lamé constant, (F/L^2).
μ	solid matrix Lamé constant, (F/L^2).
ν	Laplace transform parameter.
ξ_s	solid displacement, (L).
ξ_f	fluid displacement, (L).
ξ_r	fluid displacement relative to solid displacement, (L).
ρ_{solid}	glass bead density, (M/L^3).
ρ_f	fluid bulk density, (M/L^3).
ρ_{H_2O}	density of water, (M/L^3).
ρ_s	bulk density of the solid matrix, (M/L^3).
ρ_o	density of nonaqueous phase liquid, (M/L^3).
$\Delta\rho$	density difference between nonaqueous and fluid phase, (M/L^3).
σ	solid stress, (F/L^2).

τ	dummy integration variable.
τ^*	tortuosity, (-).
ϕ	acoustic wave frequency, (1/t).
ω	angular frequency.
Ω_1, Ω_2	defined in (4.24) and (4.25), respectively.

Abbreviations

Mol wt	molecular weight.
DNAPL	dense nonaqueous phase liquid.
NAPL	nonaqueous phase liquid.
PCE	tetrachloroethylene.
TCE	trichloroethylene.
1,1,2-TCA	1,1,2-trichloroethane.

Acknowledgments

I would like to thank my mother Janet Vogler for her unconditional love and emotional support. I also owe a debt of gratitude to my wife Shelley, who has helped me through the challenging times and is always there for me and our son Emerson. My sincere appreciation to my graduate advisor Professor Costas Chrysikopoulos for his sound advice, support, friendship, and belief in both myself and this research. I'd like to thank Professor Brett Sanders for his generous support of my work, much of which wouldn't have been completed without him. I am also grateful for the contributions from my other dissertation committee members, Professor Jan Scherfig and Professor John LaRue.

I must thank the ladies of the ARCS foundation for their support my last year in graduate school. Additional thanks are extended to the staff from the Department of Civil and Environmental engineering for looking out for me, especially Suzie, Debbie, Lorie, and Marcia. Many thanks to Ted for machining all of my experimental equipment and tolerating my shortcomings in technical drawing. Bob Turnbull and Steve Takahashi, thank you for allowing me the opportunity to work when I could and the understanding when I couldn't.

I must also recognize the friendship of Lew Pennington, Dave Jaffe, Dave Swart, and Rudy Rodriguez who were with me in the trenches for so many years of graduate school. To my office mates Matt Thomas and Richard Argal, thank you for tolerating my dissertation stress, and good luck when it's your turn.

I have never let my schooling interfere with my education.

-Mark Twain

Curriculum Vitae

Eric Todd Vogler

Education

Ph.D.:	Civil Engineering, 2003
	UNIVERSITY OF CALIFORNIA, IRVINE
Master of Science:	Geology (Hydrogeology emphasis), 1999
	SAN DIEGO STATE UNIVERSITY
Bachelor of Science:	Hydrogeology, 1995
	SAN DIEGO STATE UNIVERSITY

Awards, Honors, and Certifications

UCI Regents Fellow

National Achievement Rewards for College Scientists (ARCS) Foundation Fellow

Engineer–in–Training Certification, 2003

Employment Record

(1998–2003) TEACHING and RESEARCH ASSISTANT, Department of Civil and Environmental Engineering, University of California, Irvine.

(1995–1997) GROUNDWATER MODELER, Dudek & Associates, Inc., Encinitas, California.

(1995–1996) TEACHING ASSISTANT, Department of Geological Science, San Diego State University.

(1994–1995) ENGINEERING GEOLOGIST INTERN, Regional Water Quality Control Board, San Diego, California.

(1988–1992) United States Marine Corps, Washington D. C.

Teaching Experience

Polution Prevention and Controll – CEE168 (W03) - Teaching Assistant

Groundwater Hydrology – CEE172 (F98, F99, F00, F01, F02) - Teaching Assistant

Numerical Methods in Engineering – CEE10 (SS99) - Teaching Assistant

Physics–5LC (S00) - Teaching Assistant

Fundamental Physics Laboratory–5LC (S00) - Instructor

Basic Physics Laboratory–3LB (W99, W00) - Instructor

Introduction to Civil Engineering–CEE2 (F99) - Teaching Assistant

Geologic Investigation Lab–(F95, S96) - Instructor

Show Me Geology (K-12)–(F94, S95) - Instructor

Publications

Peer-Reviewed Journal Articles:

CHRYSIKOPOULOS, C. V. and E. T. VOGLER, Estimation of time dependent virus inactivation rates by geostatistical and resampling techniques: Application to virus transport in porous media, *Stochastic Environmental Research and Risk Assessment*, (in press), 2003.

BAO, W. M. J., E. T. VOGLER, and C.V. CHRYSIKOPOULOS, Nonaqueous liquid pool dissolution in three–dimensional heterogeneous subsurface formations, *Environmental Geology*, 43, 968-977, 2003.

VOGLER, E. T., and C. V. CHRYSIKOPOULOS, Experimental investigation of acoustically enhanced solute transport in porous media, *Geophysical Research Letters*, 29(15), 1710, 10.1029/2002-GL01534, 2002.

VOGLER, E. T., and C. V. CHRYSIKOPOULOS, Dissolution of nonaqueous phase liquid pools in anisotropic aquifers, *Stochastic Environmental Research and Risk Assessment*, 15, 33-46, 2001.

VOGLER, E. T., and J. S. SCHERFIG, Modeling BOD removal in constructed wet-

lands with mixing cell method, Comment, *Journal of Environmental Engineering*, 782-785, Aug., 2000.

Conference Proceedings:

VOGLER, E. T., and C. V. CHRYSIKOPOULOS, Effects of aquifer heterogeneity and anisotropy on mass transfer from a nonaqueous phase liquid pool, (Proceedings of the First European Bioremediation Conference), Chania, Crete, Greece, 233-236, 2001.

VOGLER, E. T., and C. V. CHRYSIKOPOULOS, Effect of acoustic waves on solute transport in porous media, Proceedings of the international conference *Protection and Restoration of the Environment VI, Volume II*, editted by A. G. Kungolos, A. B. Liakopoulos, G. P. Korfiatis, A. D. Koutsospyros, K. L. Katsifarakis, and A. C. Demetracopoulos, pp. 921–926, Skiathos, Greece, 2002.

Other Publications (Technical Reports):

CHRYSIKOPOULOS, C. V., and E. T. VOGLER, Application of acoustic pressure waves in aquifer remediation and mobilization of entrapped organic liquids, Technical Completion Report, Water Resources Center, Project UCAL–WRC–W–938, 20 pp., University of California, Davis, 2002.

Poster Presentations:

VOGLER, E. T., and C. V. CHRYSIKOPOULOS, Mass transfer from a DNAPL pool in a statistically anisotropic aquifer, *22*nd *Biennial Groundwater Conference*, 104, 1999.

VOGLER, E. T., and C. V. CHRYSIKOPOULOS, Effects of aquifer anisotropy and heterogeneity on nonaqueous phase liquid pool dissolution (Abstract), *EOS, Transactions, American Geophysical Union*, 2000.

Scientific and Professional Society Memberships

American Geophysical Union (AGU)

American Society of Civil Engineers (ASCE)

Golden Key National Honors Society

Abstract of The Dissertation

Acoustically Enhanced Nonaqueous Phase Liquid Remediation In Porous Media

by

Eric Todd Vogler

Doctor of Philosophy in Civil Engineering

University of California, Irvine, 2003

Constantinos V. Chrysikopoulos, Chair

Groundwater contamination, caused by the presence of dense nonaqueous phase liquids (DNAPLs), remains a remediation challenge due to their low aqueous solubilities and residual phase immobility. To combat this challenge, the application of acoustic waves for remediation of water saturated porous media contaminated by DNAPL ganglia is proposed and investigated in this study.

Experiments are performed to first determine the effects of acoustic waves on the transport of a conservative tracer in a water-saturated column packed with glass beads. From resulting experimental tracer data, the addition of acoustic waves, in the frequency range between 60 to 245 Hz, to a steady background fluid flow (base case) is found to enhance solute transport compared to the base case. Furthermore, the effective velocity of the solute is approximately inversely proportional to the frequency of the acoustic wave.

Next, the effects of acoustic waves on the dissolution of trichloroethylene (TCE) DNAPL ganglia in a water saturated column, packed with glass beads are investigated. Acoustic waves with pressure amplitudes ranging from 0 to 1625 Pa and frequencies ranging from 0 to 285 Hz are employed to the interstitial fluid at the inlet of the packed column. Effluent dissolved TCE concentrations are observed to increase in the presence of acoustic pressure waves compared to the case where TCE dissolution

without acoustic waves is monitored. The observed effluent dissolved TCE concentration increase is attributed to increased mass flux at the TCE-water interface, caused by acoustic waves. As an extension to the single component ganglia dissolution experiments, the impact of acoustic pressure waves on multicomponent DNAPL ganglia dissolution is also investigated. The multicomponent ganglia was composed of TCE and 1,1,2-trichloroethane (1,1,2-TCA) or TCE, 1,1,2-TCA, and tetrachloroethylene (PCE). Laboratory data from ganglia dissolution experiments with two and three component NAPL mixtures show that the greatest dissolution enhancement in the presence of acoustic waves is associated with the NAPL component having the smallest equilibrium aqueous solubility. Finally, square shaped acoustic waves are shown to lead to greater NAPL dissolution enhancement compared to sinusoidal and triangular acoustic waves.

Finally, a pore network consisting of a monolayer of glass beads is used to investigate the effects of acoustic waves on the dissolution and mobilization of perchlorethylene (PCE) ganglia. Acoustic waves with frequencies ranging from 75 to 225 Hz at a constant pressure amplitude of 3.68 kPa were applied to the inlet of the monolayer for dissolution experiments. A pore network numerical model is used to determine the effective mass transfer coefficient responsible for effluent dissolved phase PCE concentrations in the presence and absense of acoustic waves. PCE ganglia mobilization experiments are conducted using a constant acoustic wave frequency of 125 Hz and acoustic pressure amplitudes ranging from 0 to 39.07 kPa. Effluent dissolved PCE concentrations and associated effective mass transfer coefficients are observed to increase in the presence of acoustic waves with the greatest increase occuring at the lowest frequency employed, 75 Hz. Mobilization experiments show that PCE ganglia are mobilized at lower flow rates and capillary numbers when acoustic pressure waves are used. Overall, the results of this study suggest that the use of acoustic waves in aquifer remediation is a promising alternative method to traditional remediation procedures particularly for aquifers contaminated with NAPLs containing components with very low equilibrium aqueous solubilities.

Chapter 1

INTRODUCTION

1.1 Motivation

The accidental release of nonaqueous phase liquids (NAPLs), such as petroleum hydrocarbons or chlorinated solvents, to the subsurface poses a serious risk to human health because many of these compounds are carcinogenic. Moreover, only a few parts per billion of certain NAPLs can render groundwater unpotable. The removal of these compounds from groundwater aquifers is therefore pivotal in maintaining potable groundwater resources and protecting human health. Unfortunately, the remediation of these compounds, especially dense NAPLs or DNAPLs, has proved to be very challenging [*Khachikian and Harmon*, 2000].

DNAPLs, such as the chlorinated solvents: trichloroethylene (TCE), perchloroethylene (PCE), and 1,1,2-trichloroethane (1,1,2-TCA) are denser than water. Because they are denser than water they have the tendency to sink to deeper portions of aquifers, given a sufficient contaminant source volume. Once DNAPLs have migrated to deeper portions of aquifers, often hundreds of meters below ground surface and the water table, they slowly dissolve and have the potential to pollute large volumes of groundwater.

1.2 Current Remediation Methods

1.2.1 Pump–and–Treat

Currently, the most common remediation method for DNAPL contaminated aquifers is pump–and–treat. The pump–and–treat method involves drilling groundwater extraction wells and pumping large volumes of polluted groundwater that is treated at the surface. There are two principle drawbacks to the pump–and–treat method. The first drawback is that most if not all DNAPLs have very low aqueous solubilities. Because of their low aqueous solubilities their subsequent dissolution is mass transfer limited [*Powers et al.*, 1991]. The mass transfer limitation results in lengthy (on the order of tens of years) remediation times where the associated costs are high. The second drawback is a hydraulic gradient, due to the zone of influence around the extraction well, that is insufficient for mobilization of the entrapped DNAPL [*Wilson et al.*, 1990]. To reduce the remediation times and costs associated with pump–and–treat, alternative remediation methods are needed.

1.2.2 Alternative Remediation Methods

Several alternative remediations methods to pump–and–treat have been proposed and investigated. For example, the use of cosolvents which enhance dissolution by making the aqueous phase more similar to the NAPL has been investigated by Rao et al. [1997] and Brandes and Farley [1993]. Use of surfactants, which reduce interfacial tension and enhance micellular mobilization and dissolution, has also been investigated [*Pennel et al.*, 1993; *Mason and Kueper*, 1996; *Fortin et al.*, 1997]. Another remediation alternative investigated is the introduction of bacteria that enhance the degradation of NAPLs in the subsurface, a process called bioremediation [*Chaudhry*, 1994; *Seagren et al.*, 1994]. The addition of humic substances to contaminated aquifers, which increases the dissolved mobile organic carbon content of the groundwater and enhances dissolution has also been investigated [*Tatalovich et al.*,

2000]. Unfortunately, there are problems associated with each of these methods, such as the addition of more substances to the groundwater which must be removed from the water in addition to the NAPL.

1.3 Research Objectives

The purpose of this work is to investigate the effect of acoustic waves on DNAPL ganglia dissolution and mobilization. Recent studies have shown that vibration of porous media can mobilize NAPL ganglia [*Reddi and Challa*, 1994; *Reddi and Wu*, 1996; *Reddi et al.*, 1998]. In another investigation, acoustic waves were shown to enhance dissolved mass transport in saturated porous media [*Vogler and Chrysikopoulos*, 2002]. These are positive indications that the phenomena associated with vibration and/or acoustic waves may be used for enhanced remediation of DNAPLs.

Chapter 2

LITERATURE REVIEW

2.1 NAPL Dissolution in Porous Media

The dissolution of nonaqueous phase liquids (NAPLS) in water saturated porous media is a slow and mass transfer limited process [*Khachikian and Harmon*, 2000] attributed to the low aqueous solubilities of NAPLs [*Mercer and Cohen*, 1990]. A common method to predict NAPL dissolution rates in water saturated porous media involves performing laboratory column dissolution experiments with residual NAPL blobs established following drainage and imbibition displacement [*Zhou et al.,* 2000]. Using steady state dissolved aqueous effluent concentrations from column experiments, correlations relating mass transfer to aqueous phase velocity have been developed [*Powers et al.,* 1992; *Imhoff et al.*, 1993; *Powers et al.*, 1994]. In addition to the dependence of mass transfer rates on aqueous phase velocities, these studies also confirmed mass transfer rates to depend on NAPL saturations and mean particle size of the porous media which vary widely in heterogeneous media [*Powers et al.*, 1998]. Investigations of NAPL dissolution in heterogeneous systems has shown that variability in the effective permeabilities affect the relative volume of water flowing through the NAPL source zone, the perimeter surface area of the NAPL source affects the total interfacial area for mass transfer, and decreased mass transfer rates within

the NAPL source zone due to limited interfacial area and/or increased aqueous flow rates is the overall rate-limiting mass transfer factor [*Nambi and Powers*, 2000]. In addition to heterogeneities in porous media, heterogeneity in NAPL distribution also contributes to much of the apparent nonequilibrium mass transfer kinetics of NAPL dissolution [*Sorens et al.*, 1998].

2.1.1 DNAPL Pool Dissolution in Porous Media

Dense nonaqueous phase liquids (DNAPLs) are denser than water and have a tendancy to sink to deeper portions of aquifers. Given enough DNAPL contaminant source volume exists, pools may form on low permeability layers or bedrock within aquifers. If this occurs, the lower interfacial areas of pools compared to ganglia, will produce slower overall dissolution rates [*Anderson et al.*, 1992; *Johnson and Pankow*, 1992]. Developing mass transfer correlations describing the dissolution of NAPL in pooled geometry is more difficult than for residual NAPL ganglia and associated column studies because it is a three-dimensional problem [*Kachikian and Harmon,* 2000]. However, several investigations have been performed on the dissolution of NAPL pools [*Anderson et al.*, 1992; *Johnson and Pankow*, 1992; *Voudrias and Yeh*, 1994; *Chrysikopoulos et al.*, 1994; *Chrysikopoulos*, 1995; *Longino and Kueper*, 1995; *Holman and Javandel*, 1996; *Mason and Kueper*, 1996; *Chrysikopoulos and Lee*, 1998; *Kim and Chrysikopoulos*, 1999 to mention a few]. A point of interest in the research performed on NAPL pool dissolution is that the aqueous phase concentration boundary layer above the pool is shown to increase from the upstream to downstream direction resulting in decreasing local mass transfer coefficients along the length of the NAPL pool [*Chrysikopoulos*, 1995]. The effect of increasing heterogeneity and vertical anisotropy on DNAPL pool dissolution was found to decrease the average mass transfer coefficient in a two-dimensional system [*Vogler and Chrysikopoulos*, 2001]. In three-dimensions, increasing the variance of log-transformed hydraulic conductivities, representing heterogeneity, was also found to decrease the average mass transfer coefficient [*Bao et al.*, 2003].

2.1.2 Multicomponent NAPL Dissolution in Porous Media

The majority of theoretical as well as experimental studies published in the literature have focused on single component NAPL ganglia and pool dissolution in subsurface formations [e.g., *Johnson and Pankow*, 1992; *Chrysikopoulos et al.*, 1994; 2000; *Seagren et al.*, 1999; *Holman and Javandel*, 1996; *Chrysikopoulos and Lee*, 1998; *Kim and Chrysikopoulos*, 1999; *Chrysikopoulos and Kim*, 2000; *Tatalovich et al.*, 2000; *Vogler and Chrysikopoulos*, 2001; *Brusseau et al.*, 2002; *Chrysikopoulos et al.*, 2002; *Dela Barre et al.*, 2002; *Lee and Chrysikopoulos*, 2002; *Bao et al.*, 2003]. However, several studies are devoted to the investigation of the relatively complex multicomponent NAPL dissolution in water saturated as well as unsaturated porous formations [e.g., *Lee and Chrysikopoulos*, 1995; 1998; *Mukherji et al.*, 1997; *Chrysikopoulos and Lee*, 1998; *Peters et al.*, 2000; *Gaganis et al.*, 2002; *Eberhardt and Grathwohl*, 2002; *Roy et al.*, 2002; *Jawitz et al.*, 2003]. The various components of a NAPL mixture may have substantially different water solubilities. Consequently, an important complication with multicomponent NAPL dissolution is that temporal changes in the equilibrium solubility of each NAPL component must be accounted for, because the mole fraction and the nonaqueous phase activity coefficient of each component changes as the composition of the NAPL changes [*Banerjee*, 1984; *Lee and Chrysikopoulos*, 1995; *Chrysikopoulos and Lee*, 1998; *McCray and Dugan*, 2002).

2.2 Acoustic Waves in Porous Media

The use of acoustic waves in the remediation of aquifers contaminated with DNAPLs has yet to be investigated. Currently, only peripheral observations and investigations have been made or performed suggesting that acoustic waves may be an effective method for groundwater remediation. Although the theory of elastic wave propagation in water saturated porous media has been previously established by the work of Biot [1956a, 1956b], little attention has been given to applying the resulting phenomena to a groundwater remediation technique.

Wave phenomena in saturated porous media has been investigated and theoretically explored by the ground breaking work of Biot [1956a, 1956b]. Biot fully developed and theoretically explored the theory of elastic wave propagation in saturated porous media. Elastic waves, such as acoustic waves, in porous media are waves that compress and rarefy the medium, in this case saturated porous media, without causing permanent deformation. These elastic waves were theoretically found to propagate by longitudinal and transverse waves. The waves of importance for this study are the longitudinal waves because they are of compressional/dilatational nature and not rotational. It has been shown that there are two longitudinal waves, consisting of a fast wave and a slow wave, that propagate through the water saturated porous media [*Biot*, 1956a; *Biot*, 1956b; *Chandler and Johnson*, 1981; *Geerits and Kelder*, 1997; *Parra and Xu*, 1994].

2.2.1 Wave Propagation

Longitudinal fast waves that propagate through saturated porous media, per Biot's theory [1956a, 1956b], do so by compressing the fluid and solid fractions in phase. The slow wave is described by a compressional wave propagating through the porous media where the oscillatory motion of the interstitial pore fluid and solid matrix are out of phase. Experiments conducted in shock tubes to explore these theories have shown that for the fast wave, both the fluid phase and porous media skeleton are compressed, but in the slow wave the fluid is compressed and the skeleton is extended [*Van der Grinten et al.*, 1985; *Van der Grinten et al.*, 1987; *Sniekers et al.*, 1989]. The phenomena of the porous media matrix and the pore fluid being out of phase for the slow wave produces an additional interstial pore water velocity. This motion/velocity resulting from the out of phase "slow" wave is diffusive in nature and as a diffusive wave has very interesting properties. These properties, for example, follow the accumulation–depletion law at interfaces instead of the reflection–refraction law of normal waves and have an infinite speed of field propagation, though with vanishingly small amplitudes with increasing distances away from the source [*Mandelis*, 2000]. All

of these phenomena, however, result in an additional fluid velocity, specifically for the slow wave and the fast wave with a constant background flow component.

2.2.2 Effects on Pore Fluid

The study of oscillatory pore fluid velocity and its properties has been investigated in several studies. For example, Biot [1956b] addressed the breakdown of Poiseuille flow at elastic wave frequencies greater than approximately 100 Hz and determined that the friction factor between the pore fluid and pore walls increases with increasing frequency of the elastic wave. In a similar study, Qian [1998] investigated the dynamic properties of viscosity in porous media and found that the effective viscosity increases with increasing acoustic frequency. Zhou and Sheng [1989] reported that the permeability of a porous medium decreases with increasing elastic wave frequency. Cherskiy et al. [1977] performed experiments on rock core samples and determined that the permeability increases with increasing sound intensity caused by a possible destruction of water films within the pore spaces. However, it should be noted that Biot [1956b], Qian [1998], and Zhou and Sheng [1989] did not consider a background steady flow component which was experimentally accounted for by Cherskiy et al. [1977].

2.3 Acoustic Enhanced Mass Transfer

The effects of oscillatory fluid motion, such as acoustic waves, on mass transfer have only recently been investigated. For example, using a single oscillating aerocolloidal droplet, evaporation rates have been reported to be as much as five times the rate for evaporation in a stagnant gas [*Zhu et al.*, 2002]. In a similar study, heat and mass transfer from pulvarized coal particles and coal-water slurry fuel droplets were observed to increase by up to 290% by applying a high intensity acoustic field [*Ha and Yavuzkurt*, 1993a; *Ha and Yavuzkurt*, 1993b]. Heat transfer from a flat plate has

also been experimentally shown to increase by approximately an order of magnitude when using infrasound compared to natural convection [*Preston and Johnson*, 1997]. However, no investigations have been performed showing the effects of acoustic waves or oscillatory flow on enhanced mass transfer in porous media.

2.4 Acoustic Mobilization Mechanisms

There two known NAPL mobilization mechanisms that are associated with acoustics. The first method involves vibrating the porous media [*Reddi and Challa*, 1994; *Reddi and Wu*, 1996; *Reddi et al.*, 1998]. It has been shown that when vibrational forces result in the compaction of sand, viscous pressures are responsible for splitting ganglia whereas the buoyancy pressures increase the maximum sustainable NAPL ganglia length. The reverse was observed when dillatation of the soil pores occurred, which increased porosity [*Reddi and Wu*, 1996]. However, the application and research of vibratory mobilization has been limited to light nonaqueous phase liquids (LNAPLs), which tend to reside in shallow portions of aquifers such as the vadoze zone and at the water table. Since DNAPLs have the potential to contaminate deeper portions of the aquifer, the application of vibratory mobilization at greater depths would be limited by overburden stress of aquifer material.

Recently, the resonation of NAPL menisci have been investigated as a means of remediation. For example, the effects of oscillatory flow in a capillary tube on the meniscus of two imiscible fluids has been shown to depend on the amplitude and frequency of the flow field [*Hilpert et al.*, 1996]. From this research three basic types of possible meniscus motion have been determined; pinned oscillations at low amplitudes, pinned oscillations and contact line sliding at high amplitudes and low frequencies, and pinned oscillations at high amplitudes and high frequencies [*Hilpert et al.*, 1996]. If high amplitudes and low frequencies are used, it has been shown that the meniscus physically moves. Considering the two-phase liquid capillary column as porous media saturated with water and DNAPL, the use of acoustic waves may mobilize and

enhance aquifer DNAPL ganglia and blob remediation where the DNAPL is immobilized in pore spaces due to interfacial tensions and corresponding capillary pressures. However, no experiments or investigations have been performed in porous media.

Chapter 3

ACOUSTIC ENHANCED MASS TRANSPORT

3.1 Mathematical Formulation

The one–dimensional transport of a non-sorbing solute or a conservative tracer in water saturated porous media under a constant hydraulic gradient can be described by the following linear, second–order partial differential equation:

$$\frac{\partial C(x,t)}{\partial t} = -U_e \frac{\partial C(x,t)}{\partial x} + D_e \frac{\partial^2 C(x,t)}{\partial x^2}, \tag{3.1}$$

where C is the liquid phase solute concentration [M/L^3]; t is time [t]; U_e is the effective interstitial fluid velocity [L/t]; and D_e is the effective hydrodynamic dispersion coefficient [L^2/t]. The effective interstitial fluid velocity is defined as

$$U_e = U + U^*, \tag{3.2}$$

where U is the steady state, background interstitial fluid velocity [L/t] and U^* is the additional velocity component attributed to acoustic pressure [L/t]. Similarly, the effective dispersion coefficient is defined

$$D_e = D + D^* = (U + U^*)\alpha_L + \mathcal{D}_e = U_e \alpha_L + \mathcal{D}_e, \tag{3.3}$$

where $D = U\alpha_L + \mathcal{D}_e$ is the hydrodynamic dispersion coefficient [L^2/t]; α_L is the longitudinal dispersivity [L]; $\mathcal{D}_e = \mathcal{D}/\tau^*$ is the effective molecular diffusion coefficient [L^2/t] (where $\mathcal{D}$ is the molecular diffusion coefficient [L^2/t], and $\tau^* > 1$ is the tortuosity coefficient [-]); and D^* is the additional dispersion component attributed to acoustic pressure [L^2/t]. It should be noted that the concept of effective parameters has been applied in numerous groundwater flow and solute transport studies [*Valocchi*, 1989; *Chrysikopoulos et al.*, 1990, 1992; *Kabala and Sposito*, 1991; *Chrysikopoulos*, 1995]

For a finite system, the following initial and boundary conditions can be used [*Kreft and Zuber*, 1978]

$$C(x,0) = 0, \tag{3.4}$$

$$-D_e\frac{\partial C(0,t)}{\partial x} + U_e C(0,t) = M_0\delta(t), \tag{3.5}$$

$$-D_e\frac{\partial C(L,t)}{\partial x} + U_e C(L,t) = U_e C_f, \tag{3.6}$$

where $M_0 = M/A_c\theta$ is the mass injected over the cross sectional area of the column (where M is the injected mass [M], A_c is the cross sectional area of the porous medium [L^2], and θ is porosity [-]); δ is the Dirac delta function [1/t]; and C_f is the effluent flux concentration [M/L^3]. It should be noted that C corresponds to the *in situ* or resident concentration, whereas C_f is the flux concentration defined as the ratio of the solute mass flux to the volumetric fluid flux [*Kreft and Zuber*, 1978]. Initial condition (3.4) establishes a zero background concentration. Boundary condition (3.5) describes the flux influent pulse concentration. Boundary condition (3.6) describes the flux effluent solute concentration at the end of the packed column $x = L$. The solution to the governing equation (3.1) subject to conditions (3.4)–(3.6), for the effluent concentration of a one–dimensional packed column of length L is obtained by straightforward Laplace transform procedures to yield:

$$C(x,t) = \frac{xM_0}{2U_e t}\left(\frac{1}{\pi D_e t}\right)^{1/2}\exp\left[-\frac{1}{4D_e t}\left(x - U_e t\right)^2\right]. \tag{3.7}$$

It should be noted that an analytical solution to a slightly different mathematical model than the one examined in this study has been previously presented in the

literature [*DeSmedt and Wierenga*, 1979].

3.2 Experimental Design

The effect of acoustic waves on solute transport in water saturated porous media was investigated in this study by injecting a bromide tracer pulse into a 30 cm long glass laboratory column with a 2.5 cm inner diameter (Kimble Kontes, New Jersey). The column was packed with 2 mm diameter glass beads (Fisher Scientific, Pennsylvania) that were retained in the column with teflon screens placed on both the influent and effluent sides of the column. The teflon column end caps were milled to accommodate 1/4 inch stainless steel fittings (Swageloc) for 3/8 inch semi–rigid plastic tubing (Fisher Scientific, Pennsylvania). Constant flow of degassed Millipore water at a rate of 1.48 ml/min was maintained through the packed column with a microprocessor pump drive (Cole Palmer Instrument Co., Illinois). Acoustic pressure was introduced into the column through the plastic tubing with a specially designed reservoir containing a pressure transducer (TST37; Clark Sythesis, Colorado). The frequency of the acoustic pressure oscillation was controlled by a frequency generator (LG Precision, California). Acoustic pressure levels were controlled by an amplifier (Lab Gruppen, Sweden) and measured with a PCB106b pressure sensor in conjunction with a signal conditioner (PCB Piezotronics, Inc., New York) and a digital multimeter (Metex, Korea). Effluent samples were collected from a dedicated needle (sampling port) within the effluent tube. A complete schematic of the experimental apparatus employed in this study is shown in Figure 3.1.

The tracer solution was prepared by dissolving 256 mg of potassium bromide salt (KBr) (Fisher Scientific, Pennsylvania) into a liter of total solution volume to yield a final Br^- concentration of 172 mg/L. Alkali halides are the most commonly used salts for subsurface fluid tracing [*Chrysikopoulos*, 1993]. A slug of 0.6 mL of the tracer solution was instantaneously injected into the column by a side injection port midway down the column. Sample effluent volumes of 0.8 mL were collected at regular

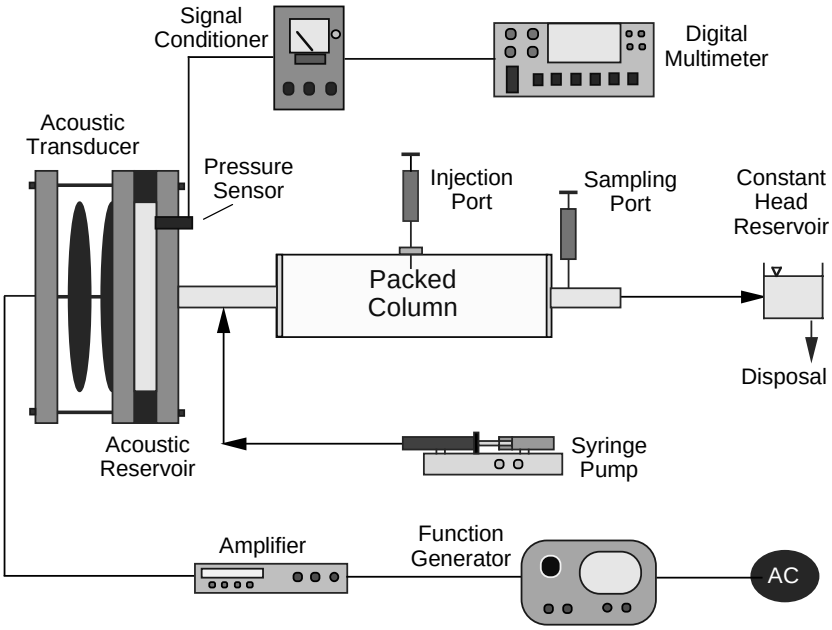

Figure 3.1: Experimental apparatus.

intervals using disposable 1.0 mL tuburculin plastic syringes (Becton Dickinson & Co., New Jersey). The Br^- concentrations of the liquid samples were determined using a Dionex DX–120 ion chromatograph (Dionex, California). The base case experiment was first conducted to determine background U, and α_L in the absence of acoustic waves (0 Hz). Subsequently, flowthrough experiments were conducted using the same procedure described for the base case, but in the presence of acoustic waves at ten different preselected acoustic frequencies.

3.3 Experimental Results

The experimental Br^- breakthrough data for the base case are presented in Figure 3.2 (solid circles) together with the breakthrough data collected in the presence of acoustic waves with frequency 60 Hz (open circles). Clearly, the presence of acoustic waves leads to a faster breakthrough of the conservative tracer. The nonlinear regression subroutine *mrqmin* [*Press et al.*, 1992] was employed to estimate the dispersivity of

the packed column $\alpha_L = 0.117$ cm and the steady state background interstitial fluid velocity $U = 0.644$ cm/min, by fitting the analytical solution derived in this work, (3.7), to the experimental breakthrough data for the base case.

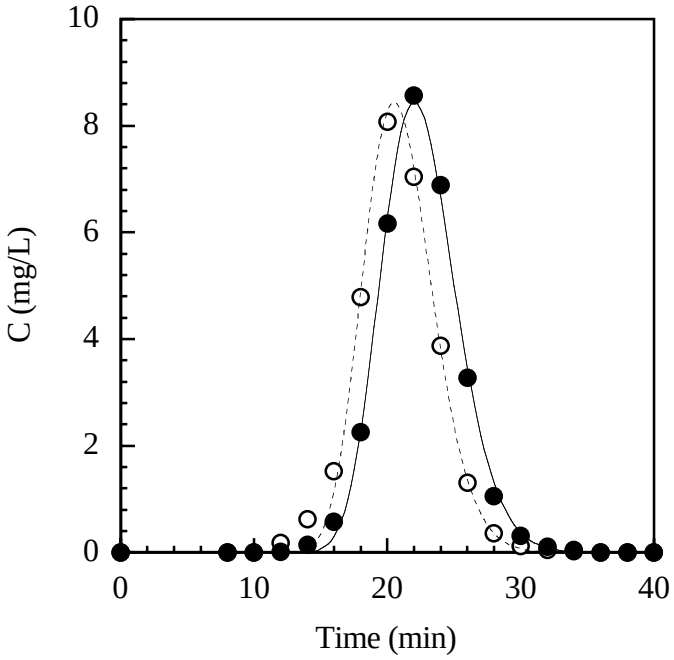

Figure 3.2: Tracer (Br^-) concentration breakthrough data (solid circles) and fitted model (solid curve) in the absence of acoustic pressure (base case) compared to breakthrough data (open circles) and fitted model (dashed curve) obtained in the presence of acoustic pressure at 60 Hz.

The effective molecular diffusion coefficient of Br^- used for the nonlinear regression procedure is $\mathcal{D}_e = \mathcal{D}/\tau^* = 8.62 \times 10^{-4}$ cm^2/min, or equivalently $\mathcal{D} = 1.2067 \times 10^{-3}$ cm^2/min [*Domenico and Schwartz*, 1990], and $\tau^* = 1.4$ [*de Marsily*, 1986]. Subsequently, the same fitting procedure was employed to determine the effective velocity (U_e), using a fixed value of α_L, for each of the ten different breakthrough data sets collected in this study in the presence of acoustic waves. The estimated effective velocity for the base case and the ten different frequencies ranging from 0 to 245 Hz at a constant pressure amplitude of 565 Pa are shown in Figure 3.3. The estimated effective dispersion coefficient for the base case and the ten different acoustic frequencies are shown in Figure 3.4. It should be noted that the values in Figure 3.4 were obtained directly from from (3.3) using the U_e values presented in

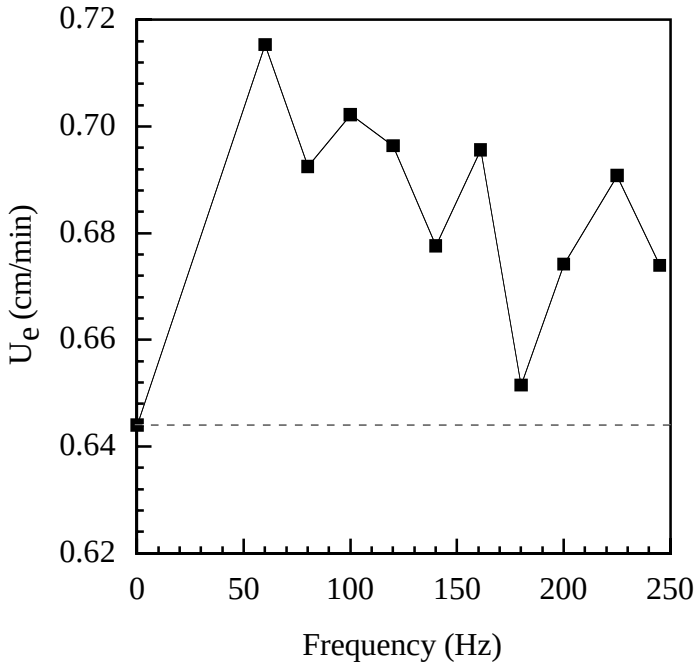

Figure 3.3: Experimentally determined effective velocity (solid squares) for various acoustic pressure frequencies. The dashed line represents the case of no acoustic waves present (base case).

Figure 3.3.

Obviously, acoustic waves, particularly at low frequencies, enhance the tracer velocity and consequently enhance tracer dispersion (see Equation (3.3)). It should also be noted that due to experimental limitations in the low acoustic frequency range, no characteristic acoustic wave frequency was found to produce a maximum enhancement of the tracer transport. However, the enhanced interstitial fluid velocity appears to be approximately inversely proportional to the acoustic frequency.

3.4 Summary

The experimental Br^- breakthrough data collected in this study indicate that acoustic waves enhance the transport of solutes in water saturated porous media. The degree of solute transport enhancement was found to be inversely proportional to the acoustic wave frequency. Due to experimental limitations, the characteristic acoustic

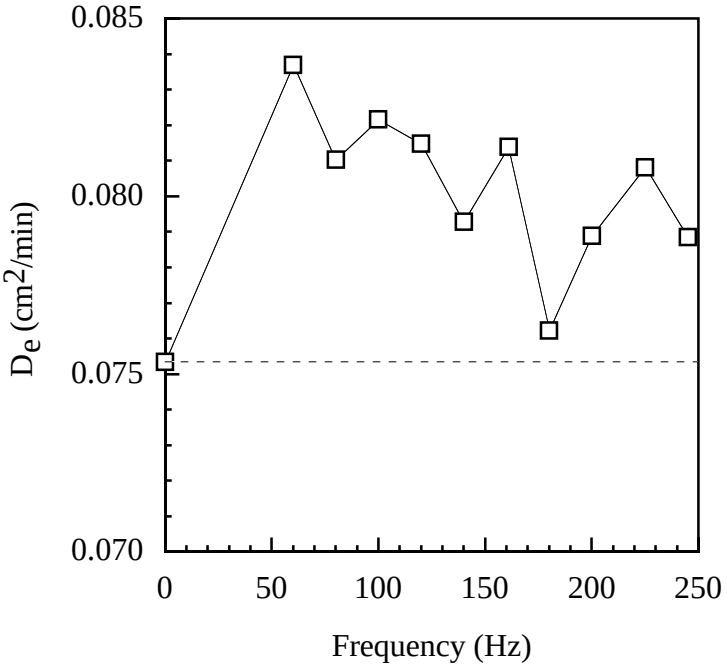

Figure 3.4: Effective dispersion coefficient (open squares) for various acoustic pressure frequencies. The dashed line represents the case of no acoustic waves present (base case).

wave frequency leading to a maximum enhancement of solute transport was not determined. However, it is assumed that this characteristic acoustic frequency, for the experimental conditions considered in this study, is within the range of the lowest frequency examined (60 Hz) and the base case (0 Hz). The experimental results suggest that further research should be undertaken to discern the governing mechanisms responsible for the enhanced transport phenomenon. The preliminary findings of this study however, may be regarded as the initial step to the development of a clean groundwater remediation method as an alternative to currently available remediation methods.

Chapter 4

ACOUSTIC ENHANCED DNAPL DISSOLUTION

4.1 Mathematical Developments

Acoustic wave propagation through one–dimensional, water saturated porous media, assuming the interstitial fluid and solid matrix are incompressible, may be described by the following two equations that account for the motion of the interstitial fluid and solid matrix, and a mass conservation equation [*de Boer et al.*, 1993]:

$$(\lambda+2\mu)\frac{\partial^2\xi_s(t,x)}{\partial x^2}-(1-\theta)\frac{\partial p(t,x)}{\partial x}-\rho_s\frac{\partial^2\xi_s(t,x)}{\partial t^2}+S\left[\frac{\partial\xi_f(t,x)}{\partial t}-\frac{\partial\xi_s(t,x)}{\partial t}\right]=0, \quad (4.1)$$

$$-\theta\frac{\partial p(t,x)}{\partial x}-\rho_f\frac{\partial^2\xi_f(t,x)}{\partial t^2}-S\left[\frac{\partial\xi_f(t,x)}{\partial t}-\frac{\partial\xi_s(t,x)}{\partial t}\right]=0, \quad (4.2)$$

$$(1-\theta)\frac{\partial^2\xi_s(t,x)}{\partial t\partial x}+\theta\frac{\partial^2\xi_f(t,x)}{\partial t\partial x}=0, \quad (4.3)$$

where μ and λ are the solid matrix Lamé constants, representing the shear modulus and the bulk modulus less 2/3 of the shear modulus, respectively; ξ_s is the solid displacement; ξ_f is the fluid displacement; x denotes spacial coordinate in the direction of flow; θ is the fluid volume fraction or porosity of the porous medium; $(1-\theta)$ is the volume fraction of solids per unit volume of the porous medium; p denotes fluid

pressure; t is time; $\rho_s = (1-\theta)\rho_{\text{solid}}$ is the solid bulk density (where ρ_{solid} is the solid density); $\rho_f = \theta\rho_{\text{H}_2\text{O}}$ is the fluid bulk density (where $\rho_{\text{H}_2\text{O}}$ is the water density); S is a function that relates the extra stress due to the relative movement between the solid and fluid [*de Boer and Ehlers*, 1990]

$$S = \frac{\theta^2\gamma}{K}, \tag{4.4}$$

where γ is the specific weight of the fluid; and K is the hydraulic conductivity of the porous medium.

Assuming that there is no initial displacement or velocity for the fluid and solid matrix, the appropriate initial conditions considered here are:

$$\xi_s(0,x) = \xi_f(x,0) = 0, \tag{4.5}$$

$$\frac{\partial\xi_s(0,x)}{\partial t} = \frac{\partial\xi_f(0,x)}{\partial t} = 0. \tag{4.6}$$

Furthermore, assuming that the porous medium is semi-infinite, the boundary conditions for the solid and fluid phases are given by:

$$\sigma(t,0) = (1-\theta)f(t) = (2\mu+\lambda)\frac{\mathrm{d}\xi_s}{\mathrm{d}x}, \tag{4.7}$$

$$\sigma(\infty,t) = p(t,\infty) = 0, \tag{4.8}$$

where σ is solid stress caused by the interaction between solid and fluid movement [*de Boer et al.*, 1993] and $f(t)$ is an acoustic pressure source function. Boundary condition (4.7) equates the stress of the solid matrix and the pressure of the fluid at the acoustic source boundary.

The solution to the boundary value mathematical problem described is obtained with the methods of de Boer et al. [1993] who have examined the governing differential equations (4.1)-(4.3) for a different set of boundary conditions. Taking Laplace transforms of (4.1)-(4.3) with respect to time variable t, and employing initial conditions (4.5) and (4.6), leads to the following set of equations:

$$(\lambda+2\mu)\frac{\mathrm{d}^2\tilde{\xi}_s(\nu,x)}{\mathrm{d}x^2} - (1-\theta)\frac{\mathrm{d}\tilde{p}(\nu,x)}{\mathrm{d}x} - (\rho_s\nu^2 + S\nu)\tilde{\xi}_s(\nu,x) + S\nu\tilde{\xi}_f(\nu,x) = 0, \tag{4.9}$$

$$-\theta\frac{\mathrm{d}\tilde{p}(\nu,x)}{\mathrm{d}x}-(\rho_f\nu^2+S\nu)\tilde{\xi}_f(\nu,x)+S\nu\tilde{\xi}_s(\nu,x)=0, \tag{4.10}$$

$$(1-\theta)\nu\frac{\mathrm{d}\tilde{\xi}_s(\nu,x)}{\mathrm{d}x}+\theta\nu\frac{\mathrm{d}\tilde{\xi}_f(\nu,x)}{\mathrm{d}x}=0, \tag{4.11}$$

where the "tilde" signifies Laplace transform defined as

$$L[\kappa(t)]=\tilde{\kappa}(\nu)=\int_0^\infty \kappa e^{-\nu t}\mathrm{d}t, \tag{4.12}$$

κ is a dummy variable, and ν is the Laplace transform parameter. Placing (4.9) through (4.11) into matrix notation results in

$$\mathbf{F}\frac{\mathrm{d}^2\mathbf{m}}{\mathrm{d}x^2}+\mathbf{G}\frac{\mathrm{d}\mathbf{m}}{\mathrm{d}x}+\mathbf{H}\mathbf{m}=\mathbf{0}, \tag{4.13}$$

where

$$\mathbf{m}=\left[\tilde{\xi}_s(\nu,x),\tilde{\xi}_f(\nu,x),\tilde{p}(\nu,x)\right]^{\mathrm{T}}, \tag{4.14}$$

the superscript T indicates transpose, and matrices $\mathbf{F}$, $\mathbf{G}$, and $\mathbf{H}$ are:

$$\mathbf{F}=\begin{bmatrix}\lambda+2\mu & 0 & 0\\ 0 & 0 & 0\\ 0 & 0 & 0\end{bmatrix} \tag{4.15}$$

$$\mathbf{G}=\begin{bmatrix}0 & 0 & -(1-\theta)\\ 0 & 0 & -\theta\\ (1-\theta)\nu & \theta\nu & 0\end{bmatrix}, \tag{4.16}$$

$$\mathbf{H}=\begin{bmatrix}-\rho_s\nu^2-S\nu & S\nu & 0\\ S\nu & -\rho_f\nu^2-S\nu & 0\\ 0 & 0 & 0\end{bmatrix}. \tag{4.17}$$

Assuming a trial solution for $\mathbf{m}$ in the form

$$\mathbf{m}=\mathbf{m}_0e^{\alpha x}, \tag{4.18}$$

where $\mathbf{m}_0$ and α are functions of the Laplace transform parameter ν. Substitution of (4.18) into (4.13) results in the following eigenvalue problem

$$(\alpha^2\mathbf{F}+\alpha\mathbf{G}+\mathbf{H})\mathbf{m}_0e^{\alpha x}=\mathbf{0}. \tag{4.19}$$

The eigenvalues are determined from the characteristic equation

$$|\alpha^2\mathbf{F} + \alpha\mathbf{G} + \mathbf{H}| = \alpha^2\{(\lambda + 2\mu)\theta^2\alpha^2 - \left[(1-\theta)^2\rho_f + \theta^2\rho_s\right]\nu^2 - S\nu\} = 0, \quad (4.20)$$

where the latter formulation in the preceding expression is the consequence of substitution of (4.15)-(4.17) followed by determinant evaluation. The roots or eigenvalues of the characteristic equation are:

$$\alpha_1 = (\Omega_1\nu^2 + \Omega_2\nu)^{1/2}, \quad (4.21)$$

$$\alpha_2 = -(\Omega_1\nu^2 + \Omega_2\nu)^{1/2}, \quad (4.22)$$

$$\alpha_3 = \alpha_4 = 0, \quad (4.23)$$

where

$$\Omega_1 = \frac{(1-\theta)^2\rho_f + \theta^2\rho_s}{(\lambda + 2\mu)\theta^2}, \quad (4.24)$$

$$\Omega_2 = \frac{S}{(\lambda + 2\mu)\theta^2}. \quad (4.25)$$

Consequently, the corresponding eigenvectors are:

$$\mathbf{q}_1 = \left[\begin{array}{ccc} \dfrac{-\theta}{(1-\theta)}, & 1, & \dfrac{-(1-\theta)\rho_f\nu^2 - S\nu}{(1-\theta)\theta(\Omega_1\nu^2 + \Omega_2\nu)^{1/2}} \end{array} \right]^{\mathrm{T}}, \quad (4.26)$$

$$\mathbf{q}_2 = \left[\begin{array}{ccc} \dfrac{-\theta}{(1-\theta)}, & 1, & \dfrac{(1-\theta)\rho_f\nu^2 + S\nu}{(1-\theta)\theta(\Omega_1\nu^2 + \Omega_2\nu)^{1/2}} \end{array} \right]^{\mathrm{T}}, \quad (4.27)$$

$$\mathbf{q}_3 = \mathbf{q}_4 = \left[\begin{array}{ccc} 0, & 0, & 1 \end{array} \right]^{\mathrm{T}}. \quad (4.28)$$

The Laplace domain solution can be expressed as

$$\mathbf{m} = A_1\mathbf{q}_1 e^{\alpha_1 x} + A_2\mathbf{q}_2 e^{\alpha_2 x} + A_3\mathbf{q}_3 + A_4 x\mathbf{q}_4, \quad (4.29)$$

where $A_1, \ldots, A_4$ are the Laplace domain constants to be determined. In view of boundary condition (4.8), it is evident that the solution can be finite at $x \to \infty$ only if $A_1 = A_4 = 0$. Thus, the Laplace domain solution reduces to

$$\mathbf{m} = A_2\mathbf{q}_2 e^{\alpha_2 x} + A_3\mathbf{q}_3. \quad (4.30)$$

In view of (4.14), (4.27), (4.28), and boundary condition (4.7), the constants A_2 and A_3 are determined as:

$$A_2 = \tilde{f}(\nu)\frac{(1-\theta)^2}{\theta(\lambda+2\mu)(\Omega_1\nu^2+\Omega_2\nu)^{1/2}}, \tag{4.31}$$

$$A_3 = \tilde{f}(\nu)\left[\theta - \frac{(1-\theta)^3\rho_f\nu^2 + (1-\theta)^2 S\nu}{\theta^2(1-\theta)(\lambda+2\mu)(\Omega_1\nu^2+\Omega_2\nu)}\right]. \tag{4.32}$$

Consequently, the Laplace domain solutions for $\tilde{\xi}_s(\nu,x)$ and $\tilde{\xi}_f(\nu,x)$ can be expressed as

$$\tilde{\xi}_s(\nu,x) = \frac{(\theta-1)}{(2\mu+\lambda)}\tilde{f}(\nu)\tilde{\Psi}(\nu,x), \tag{4.33}$$

$$\tilde{\xi}_f(\nu,x) = \frac{(1-\theta)^2}{\theta(2\mu+\lambda)}\tilde{f}(\nu)\tilde{\Psi}(\nu,x), \tag{4.34}$$

where

$$\tilde{\Psi}(\nu,x) = \frac{\exp\left[-(\Omega_1\nu^2+\Omega_2\nu)^{1/2}x\right]}{(\Omega_1\nu^2+\Omega_2\nu)^{1/2}}. \tag{4.35}$$

Taking the Laplace inverse transformation of (4.33) and (4.34) yields

$$\xi_s(t,x) = \frac{(\theta-1)}{\Omega_1^{1/2}(\lambda+2\mu)}\int_0^t f(t-\tau)\exp\left[-\frac{\Omega_2}{2\Omega_1}\tau\right]\mathrm{I}_0\left[\frac{\Omega_2(\tau^2-\Omega_1x^2)^{1/2}}{2\Omega_1}\right]\mathrm{H}(\tau-\Omega_1^{1/2}x)\mathrm{d}\tau, \tag{4.36}$$

$$\xi_f(t,x) = \frac{(1-\theta)^2}{\Omega_1^{1/2}\theta(\lambda+2\mu)}\int_0^t f(t-\tau)\exp\left[-\frac{\Omega_2}{2\Omega_1}\tau\right]\mathrm{I}_0\left[\frac{\Omega_2(\tau^2-\Omega_1x^2)^{1/2}}{2\Omega_1}\right]\mathrm{H}(\tau-\Omega_1^{1/2}x)\mathrm{d}\tau, \tag{4.37}$$

where the following Laplace inversion identities were utilized [*Abramowitz and Stegun*, 1965, p.1027]:

$$L^{-1}\{\tilde{g}_1(\nu)\tilde{g}_2(\nu)\} = \int_0^t g_1(\tau)g_2(t-\tau)\mathrm{d}\tau, \tag{4.38}$$

$$L^{-1}\{\tilde{\Psi}(\nu,x)\} = \frac{1}{\Omega_1^{1/2}}\exp\left[-\frac{\Omega_2}{2\Omega_1}t\right]\mathrm{I}_0\left[\frac{\Omega_2(t^2-\Omega_1x^2)^{1/2}}{2\Omega_1}\right]\mathrm{H}(t-\Omega_1^{1/2}x), \tag{4.39}$$

where L^{-1} is the Laplace inverse operator, I_0 is the modified Bessel function of zero order and H is the unit step function or Heaviside function. The solution for the fluid pressure is not presented here because it is just the Lagrangian multiplier of the fluid and solid displacements [*de Boer and Ehlers*, 1990] and it is not required in the present study.

The fluid displacement relative to the solid displacement may be written as

$$\xi_r(t,x) = \xi_f(t,x) - \xi_s(t,x). \tag{4.40}$$

Furthermore, a time and space dependent relative fluid velocity, $U_r(t,x)$, may be determined by differentiating (4.40) with respect to time. Because $U_r(t,x) = \mathrm{d}\xi_r(t,x)/\mathrm{d}t$ is a function of acoustic pressure and frequency which may vary between different experiments, the acoustic Reynolds number [*Ha and Yavuzkurt*, 1993a,b]

$$Re_a = \frac{U_{r_a} d}{\eta} \tag{4.41}$$

where U_{r_a} is the maximum value or amplitude of the oscillatory interstitial pore water velocity over one period of oscillation ($1/\phi$, where ϕ is the acoustic wave frequency), d is the mean grain diameter of the porous medium, and η is the kinematic fluid viscosity, will be used in this study for consistent comparison of our experimental data.

Figure 4.1 presents model simulations for fluid and solid displacements in water saturated columns packed with 1 mm (dashed curves) and 2 mm (solid curves) beads for the following acoustic source function

$$f(t) = p_s \sin(\omega t), \tag{4.42}$$

where p_s is the acoustic source fluid pressure, and $\omega = 2\pi\phi$ is the angular frequency. The curves are generated with the analytical solutions for $\xi_s(t,x)$ and $\xi_f(t,x)$, (4.36) and (4.37), respectively, where the integrals were evaluated numerically with IMSL subroutine *dqdag* [IMSL, 1991]. All of the model parameters employed are listed in Table 4.1. The displacements are evaluated at a location x=0.15 m downstream from the acoustic source with p_s=1 Pa and ϕ=225 Hz. Note that positive (ξ_s, $\xi_f > 0$) and negative (ξ_s, $\xi_f < 0$) displacements refer to directions away and toward the acoustic source, respectively. The solid displacements for the case of 2 mm beads is observed to be greater than for the case of 1 mm beads (Figure 4.1a). The same trend is observed in the simulations of the fluid displacement (Figure 4.1b). Comparison of Figures 4.1a and 4.1b indicates that the magnitude of the fluid displacement is greater than

that of the solid displacement. In addition, the equilibrium position, which refers to the position of the center of the oscillatory displacement, is initially located toward the acoustic source (negative displacement) for ξ_s and away from the acoustic source (positive displacement) for ξ_f. However, the equilibrium positions for both ξ_s and ξ_f are progressively shifted towards the zero displacement position ($\xi_s = \xi_f = 0$).

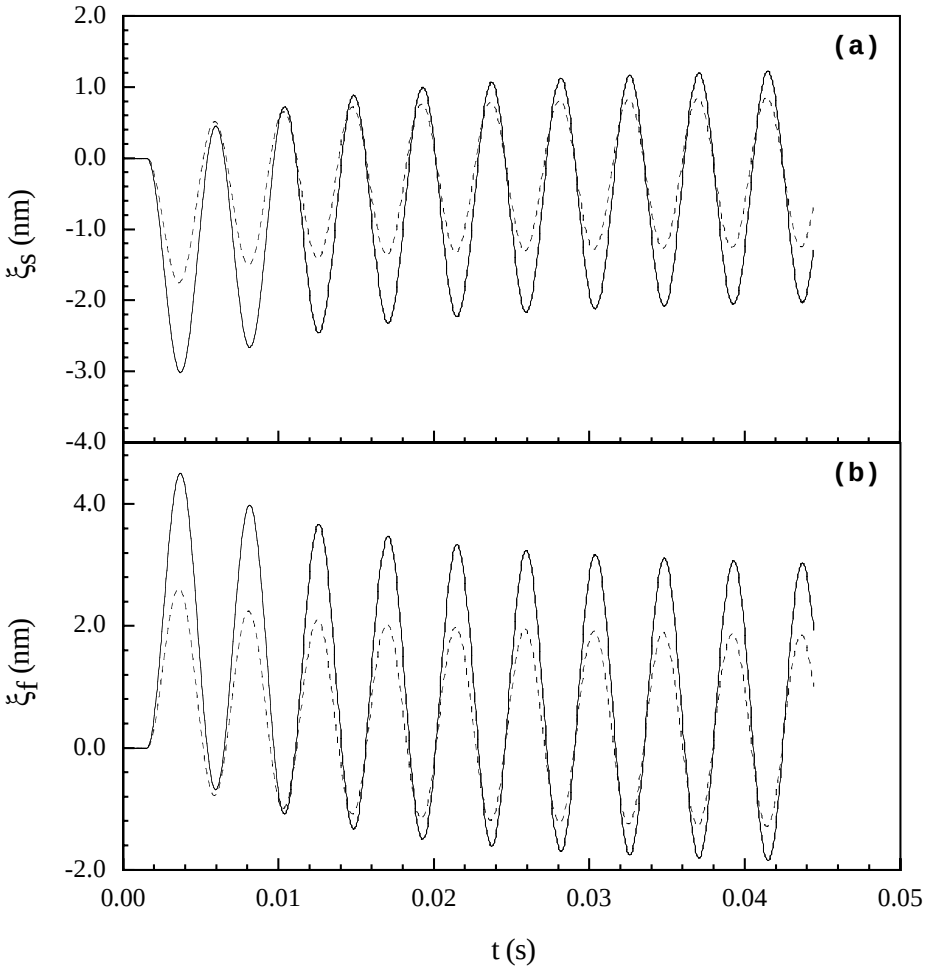

Figure 4.1: Simulated (a) solid and (b) fluid displacements as a function of time at x=0.15 m for an acoustic wave source with ϕ=225 Hz and p_s=1 Pa. Dashed and solid curves represent column packings of 1 and 2 mm beads, respectively.

Table 4.1: Column Packing Material and Fluid Properties

Parameter	Values
K†	6.158×10^{-2} m/s (for 1 mm beads)
K†	2.463×10^{-1} m/s (for 2 mm beads)
θ	0.40
ρ_{H_2O}	1000.0 Kg/m^3
ρ_{bead}	2330.0 Kg/m^3
ρ_f†	400.0 Kg/m^3
ρ_s	1398.0 Kg/m^3
η†	1.0037×10^{-6} m^2/s
λ^b	5.5833×10^6 N/m^2
μ^b	8.375×10^6 N/m^2
γ	1.0×10^5 N/m^3

† for water at 20 °C

‡ Adopted from *de Boers et al.* [1993]

The dependence of the acoustic Reynolds number, Re_a, on the distance from the acoustic source, x, acoustic wave frequency, ϕ, and acoustic source fluid pressure, p_s, is illustrated in Figure 4.2. The parameter U_{r_a}, present in the Re_a expression (4.41), is obtained by numerical approximation of the derivative $\mathrm{d}\xi_r(t,x)/\mathrm{d}t$ and evaluation of its maximum value over a period of acoustic wave oscillation, $1/\phi$. The term $\xi_r(t,x)$ is evaluated from (4.40) with $\xi_s(t,x)$ and $\xi_f(t,x)$ provided by the theoretically derived expressions (4.36) and (4.37), respectively. The simulations in Figure 4.2a indicate that Re_a decreases with increasing x. Figure 4.2b shows that Re_a reaches an asymptotic value with increasing ϕ. Figure 4.2c shows that Re_a increases linearly with increasing p_s. It should be noted that the Re_a values are consistently higher for the column packed with 2 mm beads (solid curves) than 1 mm beads (dashed curves). This is attributed to greater hydraulic conductivities and consequently, less viscous losses in the column with the greater bead size packing, due to smaller total bead surface areas per unit volume.

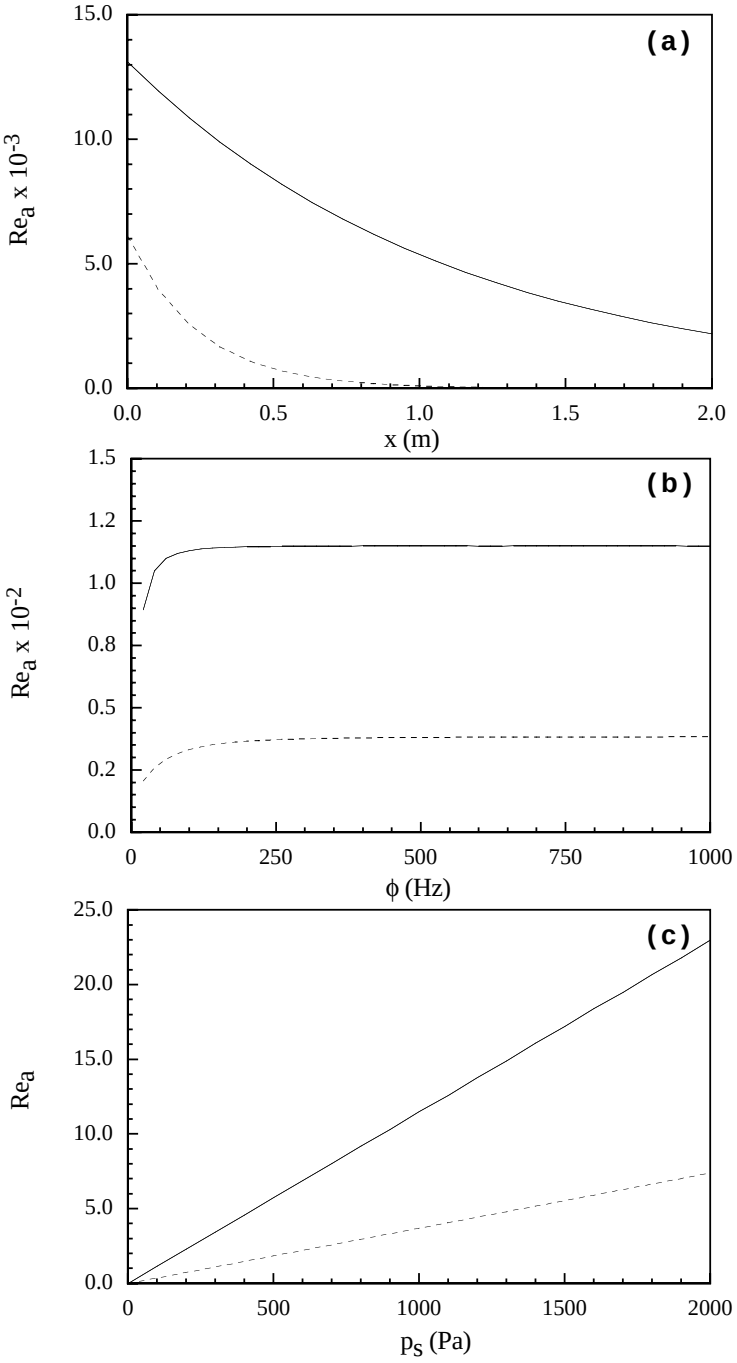

Figure 4.2: Acoustic Reynolds number as a function of (a) x, (b) ϕ, and (c) p_s (here x=0.15 m, ϕ=225 Hz, p_s=1 Pa). Dashed and solid curves represent column packings of 1 and 2 mm beads, respectively.

4.2 Experimental Procedures

The effect of acoustic pressure waves on mass transfer from a DNAPL blob in saturated porous media was investigated by conducting flowthrough dissolution experiments in a 30 cm long glass laboratory column with a 2.5 cm inner diameter (Kimble Kontes, New Jersey). The column was packed with either 1 or 2 mm diameter soda lime glass beads with a density of 2.33 g/cm^3 (Fisher Scientific, Pennsylvania). The beads were retained in the column using teflon screens and end caps on both the influent and effluent sides of the column. The teflon column end caps were milled to accommodate 1/4 inch stainless steel fittings (Swageloc) for 3/8 inch semi–rigid plastic tubing (Fisher Scientific, Pennsylvania). Constant flow of degassed Millipore water at 3.25 mL/min was maintained through the packed column with a microprocessor pump drive (Cole Palmer Instrument Co., Illinois). Acoustic pressure was introduced into the column using a custom designed acoustic reservoir containing a pressure transducer (TST37; Clark Sythesis, Colorado). The frequency of the acoustic pressure oscillation was controlled by a frequency generator (LG Precision, California). Acoustic pressure levels were controlled by an amplifier (Lab Gruppen, Sweden) and measured using PCB106b pressure sensors (PCB Piezotronics, Inc., New York). One pressure sensor was installed in the acoustic reservoir to measure the acoustic source pressure. Another sensor was placed in the effluent line, just after the packed column, to measure the effluent pressure as close to the packed column as possible. Pressure sensor measurements were made using a signal conditioner (PCB Piezotronics, Inc., New York) in addition to a digital multimeter (Metex, Korea) and oscilloscope (EZ Digital Co., Ltd, Korea). A complete schematic of the experimental apparatus is shown in Figure 4.3.

Effluent samples (0.15 mL) were collected from a dedicated needle within the effluent tube (sample port) at regular 10 minute intervals using disposable 1.0 mL tuberculin plastic syringes (Becton Dickinson & Co., New Jersey). The samples were immediately introduced into 2 mL vials (Kimble Glass, New Jersey) containing a known volume of n-pentane (Fisher Scientific, Pennsylvania). The TCE concentrations of

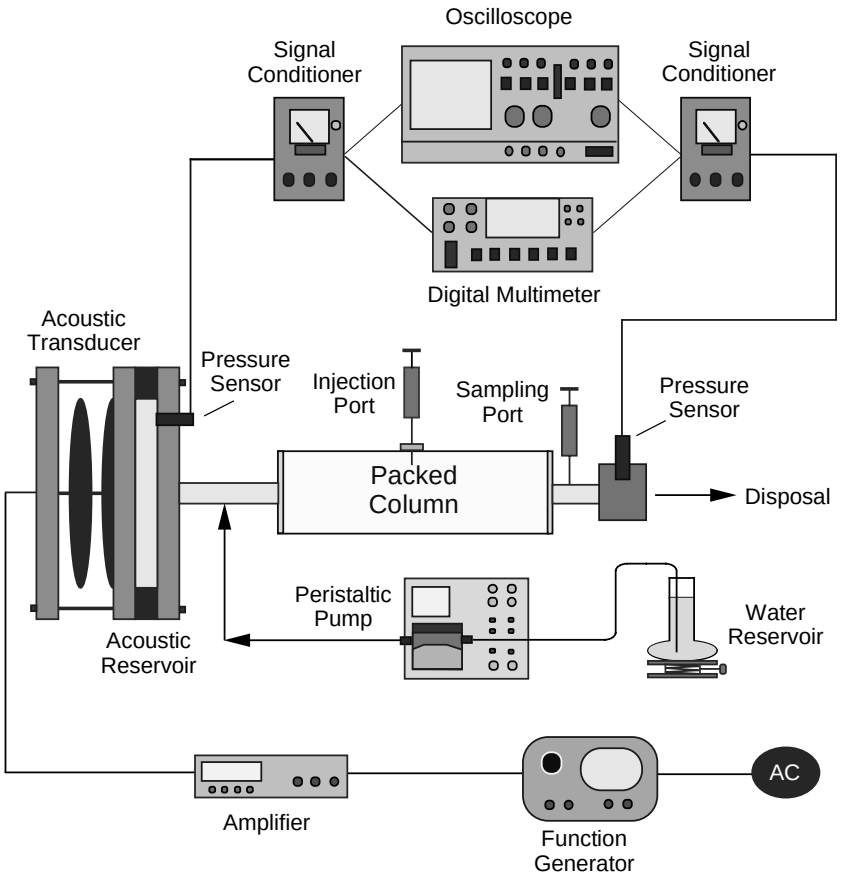

Figure 4.3: Dissolution experiment schematic.

the liquid samples were determined using a Hewlett Packard 5890 Series II gas chromatograph with an electron caption detector.

DNAPL dissolution experiments were initiated by injecting 0.05 mL of TCE (Fisher Scientific, Pennsylvania) dyed red with oil red EGN (Aldrich Chemical Co., Wisconsin) into a side injection port in the middle of the packed column and allowed to equilibrate to flow conditions within the packed column. Preliminary TCE dissolution experiments, in the absence of acoustic waves (base case) suggested that 5 pore volumes are sufficient to achieve a relatively steady effluent concentration. Moreover, it was observed that the effluent concentration remained relatively constant for over 30 pore volumes, greatly exceeding the time scale of the experiments performed in

this study. To assess the effect of acoustic waves on NAPL dissolution, a range of acoustic frequencies and amplitudes were applied at 60 minute intervals following a 120 minute period of flow without acoustic pressure.

4.3 Results and Discussion

Dissolution experiments were conducted with acoustic wave frequencies ranging from 0 (base case) to 285 Hz using a constant acoustic source fluid pressure amplitude of p_s=812 Pa. Two columns packed with 1 and 2 mm beads, respectively, were employed. Experiments were also conducted using a constant acoustic wave frequency of ϕ=245 Hz with acoustic source fluid pressures ranging from 0 (base case) to 1,625 Pa. A set of experimental data for the 2 mm bead column packing with p_s=812 Pa at ϕ=225 Hz are presented in Figure 4.4. The dissolved TCE effluent concentration is observed to increase significantly during the engagement of acoustic waves, as shown in the shaded area of Figure 4.4. It should also be noted that the effluent concentration returns to the original base case value after the acoustic pressure is discontinued. The enhanced dissolution observed is attributed to small scale displacement oscillations. These oscillations are responsible for an oscillatory pore water velocity that is sufficient to change the pore scale concentration gradient over the individual TCE-water interfacial areas.

A second acoustic wave mechanism that could have contributed to the enhancement of dissolved TCE effluent concentrations may be a physical change in the injected TCE blob configuration, which is observed in previous vibration studies [*Reddi et al.*, 1998]. This change in DNAPL blob configuration is referred to as the snap–off mechanism which causes DNAPL blobs to snap–off in individual pore bodies and consequently leads to increased DNAPL–water interfacial areas [*Chatzis et al.*, 1983; *Mohanty et al.*, 1987; *Morrow et al.*, 1988]. However, effluent concentrations are observed to return to base case values as soon as acoustic pressures were discontinued

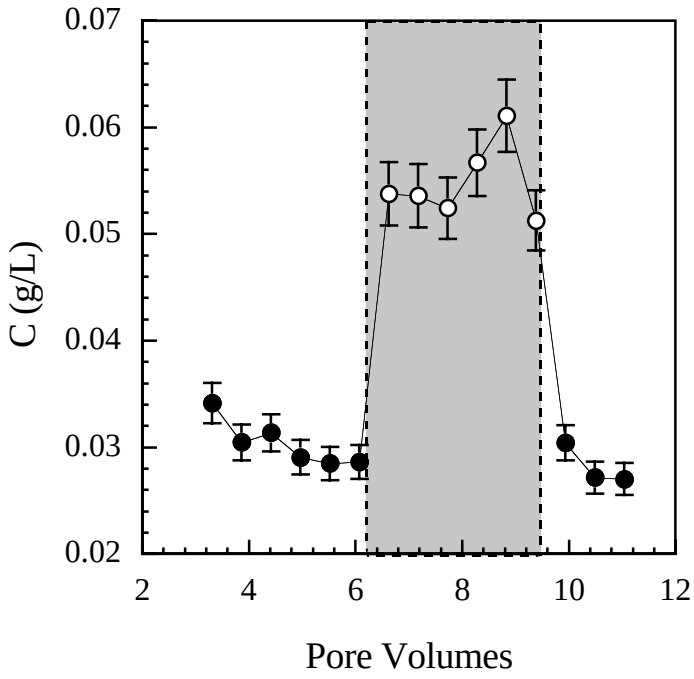

Figure 4.4: Effluent dissolved TCE concentrations from a column packed with 2 mm beads in the presence (shaded area) and absence of acoustic waves (here ϕ=225 Hz, p_s=812 Pa). Closed circles represent the base case (no acoustic pressure) and open circles in the grey shaded region represent portions of the experiment where acoustic waves are present. The bars indicate experimental error.

(see Figure 4.4). Therefore, snap–off doesn't occur during the experiments conducted in this study, and it can not be responsible for the observed increase in effluent concentrations due to the addition of acoustic waves.

In order to clearly present in a single plot the results from the various TCE dissolution experiments conducted in this study, the experimental data are expressed as the average percent change in effluent concentration

$$\Delta C = \frac{\overline{C}_{\mathrm{a}} - \overline{C}_{\mathrm{b}}}{\overline{C}_{\mathrm{b}}}, \tag{4.43}$$

where $\overline{C}_{\mathrm{a}}$ is the average of the effluent concentrations determined for the last 3 samples (1.66 pore volumes) collected in the presence of acoustic waves from each TCE dissolution experiment, and $\overline{C}_{\mathrm{b}}$ is the average of the last 3 samples collected in the absence of acoustic waves. The complete set of the experimental data collected are shown in Figure 4.5a. Note that each symbol in Figure 4.5a represents a different

TCE dissolution experiment. The greatest observed change in effluent dissolved TCE concentration due to the addition of acoustic waves is ΔC=120 and 96% for the 1 and 2 mm bead column packings, respectively, and occurs at ϕ=225 Hz. Another major ΔC peak occurs at ϕ=161 Hz. The cause of the observed ΔC peaks may be attributed to different pressures within the packed column. Although a constant acoustic source fluid pressure of p_s=812 Pa is employed here, as shown in Figure 4.5b, the effluent fluid pressures, p_e, are not constant for the different frequencies used. It should also be noted that ΔC is consistently greater for 1 mm beads than the 2 mm beads. This is attributed to greater TCE-water interfacial areas associated with the smaller bead size column packing.

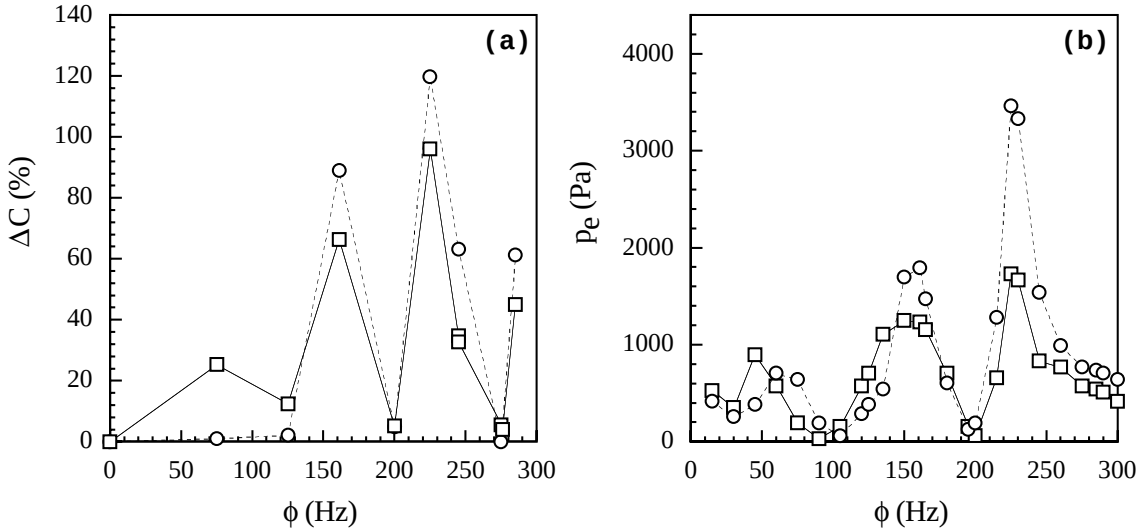

Figure 4.5: Effect of ϕ on (a) percent change in effluent dissolved TCE concentration, and (b) effluent fluid pressure (here p_s=812 Pa). Circles with dashed lines and squares with solid lines represent column packings of 1 and 2 mm beads, respectively.

Furthermore, comparison of Figures 4.5a and 4.5b shows that p_e follows the same trend as ΔC. The effluent fluid pressures are greater for the 1 mm bead than 2 mm bead column packing. A possible explanation for this is that smaller beads lead to better column packing. Furthermore, the observed p_e peaks for the different ϕ values employed with constant p_s may be caused by the presence of standing waves that can lead to location dependent acoustic pressure.

The effect of the acoustic source fluid pressure for a constant frequency of ϕ=245 Hz

on ΔC is shown in Figure 4.6, where the dotted and solid lines are the best linear fits for columns packed with 1 and 2 mm beads, respectively. Clearly, ΔC increases with increasing p_s. Furthermore, with the exception of the data collected at p_s= 1,625 Pa, ΔC is greater for the column packed with 1 mm beads than 2 mm beads. Note that two experiments were performed with the column packed with 2 mm beads at approximately p_s=800 Pa and the results were practically identical. This is an indication of the good experimental reproducibility.

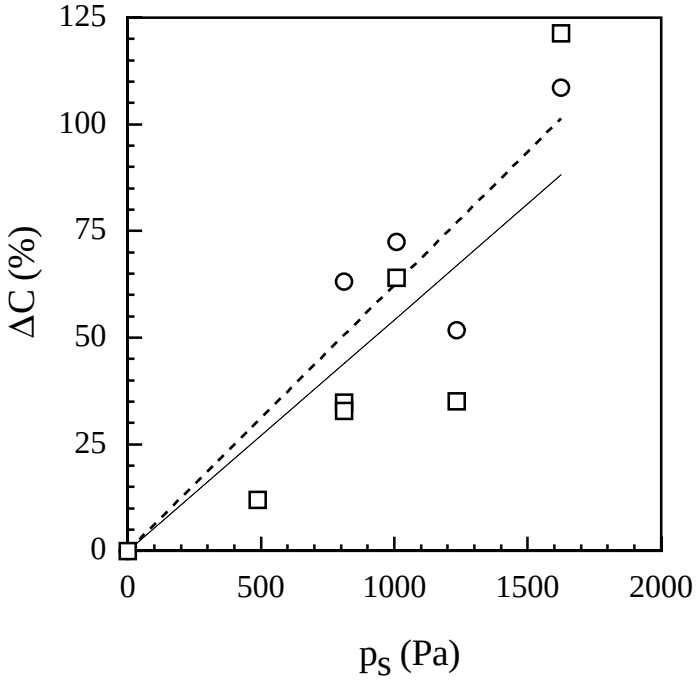

Figure 4.6: Percent change in effluent dissolved TCE concentration as a function of p_s (here ϕ=245 Hz). Circles with best fit dashed lines and squares with solid best fit lines represent column packings of 1 and 2 mm beads, respectively.

Figure 4.7 illustrates the effect of ϕ and p_s expressed as Re_a on ΔC. The dotted and solid lines correspond to the best linear fits for columns packed with 1 and 2 mm beads, respectively. Clearly, the results suggest that the TCE dissolution rate is proportional to Re_a or equivalently to the acoustically induced oscillatory pore water velocity. This is in agreement with previous studies suggesting that NAPL dissolution rates depend on the interstitial pore water velocity [*Powers et al.*, 1994; *Zhou et al.*, 2000; *Chrysikopoulos*, 1995; *Vogler and Chrysikopoulos*, 2001; *Bao et al.*, 2003].

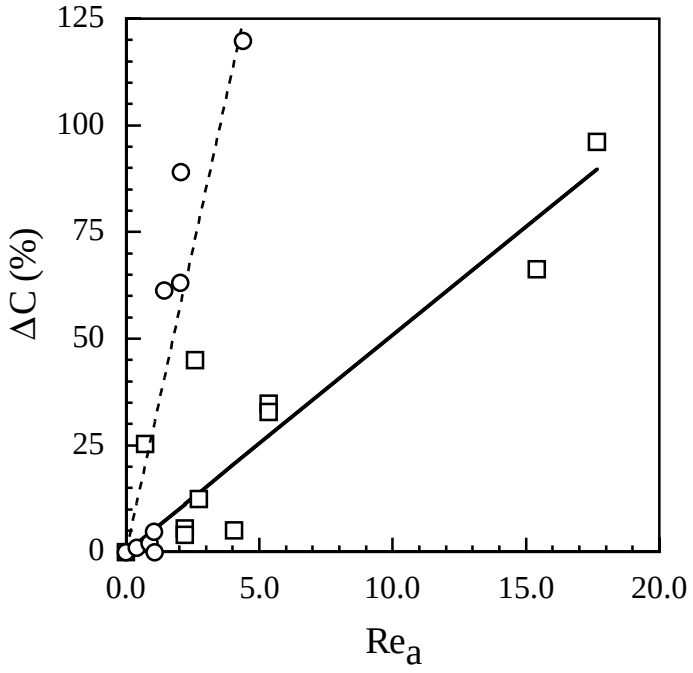

Figure 4.7: Percent change in effluent concentration as a function of Re_a. Circles with best fit dashed lines and squares with solid best fit lines represent column packings of 1 and 2 mm beads, respectively.

4.4 Summary

The effect of acoustic pressure waves on TCE ganglia dissolution in a water saturated column packed with glass beads is examined theoretically and experimentally. A mathematical model is developed to determine the acoustically induced pore fluid displacement relative to the solid matrix displacement. The acoustic Reynolds number is observed to decrease with increasing x, reach an asymptotic value with increasing ϕ, and increase linearly with increasing p_s. The experimental TCE dissolution data show that the oscillatory pore water velocity caused by the acoustic pressure waves leads to over a 100% increase in the effluent dissolved TCE concentrations. The increase in effluent concentrations is found to be proportional to the applied acoustic source pressure. In addition, although Re_a values are found to be greater for the column packed with larger beads, acoustically enhanced TCE dissolution is found to be greater in the column packed with smaller glass beads. This is due to greater TCE-water interfacial areas associated with smaller bead size column packings. The

results of this study indicate that the use of acoustic pressure waves, complementing traditional pump–and–treat methodology, may be a viable method to decrease remediation times and costs for DNAPL contaminated aquifers.

Chapter 5

ACOUSTICALLY ENHANCED MULTICOMPONENT NAPL GANGLIA DISSOLUTION

5.1 Theory

5.1.1 Multicomponent NAPL Dissolution

The aqueous phase concentration of each dissolving component of a NAPL mixture is dependent on the equilibrium aqueous solubility of the individual component. The equilibrium aqueous solubility, C_p^w [M/L^3], of component p is defined as [*Broholm and Feenstra*, 1995]:

$$C_p^w(t) = C_{s_p}\ X_p(t)\ \gamma_p(X_p) \tag{5.1}$$

where C_s is the pure component saturation concentration (solubility) [M/L^3]; X_p is the dimensionless mole fraction of component p in the nonaqueous phase [-]; and γ_p is the dimensionless activity coefficient of component p in the nonaqueous phase [-]. The activity coefficient is a correction term indicating the nonideality of a solution [*Schwarzenbach et al.*, 1993]. The higher the deviation of activity coefficients from

unity, the greater the degree of nonideality of a solution. For a NAPL mixture containing components of similar structure the nonaqueous phase activity coefficients can be approximated equal to one ($\gamma_p \simeq 1$). For the special case of an ideal solution $\gamma_p = 1$ and equation (5.1) reduces to Raoult's law [*Banerjee*, 1984]:

$$C_p^w(t) = C_{s_p} X_p(t). \tag{5.2}$$

The nonaqueous phase activity coefficient of nonideal liquid mixtures can be estimated using the UNIFAC (UNI-Functional group Activity Coefficients) method. UNIFAC was initially developed by *Fredenslund et al.* [1975] for chemical engineering applications associated with activity coefficient estimations in organic mixtures where limited or no experimental data are available and has since been improved several times [*Fredenslund et al.*, 1977; *Skjold-Jørgensen et al.*, 1979; *Gmehling et al.*, 1982; *Macedo et al.*, 1983; *Tiegs et al.*, 1987; *Hansen et al.*, 1991]. UNIFAC is based on the solution of groups concept, which does not consider a liquid mixture as a solution of molecules, but as a solution of groups (e.g., methylene, nitro, keto, amino, carboxyl). The advantage of this method is that the activity coefficients can be estimated for practically any organic molecule provided that the molecule consists of structural groups for which parameters are available.

5.1.2 Acoustic Pressure Waves in Porous Media

Acoustic waves travel in porous media by the propagation of small scale dilatations of the porous matrix. Acoustic pressure waves in porous media are considered elastic waves because the resulting strain on the solid matrix is reversible within the elastic limit of the porous medium. An elastic wave in water saturated porous media consists of a fast wave where the interstitial fluid and porous matrix move in phase and a slow wave where the interstitial fluid and porous matrix move out of phase. It should be noted that oscillatory flow of the interstitial fluid with respect to the porous medium occurs because the interstitial fluid and the porous matrix are moving out of phase in a slow wave [*Biot*, 1956a]. It has been reported in the literature that the friction

factor between the interstitial fluid and pore walls increases with increasing frequency of the elastic wave [*Biot*, 1956b]; the effective viscosity of the interstitial fluid increases with increasing acoustic frequency [*Qian*, 1998]; the permeability of a porous medium decreases with increasing elastic wave frequency [*Zhou and Sheng*, 1989]; and that vibration of porous media can mobilize NAPL ganglia [*Reddi and Wu*, 1996; *Reddi et al.*, 1998].

Based on the work by *de Boer et al.* [1993] on acoustic wave propagation through one-dimensional, semi-infinite, water saturated, incompressible porous media, assuming that there is no initial displacement or velocity for the interstitial fluid and solid matrix, the appropriate mathematical expressions describing the solid and fluid displacement caused by an acoustic pressure source can be derived as follows:

$$\xi_s(x,t) = \frac{(\theta-1)}{\Omega_1^{1/2}(\lambda+2\mu)} \int_0^t \Phi(\tau)\mathrm{d}\tau, \tag{5.3}$$

$$\xi_f(x,t) = \frac{(1-\theta)^2}{\Omega_1^{1/2}\theta(\lambda+2\mu)} \int_0^t \Phi(\tau)\mathrm{d}\tau, \tag{5.4}$$

where

$$\Phi(\tau) = f(t-\tau)\exp\Big[-\frac{\Omega_2}{2\Omega_1}\tau\Big]\mathrm{I}_0\Big[\frac{\Omega_2(\tau^2-\Omega_1 x^2)^{1/2}}{2\Omega_1}\Big]\mathrm{H}(\tau-\Omega_1^{1/2}x), \tag{5.5}$$

$$\Omega_1 = \frac{(1-\theta)^2\rho_f + \theta^2\rho_s}{(\lambda+2\mu)\theta^2}, \tag{5.6}$$

$$\Omega_2 = \frac{S}{(\lambda+2\mu)\theta^2}, \tag{5.7}$$

where ξ_s is the solid displacement [L]; ξ_f is the fluid displacement [L]; x is the spatial coordinate in the direction of flow [L]; θ is the porosity of the porous medium (liquid volume/porous medium volume) [$\mathrm{L}^3/\mathrm{L}^3$]; t is time [t]; $\rho_s = (1-\theta)\rho_{\mathrm{solid}}$ is the solid bulk density (where ρ_{solid} is the solid density) [M/L^3]; $\rho_f = \theta\rho_{\mathrm{H_2O}}$ is the fluid bulk density (where $\rho_{\mathrm{H_2O}}$ is the water density) [M/L^3]; $S = \theta^2\gamma/K$ is a function that relates the extra stress due to the relative movement between the solid matrix and interstitial fluid [L/t] (where γ is the specific weight of the fluid [F/L^3]; and K is the hydraulic conductivity of the porous medium [L/t]) [*de Boer and Ehlers*, 1990]; μ [F/L^2] and λ [F/L^2] are the solid matrix Lamé constants, representing the shear

modulus and the bulk modulus less 2/3 of the shear modulus, respectively; I_0 is the modified Bessel function of zero order; H is the unit step function or Heaviside function; and $f(t) = f(t+T)$ is a periodic, time dependent acoustic pressure source function [F/L^2] (where T is the period of oscillation [t]). Three different acoustic source function shapes are examined in the present study, the sinusoidal function defined as:

$$f(t) = p_s \sin(2\pi\phi t), \tag{5.8}$$

the triangular function expressed as:

$$f(t) = \begin{cases} p_s \left(\dfrac{2\phi t}{\pi}\right) & 0 \le t \le \dfrac{\pi}{2\phi}, \\ p_s \left(2 - \dfrac{2\phi t}{\pi}\right) & \dfrac{\pi}{2\phi} \le t \le \dfrac{3\pi}{2\phi}, \\ p_s \left(\dfrac{2\phi t}{\pi} - 4\right) & \dfrac{3\pi}{2\phi} \le t \le \dfrac{2\pi}{\phi}, \end{cases} \tag{5.9}$$

and the square function given by:

$$f(t) = \begin{cases} p_s & 0 \le t \le \dfrac{\pi}{\phi}, \\ -p_s & \dfrac{\pi}{\phi} \le t \le \dfrac{2\pi}{\phi}, \end{cases} \tag{5.10}$$

where p_s is the acoustic source fluid pressure [F/L^2]; and ϕ is the acoustic wave frequency [1/t]. The period for all three acoustic source function shapes is set to $T = 2\pi/\phi$.

The fluid displacement relative to the solid displacement may be evaluated by the following expression

$$\xi_r(x,t) = \xi_f(x,t) - \xi_s(x,t). \tag{5.11}$$

Differentiating ξ_r [L] with respect to time yields the time and space dependent relative fluid velocity

$$U_r(x,t) = \frac{\mathrm{d}\xi_r(x,t)}{\mathrm{d}t}. \tag{5.12}$$

Clearly, U_r [L/t] is oscillatory and depends on the acoustic pressure and frequency of the acoustic source. It should be noted that in this study the experimental aqueous

phase NAPL concentrations collected at various acoustic pressures are easily compared as a function of the dimensionless acoustic Reynolds number, Re_a [-], defined as [*Ha and Yavuzkurt*, 1993]

$$Re_a = \frac{U_{r_a} d}{\eta}, \tag{5.13}$$

where U_{r_a} [L/t] is the maximum value or amplitude of the oscillatory interstitial pore water velocity over one period of oscillation ($1/\phi$); d is the mean grain diameter of the porous medium [L]; and η is the kinematic fluid viscosity [L^2/t].

5.2 Materials and Methods

Multicomponent NAPL dissolution experiments were conducted in a 30 cm long glass laboratory column with a 2.5 cm inner diameter (Kimble Kontes, New Jersey). The column was packed with 1 mm diameter soda lime glass beads with density 2.33 g/cm^3 (Fisher Scientific, Pennsylvania). The beads were retained in the column using teflon screens and end caps on both the influent and effluent sides of the column. The teflon column end caps were milled to accommodate 1/4 inch stainless steel fittings (Swageloc) for 3/8 inch semi-rigid plastic tubing (Fisher Scientific, Pennsylvania). Constant flow of degassed Millipore water at a rate of $Q = 3.25$ mL/min was maintained through the packed column with a microprocessor pump drive (Cole Palmer Instrument Co., Illinois). Acoustic pressure was introduced into the column using a custom designed acoustic cell attached to a pressure transducer (TST37; Clark Sythesis, Colorado). The frequency of the acoustic pressure oscillation was controlled by a frequency generator (LG Precision, California). Acoustic pressure levels were controlled by an amplifier (Lab Gruppen, Sweden) and measured using PCB106b pressure sensors (PCB Piezotronics, Inc., New York). One pressure sensor was installed in the acoustic cell to measure the acoustic source pressure. Another sensor was placed in the effluent line, just after the packed column, to measure the effluent pressure as close to the packed column as possible. Pressure sensor measurements were made using a signal conditioner (PCB Piezotronics, Inc., New York) in addition

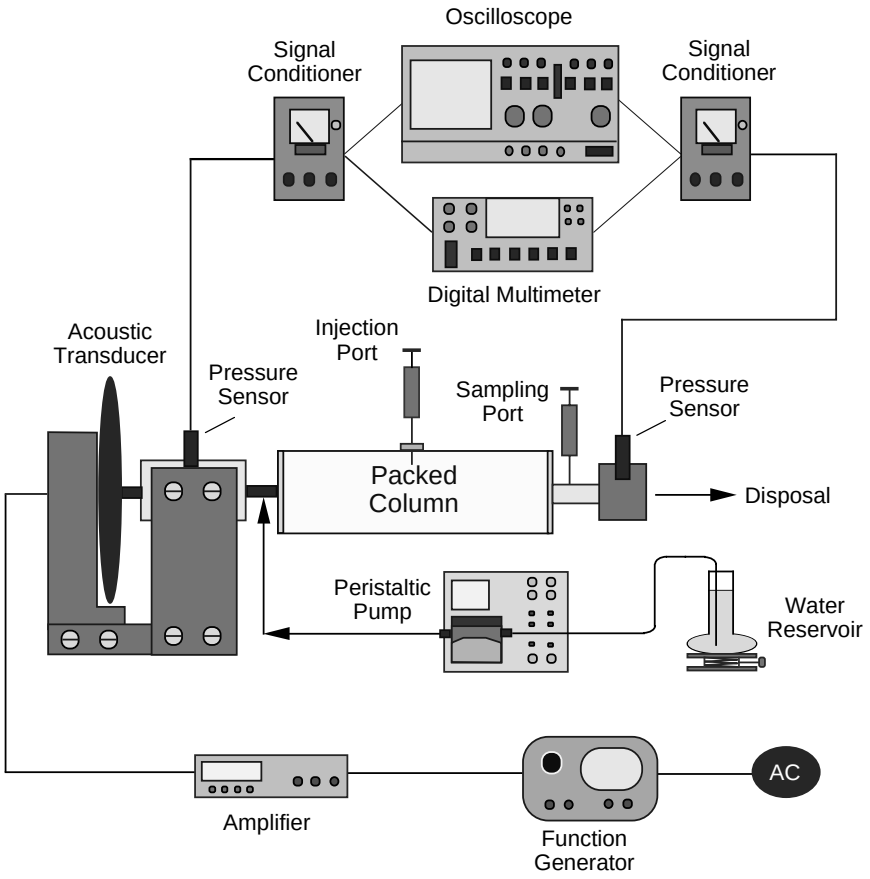

Figure 5.1: Schematic illustration of the experimental setup.

to a digital multimeter (Metex, Korea) and an oscilloscope (EZ Digital Co., Ltd, Korea). A schematic illustration of the experimental apparatus used in this study is shown in Figure 5.1.

Effluent samples (0.15 mL) were collected from a dedicated needle within the effluent tube (sample port) at regular 10 minute intervals using disposable 1.0 mL tuberculin plastic syringes (Becton Dickinson & Co., New Jersey). The samples were immediately introduced into 2 mL vials (Kimble Glass, New Jersey) containing a known volume of n-pentane (Fisher Scientific, Pennsylvania). The aqueous phase NAPL concentrations of the liquid samples were determined using a Hewlett Packard 5890 Series II gas chromatograph with an electron caption detector.

Multicomponent DNAPL dissolution experiments were initiated by injecting 0.05 mL of either Mixture A, a two-component mixture of TCE and 1,1,2-TCA, or Mixture B, a three-component mixture of TCE, 1,1,2-TCA, and PCE (Fisher Scientific, Pennsylvania) dyed with oil red EGN (Aldrich Chemical Co., Wisconsin) into a side injection port in the middle of the packed column. Subsequently, the multicomponent NAPL ganglia were allowed to equilibrate to flow conditions within the packed column. The exact composition and properties of the two NAPL mixtures employed in this study are listed in Table 5.1. To assess the effect of acoustic waves on multicomponent NAPL dissolution, a range of acoustic frequencies and amplitudes were used. Furthermore, the effects of acoustic wave source function shape (sinusoidal, triangular, and square wave) on NAPL dissolution were also investigated.

5.3 Results and Discussion

The observed effluent dissolved concentrations from the dissolution experiments conducted with NAPL mixtures A and B in the water saturated column packed with 1 mm glass beads are presented in Figure 5.2 together with the corresponding experimental error indicated by the error bars. The shaded areas represent the duration of sinusoidal acoustic pressure wave application with acoustic source fluid pressure $p_s = 15.2$ kPa and acoustic wave frequency $\phi = 275$ Hz. The experimental data indicate that in the presence of acoustic pressure waves the effluent concentrations are increased considerably for both of the NAPL mixtures considered. The increase in effluent concentrations is attributed to the presence of an oscillatory pore water velocity caused by acoustic pressure waves. It should be noted that for mixture A (Figure 5.2a) the effluent aqueous phase 1,1,2-TCA concentrations are observed to be consistently greater than the TCE concentrations during the duration of the dissolution experiment with and without the presence of the acoustic pressure waves. Similarly, for mixture B (Figure 5.2b) the effluent aqueous phase 1,1,2-TCA concentrations before and during the application of acoustic waves are greater than the TCE

concentrations and PCE concentrations are the lowest. In view of the properties listed in Table 5.1, the intuitive result is concluded that the effluent concentration level of each component is directly proportional to its pure component saturation concentration (solubility limit). Furthermore, it should be noted that as soon as the acoustic pressure waves are no longer present, the effluent concentration of each dissolved NAPL component drops to a lower level than that observed prior to the application of acoustic waves. Consequently, the observed NAPL dissolution enhancement is mainly attributed to the oscillatory pore water velocity caused by the acoustic pressure waves. Therefore, for the experimental conditions of this study, the possibility of acoustic waves increasing the ganglia surface area can be eliminated.

Table 5.1: Composition and Relevant Properties of Multicomponent NAPL Mixtures

Component	Mol wt	$C_s^{\dagger}$ (g/mole)	Density† (mg/L)	Initial X (g/cm^3)	Initial $\gamma^{\ddagger}$	Final X	Final $\gamma^{\ddagger}$
Mixture A							
TCE	131.4	1,100	1.46	0.516	1.225	0.719	1.096
1,1,2-TCA	133.4	4,400	1.44	0.484	1.124	0.281	1.354
Mixture B							
TCE	131.4	1,100	1.46	0.337	1.091	0.323	0.994
1,1,2-TCA	133.4	4,400	1.44	0.318	1.359	0.060	2.467
PCE	165.8	150	1.62	0.345	1.176	0.617	1.012

† From *Mackay et al.* [1992]
‡ Estimated by UNIFAC

Based on the effluent concentrations collected for each ganglia dissolution experiment conducted in this study under a constant volumetric flow rate through the packed column of $Q = 3.25$ mL/min, the mass of each component progressively dissolving in the aqueous phase can be estimated. For known initial masses and compositions of the multicomponent NAPL mixtures A and B, the mole fractions, X, as a function of time are determined. Subsequently, the time dependent activity coefficient, γ, of each component is estimated using UNIFAC and the corresponding equilibrium aqueous solubility, C^w, is evaluated from expression (5.1). Figure 5.3 illustrates the behavior

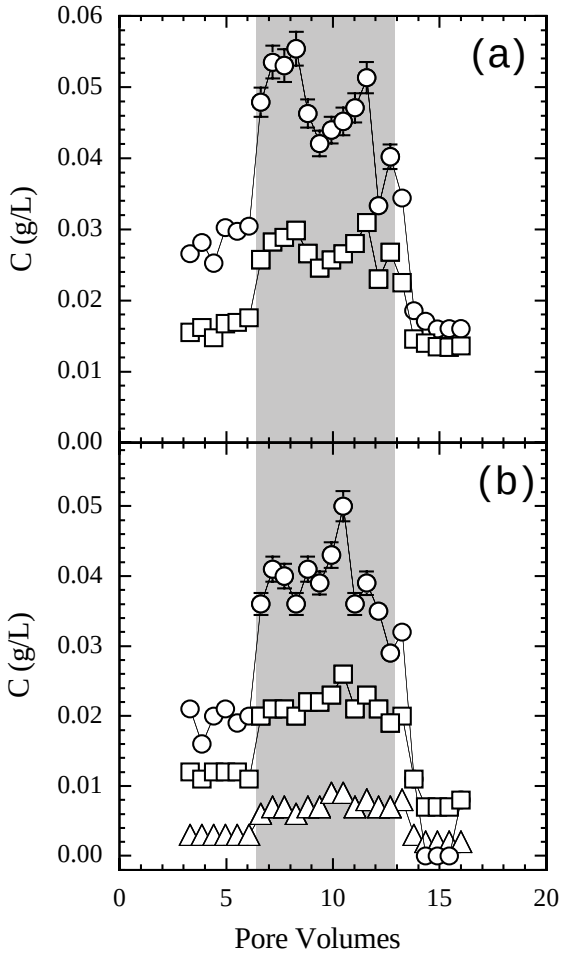

Figure 5.2: Effluent dissolved concentrations for multicomponent NAPL (a) mixture A consisiting of TCE (squares) and 1,1,2-TCA (circles), and (b) NAPL mixture B consisting of TCE (squares), 1,1,2-TCA (circles), and PCE (triangles). The shaded areas indicate the duration of acoustic wave application (here ϕ=275 Hz and p_s=15.2 kPa for a sinusoidal acoustic wave). Error bars smaller than the symbols are not presented.

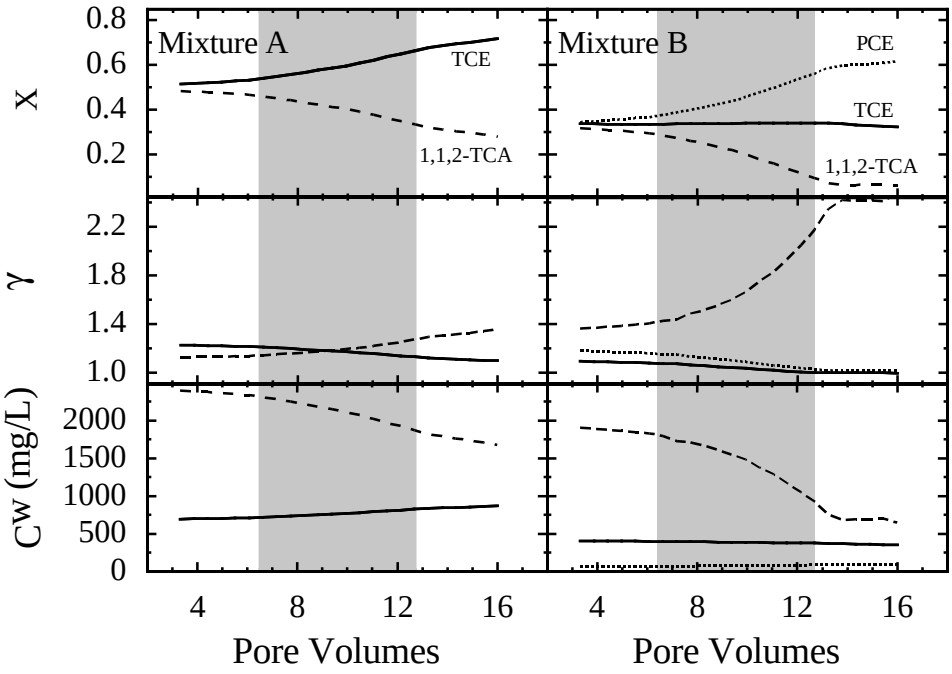

Figure 5.3: Estimated changes in mole fraction, activity coefficient and equilibrium aqueous solubility as a function of pore volumes for each of the components of ganglia mixtures A and B. The shaded areas indicate the duration of acoustic wave application. Solid, dashed, and dotted curves represent TCE, 1,1,2-TCA, and PCE, respectively (here ϕ=275 Hz and p_s=15.2 kPa for a sinusoidal acoustic wave).

of X, γ and C^w for a set of ganglia dissolution experiments with ganglia mixtures A and B. The shaded areas represent the time period where sinusoidal acoustic waves are applied to the packed column. Note that mixtures A and B cannot be considered ideal solutions because all γ's are consistently greater than one, and C^w values should be evaluated by equation (5.1). The greatest changes in X, γ and C^w are associated with the 1,1,2,-TCA component, that is the compound with the highest pure component saturation concentration, C_s (see Table 5.1). Furthermore, the rate of change of X, γ and C^w is shown to be more significant in the shaded pore volume intervals of Figure 5.3 where acoustic waves are present. For the experimental data presented in Figure 5.2, the initial and final compositions of mixtures A and B as well as the corresponding γ values are also calculated and listed in Table 5.1.

The experimental results from the various multicomponent ganglia dissolution exper-

iments conducted in this study with mixtures A and B can be presented in a single plot by expressing the experimental data as an average percent change in effluent concentration defined by

$$\Delta C = \frac{C_{\mathrm{a}} - C_{\mathrm{b}}}{C_{\mathrm{b}}}, \tag{5.14}$$

where C_{a} is the effluent concentration collected in the presence of acoustic waves; and C_{b} is the effluent concentration collected just prior to the application of acoustic waves. The complete set of the experimental data collected for mixture A (multicomponent ganglia consisting of TCE and 1,1,2-TCA), under a constant acoustic source pressure amplitude of 15.2 kPa and a sinusoidal shape function, at early and late stages of acoustic wave application are shown in Figures 5.4a and 5.4b, respectively. Note that the data for each frequency considered represents a different ganglia dissolution experiment. Comparison of Figures 5.4a and 5.4b in connection to the results of Figure 5.3 suggests that the effect of acoustic waves on ΔC is inversely proportional to C^w. Therefore, dissolution enhancement due to acoustic pressure waves is greatest for the NAPL component with the lowest equilibrium aqueous solubility (compare Figures 5.4a and 5.4b). Figure 5.4c presents the observed effluent fluid pressure, p_e [F/L^2], as a function of the acoustic wave frequency, ϕ. For different experiments p_e is not constant because it is significantly affected by the presence of standing waves and the resonant frequency of the packed column. However, comparison of Figures 5.4a, 5.4b and 5.4c indicates that ΔC is directly correlated to ϕ.

The observed ΔC at early and late stages of acoustic wave application and p_e as a function of ϕ for the various experiments conducted with mixture B (multicomponent ganglia consisting of TCE, 1,1,2-TCA and PCE), under a constant acoustic source pressure amplitude of 15.2 kPa and a sinusoidal shape function, are shown in Figures 5.5a, 5.5b and 5.5c, respectively. Similar to the results for mixture A, ΔC is directly proportional to p_e and the greatest dissolution enhancement is associated with the NAPL component having the smallest equilibrium aqueous solubility (compare Figures 5.5a and 5.5b). This is a significant result because components with very low equilibrium aqueous solubility are the most difficult components to remove from a

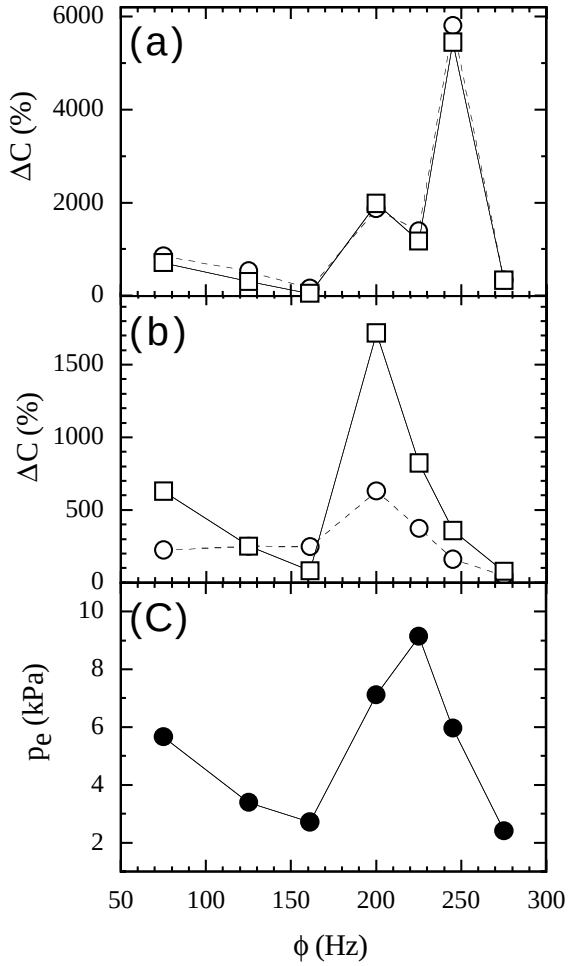

Figure 5.4: Percent change in effluent concentrations for the NAPL components present in mixture A at (a) early and (b) late times of acoustic wave application, and (c) effluent fluid pressure as a function of ϕ. Squares represent TCE and circles 1,1,2-TCA aqueous phase concentrations (here p_s=15.2 kPa for a sinusoidal acoustic wave).

contaminated aquifer with traditional remediation procedures.

In order to examine the combined effect of ϕ and p_s on NAPL ganglia dissolution, the observed percent changes in effluent concentrations, ΔC, at early and late stages of acoustic wave application as a function of Re_a are presented in Figure 5.6a and 5.6b for mixture A, and in Figure 5.6c and 5.6d for mixture B, respectively. The squares, circles and triangles correspond to TCE, 1,1,2-TCA and PCE, respectively. Furthermore, the solid, dashed and dotted lines correspond to the best linear fits of the ΔC values for TCE, 1,1,2-TCA and PCE, respectively. The Re_a values are evaluated using expression (5.13), where the parameter U_{r_a} is obtained by numerical approximation of the derivative $\mathrm{d}\xi_r(x,t)/\mathrm{d}t$ followed by determination of its maximum value over a period of acoustic wave oscillation, $1/\phi$. The term $\xi_r(x,t)$ is evaluated from equation (5.11) with $\xi_s(x,t)$ and $\xi_f(x,t)$ provided by the theoretical expressions (5.3) and (5.4), respectively. The integrals in equations (5.3) and (5.4) are evaluated numerically using IMSL subroutine *dqdag* (IMSL, 1991). All parameter values necessary for the evaluation of Re_a are listed in Table 5.3. Clearly, for mixture A, Figures 5.6a and 5.6b indicate that ΔC for both TCE and 1,1,2-TCA increases with increasing Re_a. Furthermore, the greatest ΔC increase with increasing Re_a (slope of fitted ΔC values) at the end of acoustic wave application corresponds to TCE, the component with the smallest equilibrium aqueous solubility (see Figure 5.3). Similarly, for mixture B, Figures 5.6c and 5.6d suggest that the dissolution rate of each component is proportional to Re_a or proportional to the acoustically induced oscillatory pore water velocity, and that the highest dissolution rate at the end of acoustic wave application is associated with PCE, the component with the smallest equilibrium aqueous solubility (see Figure 5.3).

The effect of the acoustic source function shape on ganglia dissolution is examined by conducting experiments with sinusoidal, triangular, and square acoustic wave source function shapes. The three acoustic wave shapes employed are plotted in Figure 5.7 using mathematical expressions (5.8)-(5.10) for acoustic wave frequency $\phi = 1$ Hz, acoustic source fluid pressure $p_s = 1$ Pa and period of oscillation $T = 2\pi/\phi$. The

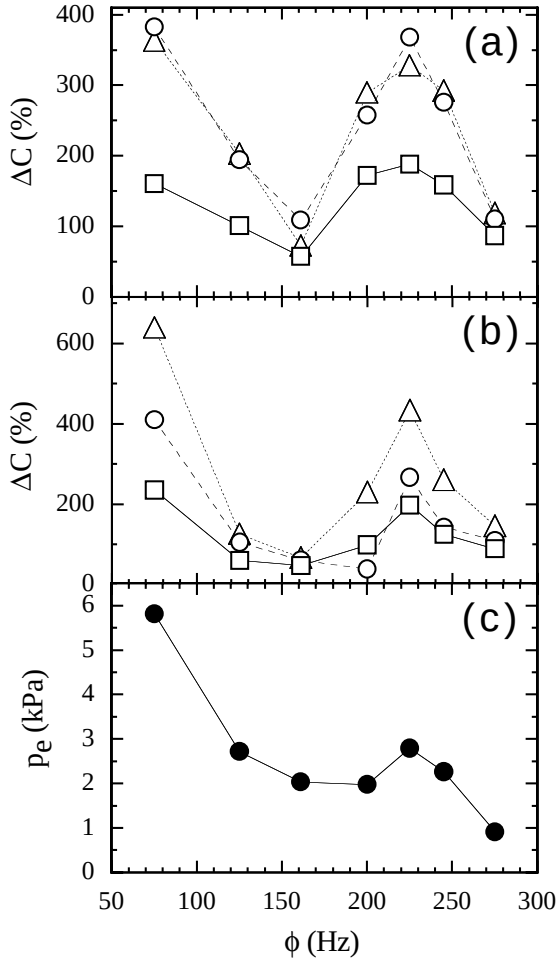

Figure 5.5: Percent change in effluent concentrations for the NAPL components present in mixture B at (a) early and (b) late times of acoustic wave application, and (c) effluent fluid pressure as a function of ϕ. Squares represent TCE, circles 1,1,2-TCA, and triangles PCE aqueous phase concentrations (here p_s=15.2 kPa for a sinusoidal acoustic wave).

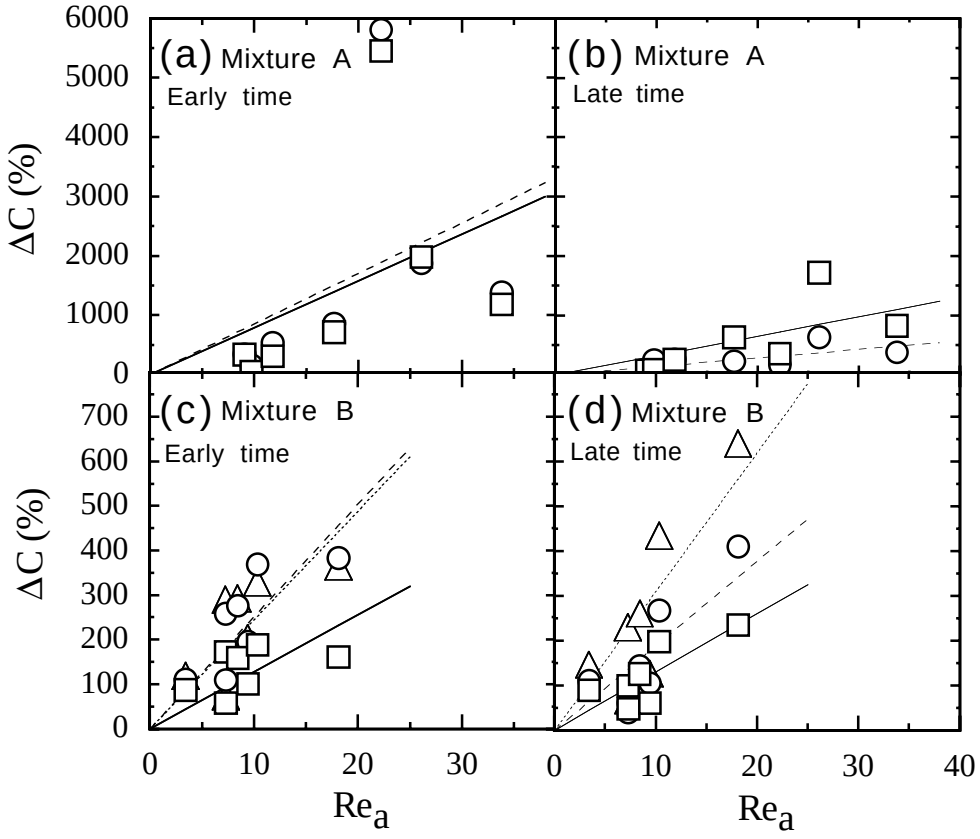

Figure 5.6: Percent change in effluent concentrations for the NAPL components present in mixture A at (a) early and (b) late times of acoustic wave application, and in mixture B at (c) early and (d) late times of acoustic wave application, respectively, as a function of Re_a. Squares with solid lines, circles with dashed lines, and triangles with dotted line correspond to the experimental data with least squares best-fit lines for TCE, 1,1,2-TCA, and PCE, respectively.

Table 5.2: Physical Properties of the Water Saturated Packed Column at 20 °C

Parameter	Value
d	1.0 mm
K	6.158×10^{-2} m/s
γ	1.0×10^5 N/m^3
η	1.0037×10^{-6} m^2/s
θ	0.40
$\lambda^\dagger$	5.5833×10^6 N/m^2
$\mu^\dagger$	8.375×10^6N/m^2
ρ_f	400.0 Kg/m^3
ρ_s	1398.0 Kg/m^3
ρ_{bead}	2330.0 Kg/m^3
ρ_{H_2O}	1000.0 Kg/m^3

† From *de Boer et al.* [1993]

observed p_e and ΔC for the dissolution experiments with mixture A are presented in Figure 5.8. The effluent fluid pressure for sinusoidal and triangular acoustic source function shapes are approximately equal, but substantially lower than the effluent fluid pressure for the square acoustic wave source function (see Figure 5.8a). The percent increase in the aqueous phase TCE and 1,1,2-TCA effluent concentrations is greatest in the presence of acoustic waves with square shape (see Figure 5.8b). The square shaped acoustic waves lead to greater effluent fluid pressure and dissolved NAPL concentrations due to their discontinuous and abrupt oscillation compared to the continuous and smooth oscillation of the sinusoidal and triangular acoustic waves.

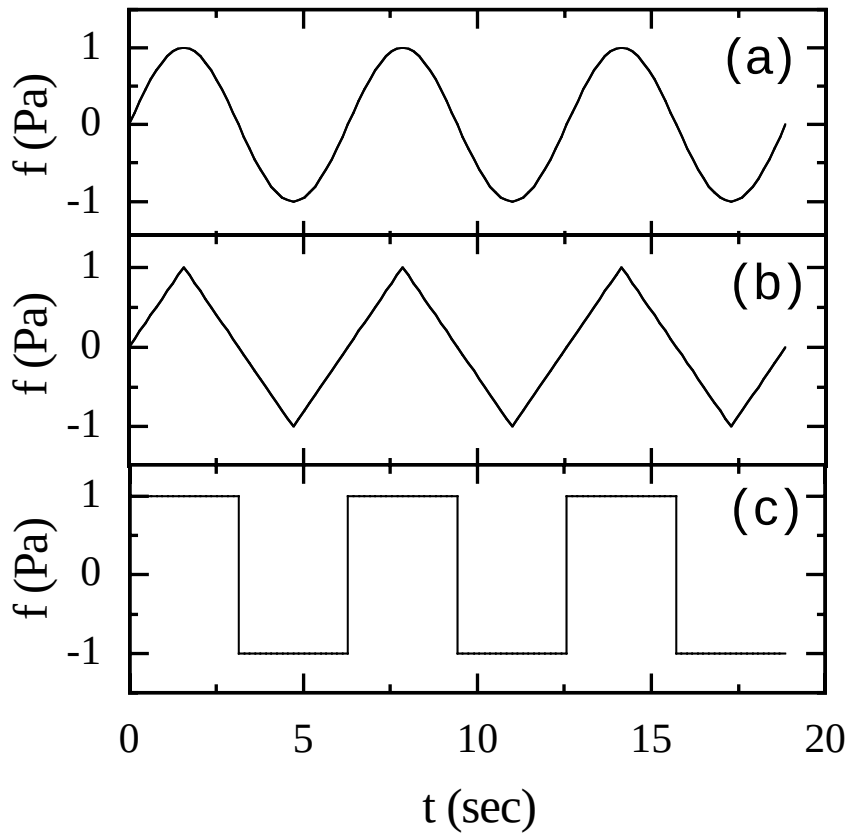

Figure 5.7: Illustration of (a) sinusoidal, (b) triangular, and (c) square acoustic wave source functions (here ϕ=1 Hz, p_s=1 Pa).

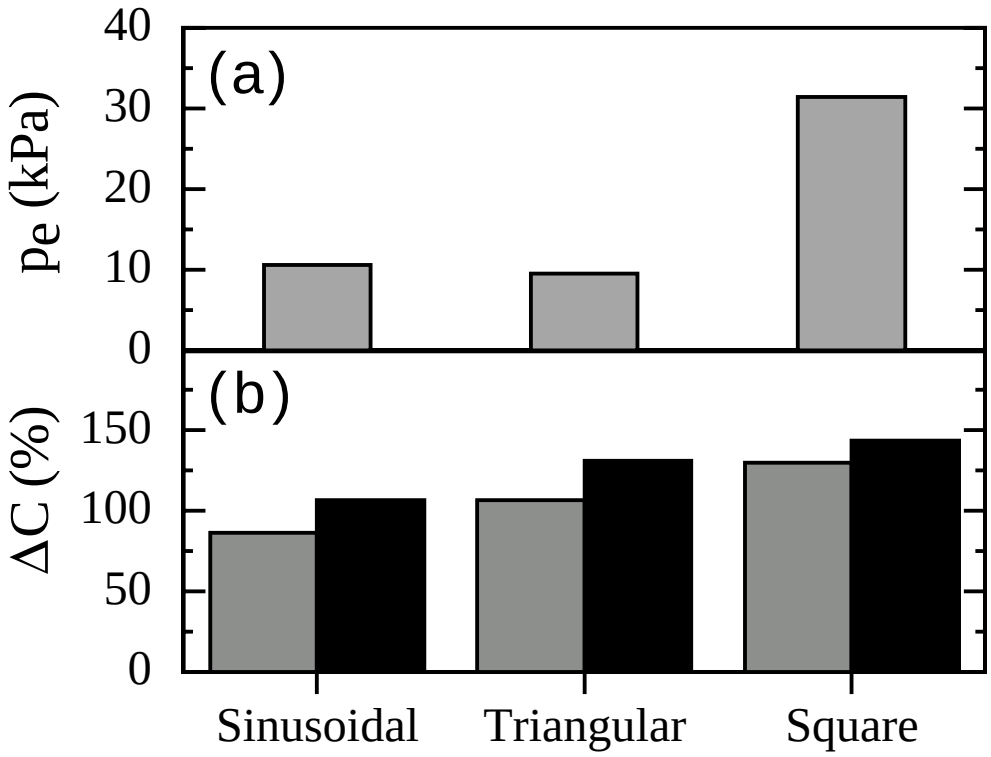

Figure 5.8: Effect of acoustic source function shape on (a) efluent fluid pressure, p_e, and (b) percent change in the effluent concentration, ΔC, of the components present in mixture A. Gray columns represent TCE, and black columns 1,1,2-TCA (here ϕ=245 Hz, p_s=15.2 kPa).

Chapter 6

PORE SCALE DNAPL DISSOLUTION and MOBILIZATION

6.1 Ganglia Dissolution Theory

NAPL ganglia dissolution is caused mainly by mass transfer across the NAPL-water interface. Assuming that the majority of NAPL ganglia interfaces are trapped at pore constrictions within a porous medium, the mass transfer across these interfaces may be described with the theory of a stagnant boundary layer in the aqueous phase [*Held and Celia*, 2001]. With the NAPL ganglia interfaces located at pore constrictions, a stagnant aqueous phase exists in the adjacent pore throats, where the pore throats act as conduits for dissolved aqueous phase DNAPL mass transport and fluid flow between pores. Imposing the aqueous equilibrium solubility constant at a NAPL-water interface, the mass flux through the stagnant aqueous phase layer may be expressed as [*Held and Celia*, 2001]

$$J_i = \frac{1}{A_i}\frac{\mathrm{d}m_i}{\mathrm{d}t} = k_i(C_s - C_i), \tag{6.1}$$

where J_i is the mass flux from each NAPL-water interface i; A_i is the interfacial area between the two fluid phases; m_i is the total mass of dissolved NAPL in the aqueous phase; k_i is the local first-order mass transfer coefficient; C_s is the equilibrium aqueous phase solubility of the DNAPL; and C_i is the aqueous phase concentration of the dissolved NAPL in an adjacent pore i. The local mass transfer coefficient is formulated from Fick's law as

$$k_i = \frac{\mathcal{D}}{l_i} \tag{6.2}$$

where D is the molecular diffusion coefficient in the aqueous phase; and l_i is the diffusion length of the stagnant aqueous phase. With respect to an elementary volume V of a porous medium, the macroscopic scale mass transfer can be derived from pore scale information as [*Held and Celia*, 2001]

$$\frac{1}{V}\sum_i [J_i A_i] = \frac{1}{V}\sum_i \left[\frac{\mathcal{D}}{l_i}(C_s - C_i)A_i\right] \equiv K_e(C_s - \overline{C}), \tag{6.3}$$

where K_e is the effective mass transfer rate coefficient; and $\overline{C}$ is the average concentration of an elementary volume.

6.1.1 Mobilization

The migration of NAPLs in porous media is a function of the NAPL source volume, NAPL and aqueous phase saturation, and gravity. For the case of light NAPLs (LNAPLs), like most petroleum hydrocarbons which are less dense than water, their downward migration reaches a terminus at the water table. If sufficient source volume exists, an LNAPL pool may form on the water table where its further movement will be controlled by its own hydraulic gradient and the relative saturations of both water and LNAPL at the water table and capillary fringe.

For denser than water nonaqueous phase liquids (DNAPLs), downward migration may not be terminated at the water table. If sufficient source volume exists, enough

DNAPL may accumulate on the water table until the air entry pressure is exceeded. Once this condition is met, the DNAPL will continue its migration downward through the saturated zone. This downward migration occurs as fingers or ganglia and will continue until the driving pressure gradient of the DNAPL ganglia is no longer sufficient to displace pore water. When this occurs, the DNAPL ganglia becomes immobile.

At the terminus of the DNAPL ganglia there exists a curved interface between the pore water and the DNAPL. This curved interface results in a pressure discontinuity between the two immiscible fluids. The difference between the pressure in the DNAPL (P_o) and the water (P_w) is defined as the capillary pressure (P_c):

$$P_c = P_o - P_w. \tag{6.4}$$

The magnitude of P_c depends on the interface curvature and may be described by the Laplace equation [*Bear*, 1972]:

$$P_c = \gamma_{ow}\left(\frac{1}{r_1} + \frac{1}{r_2}\right), \tag{6.5}$$

where γ_{ow} is the interfacial tension between the nonaqueous liquid and water, and r_1 and r_2 are the principle radii of curvature of the interface. There are several common simplifications to (6.5) for interfaces in capillary tubes and square ducts. However, for more complicated geometries, such as those contained in porous media, the capillary pressure may be represented as [*Scheidegger*, 1960; *Bear*, 1972]:

$$P_c = \frac{\gamma_{ow}\cos\beta}{r_H}, \tag{6.6}$$

where β is the contact angle of the solid-liquid-liquid interface and r_H is the hydraulic radius of the capillary which is equivalent to the ratio of void volume to surface area of the porous media. For the case of a porous medium composed of uniform diameter spherical particles, the hydraulic radius may be defined as [*Scheidegger*, 1960; *Dullien*, 1979]:

$$r_H = \frac{\theta d}{6(1-\theta)}, \tag{6.7}$$

where d is the mean particle diameter; and θ is the porosity of the porous medium.

For an immobile DNAPL ganglia to be mobilized, the capillary pressure must be met or exceeded. The conditions for mobilization have been summarized by *Dawson and Roberts* [1997] as:

$$\left(\rho_{\mathrm{H_2O}} g \frac{\mathrm{d}h_w}{\mathrm{d}z} + \Delta\rho g\right) \Delta L \geq \Delta P_c, \tag{6.8}$$

for downward displacement and

$$\frac{\mathrm{d}P_w}{\mathrm{d}x} \Delta L \geq \Delta P_c, \tag{6.9}$$

for horizontal displacement where h_w is the hydraulic head of water; $\Delta\rho$ is the difference in densities between the nonaqueous and water phase ($\Delta\rho = \rho_o - \rho_{\mathrm{H_2O}}$); g is the acceleration due to gravity; x and z denote horizontal and vertical coordinates, respectively; ΔL is the length of the DNAPL ganglia; and ΔP_c is the difference in capillary pressure between the advancing and receeding interfaces ($\Delta P_c = P_{c_1} - P_{c_2}$, where the subscripts 1 and 2 denote the advancing and receeding interfaces, respectively). In equations (6.8) and (6.9) ΔP_c represents the capillary pressure that must be overcome in order to mobilize a DNAPL ganglia [*Ng et al.*, 1977].

Generally, due to the difficulty in determining the necessary parameters for (6.8) and (6.9), especially when performing experiments where most of these parameters are difficult if not impossible to measure, mobilization criteria are presented by the dimensionless capillary number, Ca, and bond number, B. The bond number is the ratio of buoyant to capillary forces and is defined as:

$$B = \frac{\Delta\rho g (k/\theta)}{\gamma_{ow} \cos\beta}, \tag{6.10}$$

where k is the intrinsic permeability of the porous medium. For horizontal displacement, only the capillary number, which is the ratio of viscous to capillary forces, is required. The capillary number is defined as:

$$Ca = \frac{Uu}{\gamma_{ow} \cos\beta}, \tag{6.11}$$

where U is the average interstitial pore water velocity; and u is the dynamic water viscosity.

It has been shown that ganglia mobilization is highly dependent on Ca. For example, Hinkley et al. [1987] performed ganglia mobilization experiments in a monolayer of glass beads. They observed the that in a 45 degree square pack of soda lime glass beads ganglia mobilization only occurs after a fluid specific Ca, dependent on nonaqueous phase interfacial tension and contact angle, is exceeded; once in motion, the ganglia tend to align themselves with the overall flow direction and when confronted with a bifurcation they continue a regular zig-zag motion; and with increasing Ca bifurcation occurs and the ganglia begin to break up into many individual singlets. This formation of NAPL singlets is referred to as dynamic breakup [*Payatakes*, 1982].

6.2 Monolayer Design

To determine the effect of acoustic waves on DNAPL ganglia dissolution and mobilization, a two-dimensional monolayer of 3 mm diameter soda lime glass beads (Fisher Scientific, Pennsylvania) was employed. Although etched glass pore models or micromodels have been effectively used to study two–phase immiscible flow [*Lenormand and Zarcone*, 1984], a monolayer of glass beads is employed in this work to closer approximate the irregularities in fluid flow and DNAPL configuration in real porous media. Experience gained from previous studies with micromodels [*Chatzis*, 1982; *Buckley*, 1990; *Li and Yortsos*, 1995; *Jia et al.*, 1999] was utilized in the design of the monolayer used in the present study.

The monolayer of glass beads was constructed using a specially designed plexiglass acoustic retaining device or base with attached alluminum bars to suspend and attach the base to the acoustic source. A recess in the plexiglass retaining device allowed space for the glass beads and two glass plates to enclose them on top and bottom. The 1/4 inch borosilicate glass plates are surrounded by stainless steel retainers. The stainless steel retainers were used to keep the bottom glass plate and beads in place within the recess in the plexiglass base. It was also used to allow fluid and acoustic pressure to enter the monolayer on the influent and effluent side of the monolayer.

Another borosilicate glass plate is attached to the top of the beads and stainless steel retainers to enclose the device. Holes were drilled through the top glass at 45°, which can be used as NAPL ganglia injection ports. The injection ports are sealed with clear silicone sealant to make them water tight. The top glass plate is held in place by a plexiglass retainer with a cut out center to allow for the top glass plate. A 1/16 inch thick santoprene sheet was used between the plexiglass retainer, cut out around the top glass, and the monolayer base to make the monolayer water tight. Acoustic pressure is delivered to the monolayer by a diaphram attached to the acoustic source transducer.

Flow of degassed Millipore water was maintained through the monolayer with a microprocessor pump drive (Cole Palmer Instrument Co., Illinois). Acoustic source pressure was introduced into model using a pressure transducer (TST37; Clark Sythesis, Colorado). The frequency of acoustic pressure oscillation is controlled by a frequency generator (LG Precision, California). Acoustic pressure levels are controlled by an amplifier (Lab Gruppen, Sweden) and measured using two PCB106b pressure sensors (PCB Piezotronics, Inc., New York). The pressure sensors were installed within the monolayer on the influent and effluent side stainless steal bead and glass retainers. Pressure sensor measurements are made using a signal conditioner (PCB Piezotronics, Inc., New York) in addition to a digital multimeter (Metex, Korea) and oscilloscope (EZ Digital Co., Ltd, Korea). A complete schematic of the experimental apparatus is shown in Figure 6.1.

6.3 Acoustic Enhanced Dissolution

6.3.1 Experimental Procedures

DNAPL ganlia dissolution experiments were initiated by injecting 0.05 mL of tetrachloroethylene (PCE) (Fisher Scientific, Pennsylvania) dyed red with oil red EGN

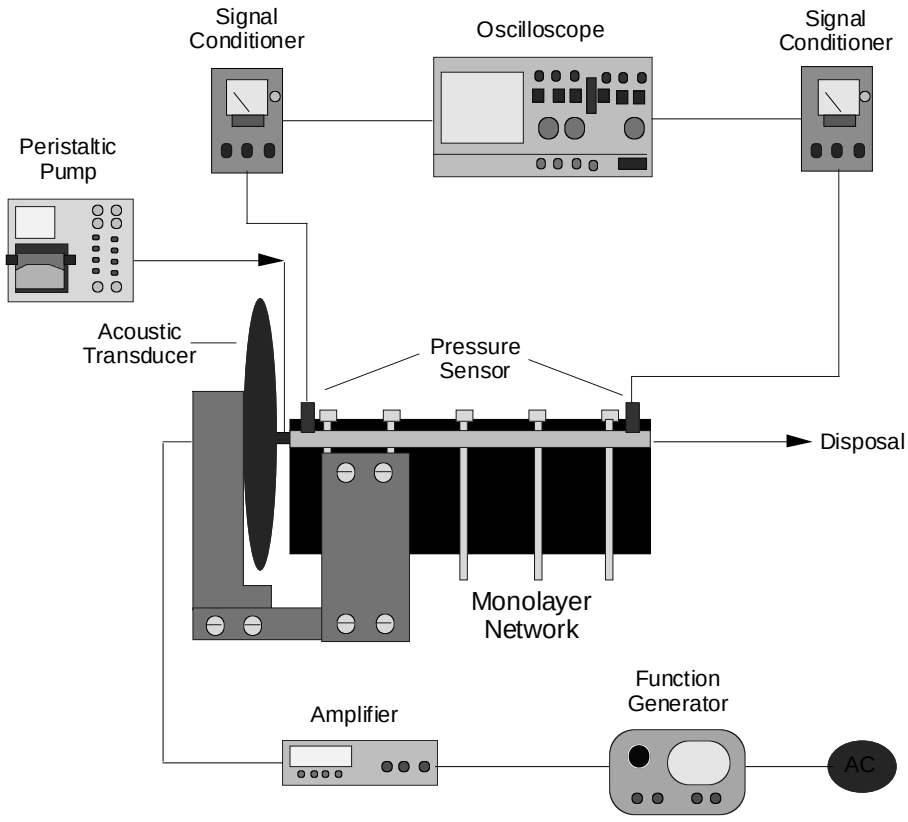

Figure 6.1: Monolayer experiment schematic.

(Aldrich Chemical Co., Wisconsin) into the center injection port in the top plate of the monolayer and allowed to equilibrate to flow conditions for a minumum of 20 pore volumes. To assess the effect of acoustic waves on PCE ganglia dissolution, a range of acoustic frequencies and background volumetric fluid flow rates were applied at intervals of 20 pore volumes following a 20 pore volume period of flow without acoustic pressure (base case).

For each DNAPL ganglia dissolution experiment effluent samples were collected at regular time intervals corresponding to 20 pore volumes. The samples were immediately introduced into 2 mL vials (Kimble Glass, New Jersey) containing a known volume of n-pentane (Fisher Scientific, Pennsylvania). The dissolved aqueous phase PCE concentrations of the liquid samples were determined using a Hewlett Packard 5890 Series II gas chromatograph with an electron caption detector.

6.3.2 Enhanced Dissolution Results

Effects of flow rate on the effluent concentration in the absence and presence of acoustic waves are shown in Figure 6.2a as open and closed circles, respectively. Each data point in Figure 6.2a represents an individual experiment and it is the average of 3 consecutive samples taken at approximately the same time, from the effluent stream. The error bars indicate the experimental error evaluated as the standard deviation of the averaged samples. The experimental data are also expressed as the average percent change in the effluent concentration (Figure 6.2b) in order to clearly present the results from the various PCE dissolution experiments conducted in this study in a single plot. The average percent change is defined as:

$$\Delta C = \frac{\overline{C}_{\mathrm{a}} - \overline{C}_{\mathrm{b}}}{\overline{C}_{\mathrm{b}}}, \tag{6.12}$$

where $\overline{C}_{\mathrm{a}}$ is the average effluent concentration collected in the presence of acoustic waves from each PCE dissolution experiment, and $\overline{C}_{\mathrm{b}}$ is the average effluent concentration collected in the absence of acoustic waves.

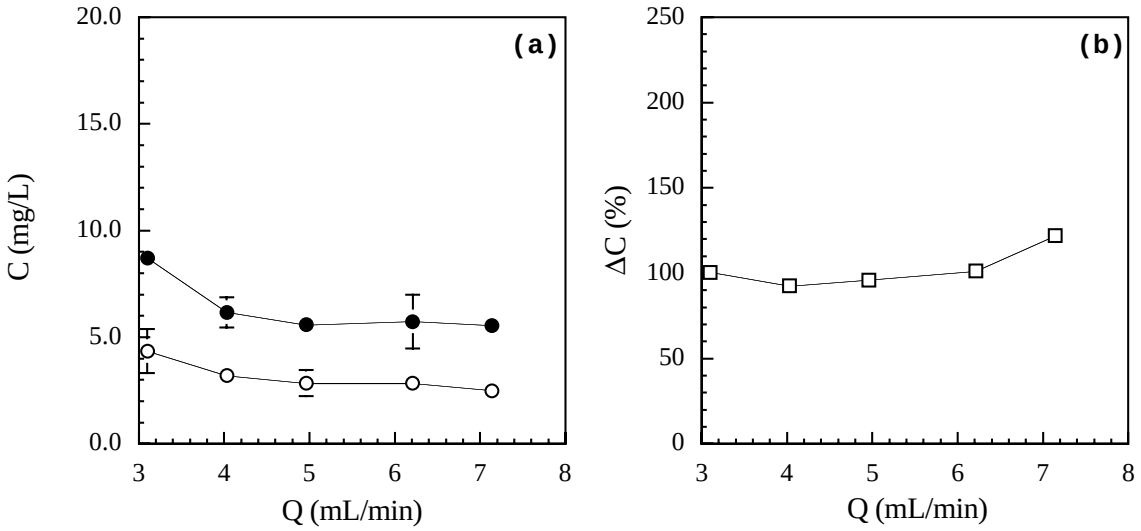

Figure 6.2: The effect of the volumetric flow rate on the (a) average effluent base case (open circles) and acoustic case (solid circles) concentrations compared to volumetric flow rate and (b) its effect on ΔC. For the acoustic case constant $\phi = 125$ Hz and p_s=3.68 kPa were used.

The experimental results presented in Figure 6.2a indicate that all effluent concentrations measured in the absence and presence of acoustic waves are observed to slightly decrease with increasing flow rate. The most pronounced decrease occurs between approximately 3 to 4 mL/min, the lowest flow rates used. However, the effluent concentrations collected in the presence of acoustic waves are consistently greater than the base case effluent concentrations. Figure 6.2b shows that ΔC due to the addition of acoustic waves is consistently about 100%. However, the effect of increasing the background volumetric flow rate on ΔC is essentially negligible for the flow rates used in this study. Clearly, for the range of background flow rates used in this study, the experimental data indicate that there is a significant PCE ganglia dissolution enhancement. The observed ganglia dissolution enhancement is attributed to the oscillatory fluid velocity due to the addition of acoustic waves. This oscillatory fluid velocity at the pore scale is probably changing the concentration gradient at the PCE ganglia-water interfaces, the PCE molecular diffusion coefficient, the mass transfer coefficient, or a combination of all three processes in order tocause the observed in-

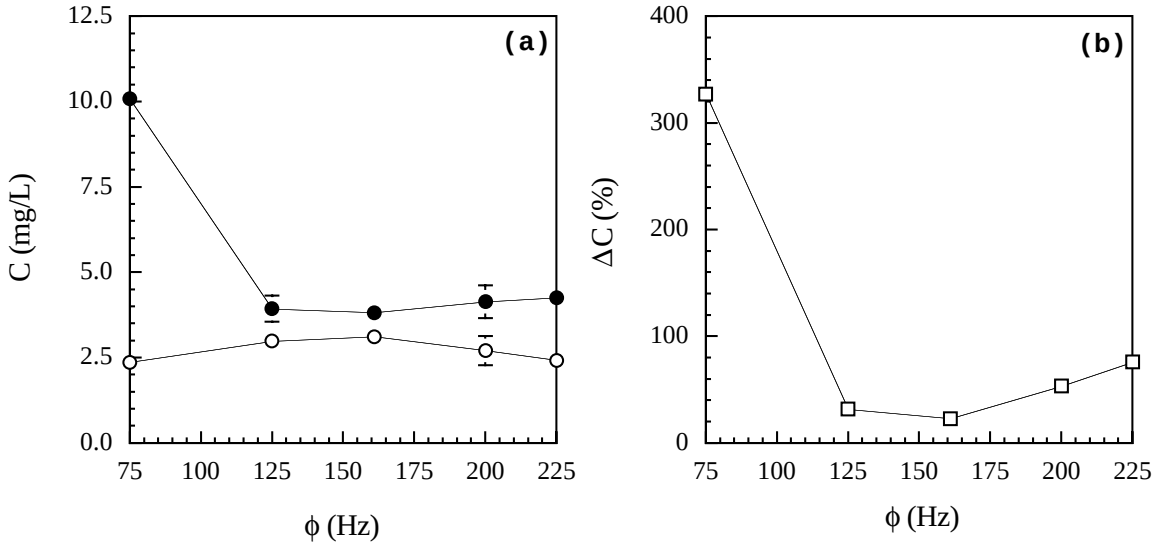

Figure 6.3: The effect of acoustic frequency ϕ on the (a) average effluent base case (open circles) and acoustic case (solid circles) concentrations compared to volumetric flow rate and (b) its effect on ΔC with constant $p_s = 3.68$ kPa and background volumetric flow rate $Q = 4.96$ mL/min.

creased effluent dissolved phase aqueous PCE concentrations shown in Figures 6.2a and b.

The effect of acoustic wave frequency, ϕ, in the range of 75 to 225 Hz, on the effluent concentration and ΔC for a constant source pressure $p_s = 3.68$ kPa using a constant background volumetric fluid flow of $Q = 4.96$ mL/min, is shown in Figure 6.3. The average effluent dissolved PCE concentration in the absence of acoustic waves (open circles) and for the case of acoustic waves (solid circles) compared to ϕ is presented in Figure 6.3a. The greatest effluent concentraton due to the presence of acoustic waves occurs at the lowest frequency used, $\phi = 75$ Hz. For frequencies ranging from 125 to 225 Hz, the effluent dissolved phase PCE concentrations exhibit a minor increase with increasing ϕ. Figure 6.3b shows that there is over a 300% increase in effluent PCE concentrations for $\phi = 75$ Hz. A minimum increase of 23% is observed at $\phi = 161$ Hz. Note that ΔC is then observed to increase to approximately 76% at 225 Hz.

The maximum ΔC observed at the lowest frequency used for this work ($\phi = 75$ Hz) may potentially be attributed to the presence of the "slow wave," where the fluid within the pore space oscillates 180 degrees out of phase with the porous media bulk

matrix [*Biot*, 1956a,b]. It has also been shown that lower frequency acoustic waves are less attenuated in porous media due to lower frictional forces along the pore walls [*Biot*, 1956a,b]. The effluent pressure recorded for the experiment at $\phi = 75$ Hz, with a constant acoustic source pressure amplitude of $p_s = 3.68$ kPa, was 2.95 kPa. This effluent pressure p_e is approximately 3 times greater than the p_e recorded for the experiments using different frequencies. The effluent pressure recordings are an indication of the acoustic wave attenuation. With the greatest p_e occuring for the lowest frequency, which is in agreement with the work by Biot [1956a,b], it is infered that the oscillatory pore water velocity must also be the greatest for low frequencies, also in agreement with Biot [1956a,b], and responsible for the greatest observed ΔC (Figure 6.3).

6.3.3 Pore Network Model

The glass beads in the monolayer experimental apparatus can be represented as a hexagonal latice pore network model. Consequently, effective mass transfer coefficients and the associated dissolution enhancement due to acoustic waves may be modeled. Using a simplified advective transport model based on the models used by Held and Celia [2001] and Jia et al. [1999], volumetric fluid flow and dissolved aqueous phase PCE concentrations are determined by

$$\frac{1}{V_i}\frac{\Delta C_i}{\Delta t} = \sum_j \left[G_{i,j}\Delta p_{i,j} C_{i,j}\right] + \sum_j \left[J_j A_j\right], \tag{6.13}$$

where V_i denotes the pore volume i; ΔC_i is the change in concentration at pore i per change in time Δt; $\Delta p_{i,j}$ is the difference in pore fluid pressures in the pores j surrounding pore i; and $G_{i,j}$ is the conductance of a pore throat connecting pores j to pore i defined using a shape factor or dimensionless hydraulic radius as [*Patzek and Silin*, 2001]

$$G_{i,j} = \frac{3}{5}\frac{A_p^3}{ull_p^2}, \tag{6.14}$$

where A_p is the cross sectional area of a pore throat connecting two pore spaces; u is dynamic fluid viscosity; l is the separaton distance between two pores included in the conductance term for convenience; and l_p is the perimeter of a pore throat connecting two pore spaces. Because the hydraulic resistance to flow is mostly in the pore throats connecting pores and considering real pore bodies and throats of complex and variable cross sections, the throats are approximated as cylindrical ducts (noncircular capillaries) of constant but arbitrary cross-section [*Patzek and Silin*, 2001]. For the network model used in this work representing the glass bead monolayer, l, l_p, and A_p are considered constant for all pores and pore throats. Parameter values used in the network model are given in Table 6.1.

Table 6.1: Network Model Parameters

Parameter	Values
A_p†	2.73×10^{-2} cm^2
l†	0.173 cm
l_p†	0.423 cm
u‡	8.90×10^{-3} g/cm s

† for 3 mm beads
‡ for water at 20 °C

The network model is composed of $N_x = 36$ pores in the direction of flow and $N_y = 29$ pores wide. The volumetric flow rate $Q_{i,j}$ through the hexagonal lattice representation of the pores of the monolayer is defined as

$$Q_{i,j} = \sum_j G_{i,j} \Delta p_{i,j} = 0. \tag{6.15}$$

The transport of dissolved aqueous phase PCE, originating from an immobile ganglion, through the network is determined by solving (6.13) and using (6.15). The mass flux of PCE across the individual PCE ganglia-water interfaces is given by (6.3). The interest of this work is to determine the effect of acoustic pressure waves on the dissolution of PCE ganglia, experimentally represented by the change in effluent dissolved aqueous phase PCE concentrations in the presence of acoustic pressure waves. The

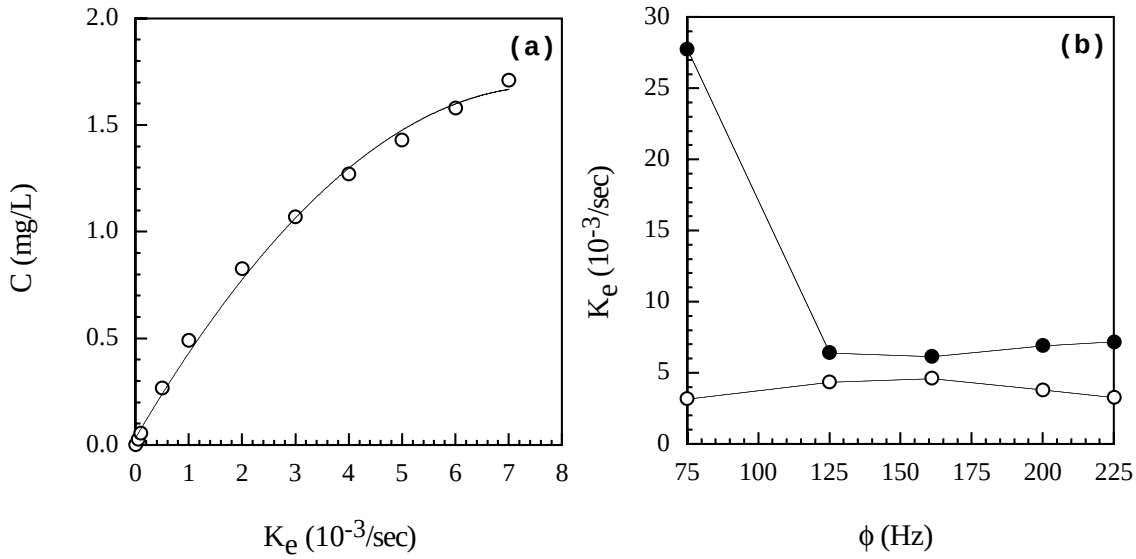

Figure 6.4: Network model (a) C shown by open circles compared to K_e where the line represents a least squares best polynomial fit and (b) K_e values corresponding to base case (open circles) and acoustic case C (solid circles) for ϕ=75 to 225 Hz.

effective mass transfer coefficient K_e defined in (**??**) is therefore considered to be dependent on local concentration gradients at the pore scale for this work. This overall time independent effective mass transfer coefficient is then used to determine the effluent concentration from the network model. To reproduce the effluent dissolved PCE concentrations for the case of constant $Q = 4.96$ mL/min observed in the experimental results (Figure 6.3), the network model was calibrated to the set flow rate and K_e was varied to produce a relationship between K_e and C, shown in Figure 6.4.

Figure 6.4a shows good agreement between the best fit polynomial line ($C = -2.99K_e + 0.45K_e$) and the numerical results from the network model. In Figure 6.4b, the K_e is clearly shown to be greater for the case of acoustic pressure compared to the base case. Moreover, the maximum increase in K_e occurs for the lower frequency similar to the maximum ΔC being the greatest for the 75 Hz wave (Figure 6.3b).

6.4 Acoustic Enhanced Mobilization

6.4.1 Experimental Procedures for Mobilization

The effect of acoustic waves on the mobilization of PCE ganglia is investigated by conducting experiments using the glass bead monolayer as in the dissolution experiments with the same equipment controlling fluid flow rates, acoustic pressure, and pressure recording. Experimental observations are made using a digital camera (Olympus C2500L, Melville, New York) with a combination of macro lenses.

Mobilization experiments of PCE ganglia are conducted by first injecting approximately 0.05 mL of PCE dyed red with oil red EGN into a center injection port in the top plate of the monolayer. After the initial PCE ganglia configuration is recorded, the flow rate is incrementally increased until ganglia mobilization is achieved in the absence of acoustic pressure (base case). When mobilization is achieved in the absence of acoustic waves, the fluid flow rate is discontinued and the new ganglia configuration is recorded. Acoustic pressure is then applied using a frequency $\phi = 125$ Hz and the flow rate incrementally increased until mobilization is again achieved. This process is repeated for a range of acoustic source pressures p_s and flow rates until the ganglia are completely mobilized and exit the monolayer.

The fluid flow rate responsible for mobilizing the PCE ganglia in the presence of acoustic waves is compared to the fluid flow rate that mobilizes the ganglia in the absence of acoustic pressure using the Capillary number Ca defined by (6.11). The parameters used to determine the respective Ca are: U which is determined by dividing Q by the cross sectional area to flow of the glass bead monolayer (1.35 cm^2) and its porosity (0.39); the dynamic fluid viscosity u =1.0019 cp; and the contact angle β, which is set to be equal to unity. The capillary pressure P_c calculated for an arbitrary PCE-water interface using (6.6) and (6.7), with γ_{ow}=44.4 dynes/cm [*Mercer and Cohen*, 1990] and $r_H = 3.23 \times 10^{-2}$ cm, is 137.38 Pa.

6.4.2 Enhanced Mobilization Results

Figure 6.5 shows the evolution of a 12 pore PCE ganglion for the case of acoustic pressure waves and that of no acoustic pressure where the background fluid flow direction is from left to right. The initial ganglion configuration is shown in Figure 6.5a. After the ganglion was emplaced the flow rate was increased until mobilization was achieved at $Ca = 9.44 \times 10^{-3}$ in the absence of acoustic pressure (Figure 6.5b). Acoustic pressure was applied with an acoustic source pressure amplitude p_s=7.35 kPa and Q was incrementally increased until mobilization was attained. Figure 6.5c shows the ganglion to begin to split into two separate ganglia at p_s=7.35 kPa and $Ca = 7.00 \times 10^{-3}$, which is lower than the Ca required for mobilization in Figure 6.5b. After the ganlion split into two separate ganglia, the acoustic pressure was discontinued and Q was increased to cause mobilization. Mobilization was unable to be observed for the highest $Ca = 1.16 \times 10^{-2}$ used without the use of acoustic pressure (Figure 6.5d). Acoustic pressure was again employed with p_s=11.03 kPa and $Ca = 7.31 \times 10^{-3}$. Initially, no mobilization occured; however, the larger of the two ganglia was observed to shrink in length (Figure 6.5e). Soon after, the larger of the two ganglia split again and become mobilized for the same p_s and Ca (Figure 6.5f).

An additional PCE gangia mobilization experiment was conducted using an 18 pore ganglion to determine the effects of acoustic waves on a larger size ganglion. Figure 6.6 shows the gangion evolution for a range of p_s and Ca. The initial ganglion configuration is shown in Figure 6.6a. In the absence of acoustic waves, mobilization is achieved at $Ca = 1.15 \times 10^{-2}$ (Figure 6.6b). The background flow was then discontinued and acoustic pressure added. Figures 6.6c and d show that no mobilization is achieved for a $p_s = 4.13$ kPa and a range of Ca from 1.87×10^{-4} to 1.17×10^{-2}, respectively. It should be noted that $Ca = 1.17 \times 10^{-2}$ is the greatest Ca value possible for the experimental equipment used in this study. Keeping the Ca constant, the p_s was then increased to 13.79 kPa again resulting in no observable mobilization (Figure 6.6e). Figure 6.6f shows the evolution of the ganglia to begin to thicken at

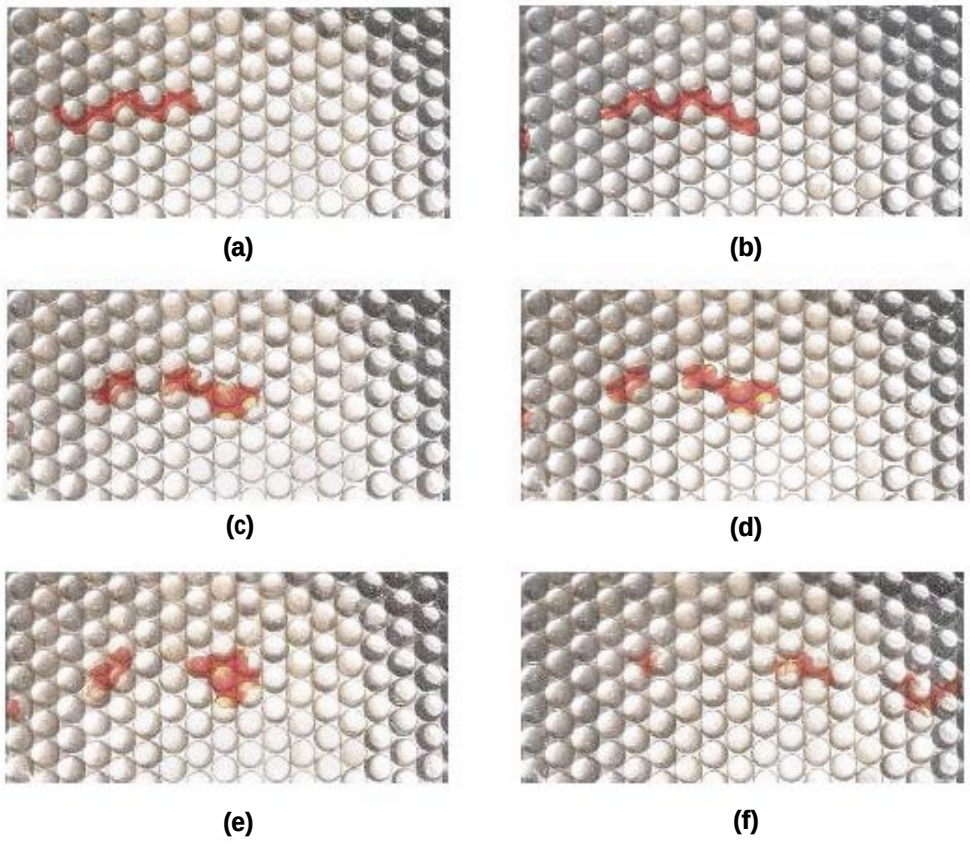

Figure 6.5: Evolution of PCE ganglia for (a) initial configuration where $p_s = 0.0$ kPa, (b) mobilization at $p_s = 0.0$ kPa and $Ca = 9.44 \times 10^{-3}$, (c) $p_s = 7.35$ kPa and $Ca = 7.00 \times 10^{-3}$, (d) $p_s = 0.0$ kPa and $Ca = 1.16 \times 10^{-2}$, (e) $p_s = 11.03$ kPa and $Ca = 7.31 \times 10^{-3}$, and (f) $p_s = 11.03$ kPa and $Ca = 7.31 \times 10^{-3}$.

the down gradient side (right) for the same Ca but with a greater p_s of 22.98 kPa. Figure 6.6g for a $p_s = 39.07$ kPa and a reduced $Ca = 1.02 \times 10^{-2}$ shows thinning of the ganglion at the down gradient side. The ganglion was then observed to become mobilized and move as a complete "blob" with the background fluid flow in Figure 6.6h, for the same p_s but an increased $Ca = 1.05 \times 10^{-2}$.

Figure 6.7 shows a close up view of the mobilized ganglion evolution from Figure 6.6h. There is minor difference between the ganglion configuration between Figures 6.7a and b, however, Figure 6.6c shows the gangion to invade neighboring downgradient pores. Figure 6.7d shows the ganglion to continue to invade downgradient pores but also begin to shrink three pores from the down gradient edge. This thinning continues,

shown in Figure 6.7d, resulting in the ganglion splitting. Rapid mobilization is then observed to occur for the downgradient ganglion and is shown in Figure 6.7f.

6.5 Summary

The effect of acoustic pressure waves on PCE ganglia dissolution and mobilization in a monolayer of glass beads is investigated. The effluent dissolved aqueous PCE concentration is observed to increase in the presence of acoustic waves compared to the case with no acoustic waves. Increasing the background fluid flow rates did not have a significant effect on dissolution enhancement caused by the addition of acoustic waves. The greatest dissolution enhancement, occurs at the lowest ϕ used in this study (75 Hz). A pore network numerical model is used to estimate K_e under various conditions. It was shown that K_e for the case where acoustic waves are present is at a maximum at low ϕ but it is consistently greater than the estimated K_e in the absence of acoustic waves. The enhanced ΔC and K_e for the dissolution and pore network experiments is attributed to an oscillatory pore water velocity component caused by the presence of acoustic waves.

Mobilization experiments show that PCE ganglia are mobilized at lower flow rates and associated Ca compared to base case mobilization experiments. Larger PCE ganglia are mobilized at lower Ca. The addition of acoustic waves also contributes to the splitting of ganglia into smaller discontinuous ganglia. The PCE ganglia, immobile for the largest Ca possible for these experiments, were mobilized after acoustic pressure waves were added causing P_c to be exceeded. The results of this research suggests that the addition of acoustic waves may reduce remediation times if employed as a remediation method. Furthermore, acoustic waves may be used to mobilize as well as to split DNAPL ganglia into smaller individual discontinuous ganglia. Ganglia splitting is beneficial in aquifer remediation applications because the DNAPL-water interfacial areas are increased and subsequent dissolution rates are greater. Overall, the combined use of acoustic waves and traditional pump-and-treat methods may reduce the

times and associated costs of remediating sites contaminated with DNAPLs.

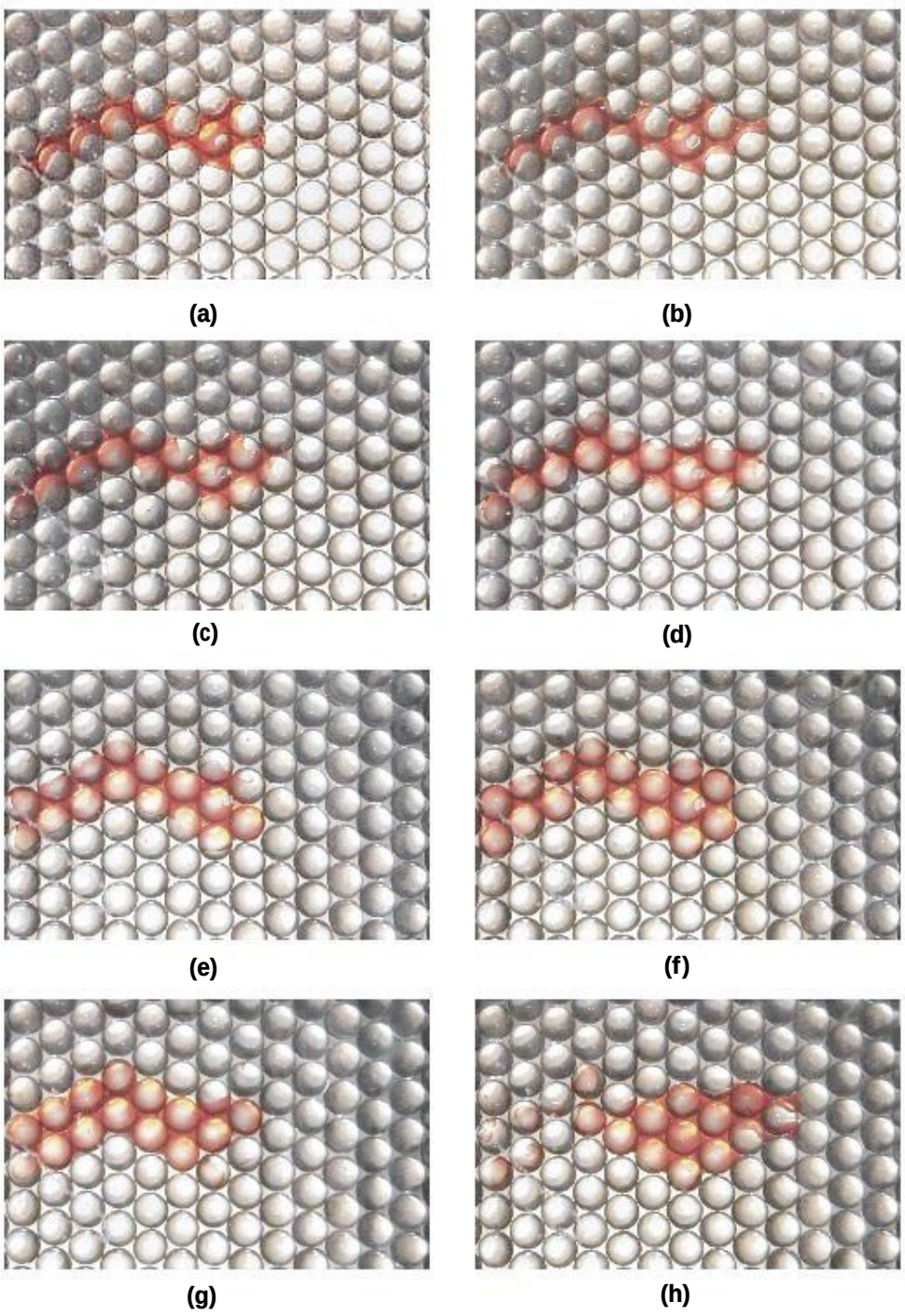

Figure 6.6: Evolution of PCE ganglia for (a) initial configuration where $p_s = 0.0$ kPa, (b) mobilization at $p_s = 0.0$ kPa and $Ca = 1.15 \times 10^{-2}$, (c) $p_s = 4.13$ kPa and $Ca = 1.87 \times 10^{-4}$, (d) $p_s = 4.13$ kPa and $Ca = 1.17 \times 10^{-2}$, (e) $p_s = 13.79$ kPa and $Ca = 1.17 \times 10^{-2}$, and (f) $p_s = 22.98$ kPa and $Ca = 1.17 \times 10^{-2}$, (g) $p_s = 39.07$ kPa and $Ca = 1.02 \times 10^{-2}$, and (h) $p_s = 39.07$ kPa and $Ca = 1.05 \times 10^{-2}$.

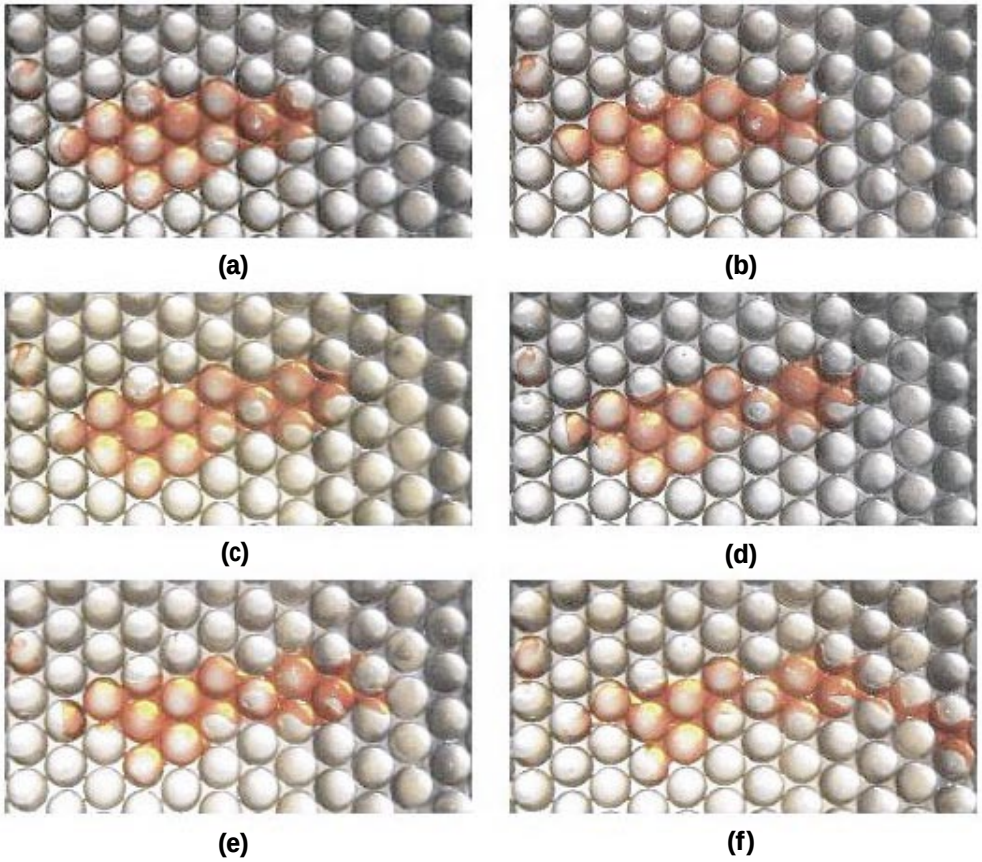

Figure 6.7: Continuation and close up of PCE ganglia evolution at $p_s = 39.07$ kPa and $Ca = 1.05 \times 10^{-2}$.

Chapter 7

SUMMARY and FUTURE RESEARCH

7.1 Summary and Conclusions

The use of acoustic waves in the remediation of aquifers contaminated with DNAPLs was examined. In order to ascertain the effect of acoustic waves on the dissolved phase transport in water saturated porous media, Br^- tracer experiments were conducted. The tracer experiment was conducted in a water saturated column filled with glass beads of uniform diameter, where the acoustic waves were applied at a constant acoustic pressure amplitude but a range of frequencies. A one-dimensional form of the advection dispersion equation, representing the mass transport of dissolved mass from a slug injection used in the column experiments, was solved analytically. The analytical soultion was used in a non-linear least squares fitting routine, written to fit the effluent Br^- concentrations from the column experiments. The fitting routine was first employed to estimate the dispersivity of the packed column and the steady state background interstitial fluid velocity for the case of no acoustic waves. Once the background interstitial velocity and dispersivity was determined, the fitting routine was used to determine the effective interstitial fluid velocity of dissolved Br^- for

effluent column concentrations in the presence of acoustic waves, using a fixed value of dispersivity. The effective interstitial fluid velocity, attributed to the presence of acoustic waves, was found to be inversely proportional to frequency. An acoustic frequency producing a maximum effective interstitial fluid velocity could not be found due to experimental equipment limitations in the low frequency range.

The effect of acoustic pressure waves on TCE ganglia dissolution in a water saturated glass bead packed column was investigated both experimentally and theoretically. A mathematical model was developed to depict the motion of the porous media and the interstitial pore water in response to an acoustic pressure source. The mathematical model was solved as an eigenvalue problem using the method of Laplace transforms. Using the solution for the solid and fluid motion, an oscillatory relative velocity for the interstitial pore fluid was determined. The oscillatory relative interstitial fluid velocity was then used in determining the acoustic Reynolds number to compare dissolution experiments using different frequencies and influent fluid pressures. The acoustic Reynolds number was found to decrease with increasing distance from the acoustic pressure source and reach an assymptotic value with increasing frequency. The acoustic Reynolds number was also found to increase linearly with increasing acoustic source fluid pressure amplitude. The effluent dissolved phase TCE concentrations in the presence of acoustic pressure waves, from the column dissolution experiments, were observed to be over 100% higher due to the addition of the oscillatory pore water velocity caused by the presence of acoustic waves than without acoustic waves. The increase in effluent TCE concentration was also found to be proportional to the applied acoustic source pressure amplitude. Acoustic Reynolds numbers, determined for the dissolution experiments, were found to be higher for the case when the column was packed with larger glass beads. However, the increase in effluent TCE concentration was observed to be greater for the case of the column packed with smaller diameter glass beads. This is attributed to greater TCE-water interfacial areas associated with smaller diameter bead column packing.

The impact of acoustic pressure waves on multicomponent nonaqueous phase liquid

(NAPL) ganglia dissolution in water saturated columns packed with glass beads was investigated. Nonideal multicomponent ganglia liquid mixture aqueous phase solubilities were accounted for by determining nonaqueous phase activity coefficients. Laboratory data from dissolution experiments with two and three component NAPL mixtures composed of either TCE and 1,1,2-TCA or TCE, 1,1,2-TCA, and PCE, show that acoustic waves significantly enhance ganglia dissolution due to the oscillatory interstitial water velocity caused by the acoustic waves. The data collected also indicate that dissolution enhancement is directly proportional to the acoustic wave frequency. Furthermore, it was demonstrated that the greatest dissolution enhancement in the presence of acoustic waves is associated with the NAPL component having the smallest equilibrium aqueous solubility. Finally, square shaped acoustic waves were shown to lead to greater NAPL dissolution enhancement compared to sinusoidal and triangular acoustic waves.

The pore scale effects of acoustic waves on DNAPL dissolution was investigated by conducting PCE ganglia dissolution and mobilization experiments in a monolayer of glass beads. A pore network model was also developed to determine the effective mass transfer coefficient for dissolution experiments conducted without acoustic pressure waves and the mass transfer enhancement due to the presence of acoustic waves. Increasing background volumetric fluid flow for PCE ganglia dissolution experiments conducted at a constant acoustic frequency and source pressure amplitude was found to have a negligable effect on the change in effluent dissolved phase PCE concentration due to the addition of acoustic waves. Overall, the percent change in efluent dissolved phase PCE concentration was shown to be approximately 100% for all flow rates used. The effluent dissolve phase PCE concentration was found to be the greatest at the lowest acoustic wave frequency used (75 Hz). Effective mass transfer coefficients, determined for PCE ganglia dissolution experiments conducted in the monolayer for a range of frequencies, was also found to be a maximum at low frequencies similar to results of effluent dissolved phase PCE concentrations over the same frequency range. The enhanced percent change in effluent concentration and effective mass transfer

coefficient is attributed to an oscillatory pore water velocity component caused by the presence of acoustic waves. PCE ganglia mobilization experiments show that ganglia are mobilized at lower flow rates and associated Ca for the case of acoustic pressure waves compared to base case mobilization experiments. The addition of acoustic waves also enhances the splitting of ganglia into smaller discontinuous ganglia.

The results presented in this dissertation demonstrated that the use of acoustic waves enhance mass transport and increase the effective interstitial fluid velocity in water saturated porous media. The enhancement of DNAPL dissolution, both multicomponent and single component, due to addition of acoustic waves suggest that acoustic waves may be a viable method of remediation for aquifers contaminated with DNAPLs. The mobilization and break up of PCE ganglia demonstates the benefits of applying acoustic waves to DNAPL contaminated sites is two-fold. Mobilization and subsequent recovery may be possible in addition to increasing the DNAPL-water interfacial areas that will enhance dissolution. The combined use of acoustic waves and traditional pump-and-treat technology may therefore be a cost and time effective method to remediate aquifers contaminated with DNAPLs.

7.2 Recommended Future Research

The enhanced mass transport and effective interstitial fluid velocity presented in Chapter 3 can be extended to real homogeneous and heterogenous real porous media, such as well to poorly sorted sands. Using different equipment to provide lower frequency acoustic waves will also enable the characteristic frequency, that results in a maximum effective interstitial fluid velocity for frequencies greater than the zero, to be determined.

The work presented in Chapter 4 can be improved by further developing mathematical models that describe the resonance frequencies observed as peaks in the effluent fluid pressures. This will enable better correlations to be determined between the acoustic Reynolds number and the enhanced TCE dissolution.

Enhanced multicomponent DNAPL ganglia dissolution, presented in Chapter 5 may be further investigated by using a solid organic contaminate where the volume and interfacial areas can be well defined. With a well defined interfacial area, mass transfer correlations may be developed for given acoustic Reynolds numbers.

Pore scale DNAPL ganglia dissolution and mobilization due to the addition of acoustic waves in Chapter 6 can be furthered by modifying the monolayer to a pore network. A pore network will facilitate the measurement of interfacial areas and simplify the mathematical description of the interstitial fluid flow. Moreover, the use of lattice-Boltzmann modeling may enable the contribution of an oscillatory interstitial pore fluid velocity due to acoustic pressure waves, on both mass transfer and ganglia mobilization, to be further described in greater detail.

Chapter 8

REFERENCES

Abramowitz, M., and I. A. Stegun, Handbook of Mathematical Functions, National Bureau of Standards, Washington D.C., 1965.

Adachi, J., S. Okamato, and M. Adachi, The effect of sound on the rate of heat transfer from a cylinder placed normal to an air stream, *Bull. Japn Soc. Mech. Engr*, 122, 172, 1979.

Adamson, A. W., *Physical Chemistry of Surfaces*, John Wiley and Sons, N. Y., 1982.

Anderson, M. R., R. L. Johnson , and J. F. Pankow , Dissolution of dense chlorinated solvents into groundwater, 3, Modeling contaminant plumes from fingers and pools of solvent, *Environ. Sci. Technol.*, 26, 901-908, 1992.

Aris, R. On the dispersion of a solute in pulsating flow through a tube, *Proc. Royal Soc. A*, 259(1298), 370–376, 1960.

Banerjee, S., Solubility of organic mixtures in water, *Environ. Sci. Technol.*, 18(8), 587-591, 1984.

Bao, W. M. J., E. T. Vogler, and C. V. Chrysikopoulos, Nonaqueous phase liquid pool dissolution in three-dimensional heterogeneous subsurface formations, *Environ.*

Geol., 43, 968-977, 2003.

Barron, J. T., W. K. Van Moorhem, and J. Majdalani, A novel investigation of the oscillatory field over a transpiring surface, *J. Sound Vibration*, 235(2), 281-297, 2000.

Baxi, C. B. and A. Ramachandran, Effect of vibration on heat transfer from spheres, *SAME J. Heat Transfer*, 337-344, 1969.

Bear, J., *Dynamics of Fluids in Porous Media*, Dover Publications, Inc., NY, 764 pp., 1972

Beresnev, I. A. and P. A. Johnson, Elastic-wave stimulation of oil production: A review of methods and results, *Geophysics*, 59(6), 1000–1017, 1994.

Biot, M. A., Theory of propagation of elastic waves in a fluid-filled porous solid. I. Low-frequency range, *J. Acoust. Soc. Am.*, 28(2), 168–178, 1956a.

Biot, M. A., Theory of propagation of elastic waves in a fluid-filled porous solid. II. High-frequency range, *J. Acoust. Soc. Am.*, 28(2), 179–191, 1956b.

Bird, R. B., W. E. Stewart, and E. N. Lightfoot, *Transport Phenomena*, John Wiley and Sons, N. Y., 1960.

Brandes, D. and K. J. Farley, Importance of phase behavior on the removal of residual DNAPLs from porous media by alcohol flooding, *Water Environ. Res.*, 65(7), 869–878, 1993.

Broholm, K., and S. Feenstra, Laboratory measurements of the aqueous solubility of mixtures of chlorinated solvents, *Environ. Toxicol. Chem.,* 14, 9-15 1995.

Buckley, J. S., In: Morrow, N. R. (Ed.), Interface Phenomena in Petroleum Recovery, Marcel Dekker, NY, 1990

Brusseau, M.L., Z. Zhang, N. T. Nelson, R. B. Cain, G. R. Tick, and M. Oostrom, Dissolution of nonuniformly distributed immiscible liquid: Intermediate-scale experiments and mathematical modeling, *Environ. Sci. Technol.,* 36, 1033-1041, 2002.

Carslaw, H. S., and J. C. Jaeger, *Conduction of HEat in Solids*, Clarendon, Oxford, 1959.

Chandler, R. N. and D. L. Johnson, The equivalence of quasistatic flow in fluid-saturated porous media and Biot's slow wave limit of zero frequency, *J. Appl. Phys.*, 52(5), 3391-3395, 1981.

Chatwin, P. C., On the longitudinal dispersion of passive contaminant in oscillatory flows in tubes, *J. Fluid Mech.*, 71(3), 513–527, 1975.

Chatzis, I., N. R. Morrow, and H. T. Lim, Magnitude and detailed structure of residual oil saturation, *Soc. Pet. Eng. J.*, 24, 311–326, 1983.

Chatzis, I., PRRC Report No. 82-12, New Mexico Petroleum Recovery Research Center, Socorro, NM, 1982.

Chaudhry, G. R., *Biological Degradation and Bioremediation of Toxic Chemicals*, 515 pp., Dioscorides Press, Portland, 1994.

Cherskiy, N. V., V. P. Tsarev, V. M. Konovalov, and O. L. Kuznetsov, The effect of ultrasound on permeability of rocks to water, *Transact. USSR Acad. Sci., Earth Sci. Sect.*, 232, 201–204, 1977.

Chrysikopoulos, C. V., Artificial tracers for geothermal reservoir studies, *Environ. Geol.*, 22, 60–70, 1993.

Chrysikopoulos, C. V., E. A. Voudrias, M. M. Fyrillas, Modeling of contaminant transport resulting from dissolution of nonaqueous phase liquid pools in saturated porous media, *Transp. Porous Media.*, 16, 125-145, 1994.

Chrysikopoulos, C. V., Three–dimensional analytical models of contaminant transport from nonaqueious phase liquid pool dissolution in saturated subsurface formations, *Water Resour. Res.*, 31(4), 1137-1145, 1995a.

Chrysikopoulos, C. V., Effective parameters for flow in saturated heterogeneous porous media, *J. Hydrol.*, 170, 181-198, 1995b.

Chrysikopoulos, C. V., K. Y. Lee, and T. C. Harmon, Dissolution of a well–defined trichlorethylene pool in saturated porous media: Experimental design and aquifer characterization, *Water Resour. Res*, 36(7), 1687-1696, 2000.

Chrysikopoulos, C. V., K. Y. Lee, Contaminant transport resulting from multicomponent nonaqueous phase liquid pool dissolution in three-dimensional subsurface formations. *J. Contam. Hydrol.*, 31(1-2), 1-21, 1998.

Chrysikopoulos, C. V., P. K. Kitanidis, and P. V. Roberts, Analysis of one–dimensional solute transport through porous media with spatially variable retardation factor, *Water Resour. Res.*, 26(3), 437–446, 1990.

Chrysikopoulos, C. V., P. K. Kitanidis, and P. V. Roberts, Generalized Taylor–Aris moment analysis of the transport of sorbing solutes through porous media with spatially–periodic retardation factor, *Transp. Porous Media*, 7(2), 163–185, 1992.

Chrysikopoulos, C. V., P-Y. Hsuan, M. M. Fyrillas, Bootstrap estimation of the mass transfer coefficient of a dissolving nonaqueous phase liquid pool in porous media *Water Resour. Res.*, 38(3), 1026, doi:10.1029/2001WR000661, 2002.

Chrysikopoulos, C. V., P-Y. Hsuan, M. M. Fyrillas, K. Y. Lee, Mass transfer coefficient and concentration boundary layer thickness for a dissolving NAPL pool in porous media, *J. Hazardous Materials*, B97, 245-255, 2003.

Chrysikopoulos, C. V., T-J. Kim, Local mass transfer correlations for nonaqueous phase liquid pool dissolution in saturated porous media. *Transp. Porous Media.*,

38(1-2), 167-187, 2000.

Cooper, P. J., J. C. Sheridan, and C. J. Flood, The effect of sound on forced convection over a flat plate, *Int. J. Heat Fluid flow* 7, 61-68, 1986.

Coulson, J. M., and J. F. Richardson, *Chemical Engineering*, McGraw Hill, N. Y., 1954.

Dawson, H. E., and P. V. Roberts, Influence of viscous, gravitational, and capillary forces on DNAPL saturation, *Ground Water*, 35(2), 261-269, 1997.

de Boer, R. and W. Ehlers, Uplift, friction and capillarity - three fundamental effects for liquid-saturated porous solids, *Int. J. Solids Structures*, 26, 43-57, 1990.

de Boer, R. and W. Ehlers, and Z. Liu, One-dimensional transient wave propagation in fluid-saturated incompressible porous media, *Archive of Appl. Mechanics*, 63, 59-72, 1993.

Dela Barre, B. K., T. C. Harmon, and C. V. Chrysikopoulos, Measuring and modeling the dissolution of nonideally shaped dense nonaqueous phase liquid pools in saturated porous media, *Water Resour. Res*, 38(8), doi: 10.1029/2001/WR000444, 2002.

del Rio, J. A., M. L. De Haro, and S. Whitaker, Enhancement in the dynamic response of a viscoelastic fluid flowing in a tube, *Phys. Rev. E*, 58(5), 6323–6327, 1998.

de Marsily, G., *Quantitative Hydrogeology, Groundwater Hydrology for Engineers*, 440 pp., Academic Press, San Diego, California, 1986.

Demond, A. H. and P. V. Roberts, Effect of interfacial forces on two-phase capillary pressure-saturation relationships, *Water Resour. Res.*, 27, 423-437, 1991.

Desai, F. N., A. H. Demond, and K. F. Hayes, Influence of surfactant sorption on capillary pressure saturation relationships, in *Transport and Remediation of Sub-*

surface Contaminants: Colloidal, Interfacial and Surfactant Phenomena, Sabatini, D. and R. Knox, American Chem. Soc., Washington DC, 133-148, 1992.

DeSmedt, F. and P. J. Wierenga, A generalized solution for solute flow in soils with mobile and immobile water, *Water Resour. Res.*, 15, 1137–1141, 1979.

Domenico, P. A. and F. W. Schwartz, *Physical and Chemical Hydrogeology*, 824 pp., Wiley, New York, 1990.

Domenico, S. N., Elastic properties of unconsolidated porous sand reservoirs, *Geophysics*, 42(7), 1339-1368, 1977.

Dullien, F. A. L., *Porous Media. Fluid Transport and Pore Structure*, Academic Press, NY, 396 pp., 1979.

Eberhardt, C., P. Grathwohl, Time scales of organic contaminant dissolution from complex source zones: coal tar pools vs. blobs, *J. Contam. Hydrology.*, 59(1-2), 45-66, 2002.

Engelbrecht, H. and L. Pretorius, The effect of sound on natural convection from a vertical flat plate, *J. Sound Vibration*, 158(2), 213-218, 1992.

Fenwick, D. H. and M. J. Blunt, Three-dimensional modeling of three phase imbibition and drainage, *Adv. Water Res.*, 21(2), 121-143, 1998.

Fortin, J., W. A. Jury, and M. A. Anderson, Enhanced removal of trapped non-aqueous phase liquids from saturated soil using surfactant solutions, *J. Contam. Hydrol.*, 24(3-4), 247–267, 1997.

Fredenslund, A., J. Gmehling, P. Rasmussen, *Vapor-liquid Equilibria Using UNIFAC*, Elsevier: New York, 1977.

Gaganis, P., H. K. Karapanagioti, V. N. Burganos, Modeling multicomponent NAPL transport in the unsaturated zone with the constituent averaging technique, *Adv.*

Water Resour., 25, 723-732, 2002.

Geerits, T. W. and O. Kelder, Acoustic wave propagation through porous media: Theory and experiments, *J. Acoust. Soc. Am.*, 102(5), 2495–2510, 1997.

Gmehling, J., P. Rasmussen, A. Fredenslund, Vapor-liquid equilibria by UNIFAC group contribution, 2, Revision and extension, *Ind. Eng. Chem. Process Des. Dev.*, 21, 118-127, 1982.

Greenkorn, R. A., *Flow Phenomena in Porous Media*, Marcel Dekker, New York, 1983.

Ha, M. Y., and S. Yavuzkurt, A theoretical investigation of acoustic enhancement of heat and mass transfer–II. Oscillating flow with a steady velocity component, *Int. J. Heat Mass Transfer*, 36(8), 2193-2202, 1993.

Ha, M. Y., and S. Yavuzkurt, A theoretical investigation of acoustic enhancement of heat and mass transfer–I. Pure oscillating flow, *Int. J. Heat Mass Transfer*, 36(8), 2183-2192, 1993.

Ha, M. Y., S. Yavuzkurt, and K. Kim, Heat transfer past particles entrained in an oscillating flow with and without a steady velocity, *Int. J. Heat Mass Transfer*, 36, 949-959, 1993.

Hamilton, E. L., Compressional wave attenuation in marine sediments, *Geophysics*, 37(4), 620-646, 1972.

Hamilton, E. L. and R. T. Bachman, Sound velocity and related properties of marine sediments, *J. Acoust. Soc. Am.*, 72(6), 1891-1904, 1982.

Hansen, H. K., P. Rasmussen, A. Fredenslund, M. Schiller, J. Gmehling, Vapor-liquid equilibria by UNIFAC group contribution, 5, Revision and extension, *Ind. Eng. Chem. Process Des. Dev.*, 30, 2352-2355, 1991.

Held, R. J., and M. A. Celia, Pore-scale modeling and upscaling of nonaqueous phase liquid mass transfer, *Water Resour. Res.*, 37(3), 539-549, 2001.

Hilpert, M. and C. T. Miller, Experimental investigation on the resonance of a liquid column in a capillary tube, *J. Colloid and Interface Sci*, 219, 62-68, 1999.

Hilpert, M., D. Stopper, and G. H. Jirka, Resonance of a liquid column in a capillary tube, *J. Appl. Math. Phys.*, 1–14, 1996.

Hilpert, M., G. H. Jirka, and E. J. Plate, Capillary-induced resonance of oil blobs in capillary tubes and porous media, *Geophysics*, 65(3), 874-883, 2000.

Hinkley, E. R., M. M. Dias, and A. C. Payatakes, On the motion of oil ganglia in porous media, *PhysicoChemical Hydrodynamics*, 8(2), pp. 185-211, 1987.

Holman, H.-Y.N., I. Javandel, Evaluation of transient dissolution of slightly water-soluble compounds from a light nonaqueous phase liquid pool, *Water Resour. Res.*, 32(4), 915-923, 1996.

Hovem, J. M. and G. D. Ingrem, Viscous attenuation of sound in saturated sand, *J. Aoust. Soc. Am.*, 66(6), 1807-1812, 1979.

Jawitz, J. W., D. Dai, P. S. C. Rao, M. D. Annble, R. D. Rhue, Rate-limited solubilization of multicomponent nonaqueous-phase liquids by flushing with cosolvents and surfactants: Modeling data from laboratory and field experiments, *Environ. Sci. Technol.*, 37, 1983-1991, 2003.

Imhoff, P. T., P. R. Jaffe, and G. F. Pinder, An experimental study of complete dissolution of nonaqueous phase liquid in saturated porous media, *Water Resour. Res.*, 30, 307-320, 1993.

Imhoff, P. T., S. N. Gieyzer, J. F. McBride, L. A. Vancho, I. Okuda, and C. T. Miller, Cosolvent-enhanced remediation of residual dense nonaqueous phase liquids; Experimental investigation, *Environ. Sci. Technol.*, 29(8), 1966-1976, 1995.

IMSL, *IMSL MATH/LIBRARY user's manual*, 2.0, IMSL, Houston, 1991.

Jia, C., K. Shing, and Y. C. Yortsos, Visualization and simulation of non-aqueous phase liquids solubilization in pore networks, *J. Contam. Hydrol.*, 35, 363-387, 1999.

Jimenez, C. and P. J. Sullivan, Contaminant dispersion in some time–dependent laminar flows, *J. Fluid Mech.*, (142), 57–77, 1984.

Johnson, R. L., J. F. Pankow, Dissolution of dense chlorinated solvents into groundwater, 2, Source functions for pools of solvent, *Environ. Sci. Technol.*, 26(5), 896-901, 1992.

Kabala, Z. J., and G. Sposito, A stochastic model of reactive solute transport with time–varying velocity in a heterogeneous aquifer, *Water Resour. Res.*, 27(3), 341–350, 1991.

Kalinitchenko, V. A. and S. Ya. Sekerj-Zenkovitch, On the immiscible fluid displacement in a capillary under oscillating pressure drop, *Exp. Thermal Fluid Sci.*, 18, 244–250, 1998.

Khachikian, C., and T. C. Harmon, Nonaqueous phase liquid dissolution in porous media: Current state of knowledge and research needs, *Transp. Porous Media*, 38, 3–28, 2000.

Kim, T. and C. V. Chrysikopoulos, Mass transfer correlations for nonaqueous phase liquid pool dissolution in saturated porous media, *Water Resour. Res.*, 35(2), 449-459, 1999.

Kline, S. J., *Similtude and Approximation Theory*, McGraw-Hill, N. Y., 1965.

Komoto, H., A study on heat transfer from a horizontal circular cylinder in a progressive sound field, s bull. Jpn Soc. Mech. Engrs, 29, 258, 1986.

Kreft, A. and A. Zuber, On the physical meaning of the dispersion equation and its solutions for different initial and boundary conditions, *Chem. Eng. Sci.*, 33, 1471–1480, 1978.

Lee, K. Y., and C. V. Chrysikopoulos, Dissolution of a well-defined trichloroethylene pool in saturated porous media: experimental results and model simulations, *Water Res.*, 36, 3911-3918, 2002.

Lee, K. Y., C. V. Chrysikopoulos, NAPL pool dissolution in stratified and anisotropic porous formations, *J. Environ. Eng., ASCE.*, 124(9), 851-862, 1998.

Lee, K. Y., C. V. Chrysikopoulos, Numerical modeling of three-dimensional contaminant migration from dissolution of multicomponent NAPL pools in saturated porous media, *Environ. Geology*, 26(3), 157-165 1995.

Legait, B., Laminar flow of two phases through a capillary tube with variable square cross section, *J. Col. and Int. Sci.*, 96(1), 28-38, 1983

Legait, B., P. Sourieau, and M. Combarnous, Inertia, viscosity, and capillary forces during two-phase flow in a constricted capillary tube, *J. Col. and Int. Sci.*, 91(2), 400-411, 1983.

Lenhard, R. J. and J. C. Parker, Measurement and prediction of saturation-pressure relationships in three-phase porous media systems, *J. Contam. Hydrol.*, 1, 407-424, 1987.

Lenormand, R., C. Zarcone, and A. Sarr, Mechanism of displacement of one fluid by another in a network of capillary ducts, *J. Fluid Mech.*, 135, 337-353, 1983.

Lenormand, R. and C. Zarcone, Role of roughness and edges during imbibition in square capillaries, paper SPE 13264, *Proceedings of the 1984 SPE Annual Technical Conference and Exhibition*, Houston, TX, 1984.

Li, A., A. W. Andren, and S. H. Yalkowsky, Choosing a cosolvent; Solubilization of

napthalene and cosolvent property, *Environ. Toxicol. Chem.*, 15(12), 2233–2239, 1996.

Li, X., and Y. C. Yortsos, Visualization and simulation of bubble growth in pore networks, *AIChE J.*, 41, 214-223, 1995.

Macedo, E. A., U. Weidlich, J. Gmehling, P. Rasmussen, Vapor-liquid equilibria by UNIFAC group contribution, 3, Revision and extension, *Ind. Eng. Chem. Process Des. Dev.*, 22, 676-684, 1983.

Majdalani, J., J. Barron, and W. K. Van Moorhem, Inception of turbulence in the stokes boundary layer over a transpiring wall, Transaction ASME, 124, 678-684, 2002.

Mandelis, A., Diffusion waves and their uses, *Physics Today*, August, 29-34, 2000.

Manga, M., Dynamics of drops in branched tubes, *J. Fluid Mech.*, 315, 105-117, 1996.

Marthelli, R. C. and L. M. Boelter, The effect of vibration on heat transfer by free concection from a horizontal cylinder, *Proceedings of the 5th International Congress of Applied Mechanics*, 578-584, 1939.

Martinez, M. J. and K. S. Udell, Axisymmetric creeping motion of drops through circular tubes, *J. Fluid Mech.*, 210, 565-591, 1990.

Mason, A. R. and B. H. Kueper, Numerical simulation of surfactant-enhanced solubilization of pooled DNAPL, *Environ. Sci. Tech.*, 30(11), 3205–3215, 1996.

McCray, J. E., P. J. Dugan, Nonideal equilibrium dissolution of trichloroethene from a decane-based nonaqueous phase liquid mixture: Experimental and modeling investigation, *Water Resour. Res.*, 38(7), doi:10.1029/2001WR000883, 2002.

McLeroy, E. C. and A. De Loach, Sound speed and attenuation from 15 to 1500 kHz, measured in natural sea-floor sediments, *J. Acoust. Soc. Am.*, 44(4), 1148-1150,

1968.

Mercer, J. W., and R. M. Cohen, A review of immiscible fluids in the subsurface: properties, model characterization and remediation, *J. Contam. Hydrol.*, 6, 107-163, 1990.

Mohanty, K. K., H. T. Davis, and L. E. Scriven, Physics of oil entrapment in water wet rocks, *Soc. Pet. Eng. Reservoir Eng.*, 2, 113–127, 1987.

Moore, T. F. and R. L. Slobod, The effect of viscosity and capillarity on the displacement of oil by water, *Producers Monthly*, 20(10), 20-30, 1956.

Morrow, N. R., I. Chatzis, and J. J. Taber, Entrapment and mobilization of residual oil in bead packs, *Soc. Pet. Eng. Reservoir Eng.*, 3, 211–218, 1988.

Morrow, N. R., Interplay of capillary, viscous, and buoyancy forces in the mobilzation of residual oil, *J. Can. Pet. Technol.*, 18(3), 35-46, 1979.

Mukherji, S., C. A. Peters, W. J. Weber, Jr., Mass transfer of polynuclear aromatic hydrocarbons from complex DNAPL mixtures, *Environ. Sci. Technol.*, 31, 416-423, 1997.

Nambi, I. M., and S. E. Powers, NAPL dissolution in heterogeneous systems: an experimental investigation in a simple heterogeneous system, *J. Contam. Hydrol.*, 44, 161-184, 2000.

Ng, K. M., H. T. Davis, and L. E. Scriven, Visualization of blob mechanics in flow through porous media, *Chem. Eng. Sci.*, 33, pp. 1009-1017, 1977.

O'Connell, R. J. and B. Budiansky, Viscoelastic properties of fluid-saturated cracked solids, *J. Geophys. Res.*, 82, 5719-5736, 1977.

Okuda, I., J. F. McBride, S. N. Gleyzer, and C. T. Miller, Physicochemical transport processes affecting the removal of residual DNAPL by nonionic surfactant

solutions, *Environ. Sci. and Tech.*, 30(6), 1852-1860, 1996.

Parra, J. O. and P. Xu, Dispersion and attenuation of acoustic guided waves in layered fluid-filled porous media, *J. Acoust. Soc. Am.*, 95(1), 91–98, 1994.

Patzek, T. W., and D. B. Silin, Shape factor and hydraulic conductance in noncircular capillaries, *J. Colloid Interface Sci.* 236, 295-304, 2001.

Payatakes, A. C., Dynamics of oil ganglia during immiscible displacement in water-wet porous media, *an. Rev. Fluid Mech.*, 14, pp. 365-393, 1982.

Pennel, K. D., L. M. Abriola, and W. J. Weber, Surfactant–enhanced solubilization of residual dodecane in soil columns. 1. Experimental investigation, *Environ. Sci. Tech.*, 27, 2332-2340, 1993.

Pennel, K. D., M. Jin, L. M. Abriola, and G. A. Pope, Surfactant enhanced remediation of soil columns contaminated by residual tetrachloroethylene, *J. Contam. Hydrol.*, 16, 35-53, 1994.

Peters, C. A., K. H. Wammer, C. D. Knightes, Multicomponent NAPL solidification thermodynamics. *Transp. Porous Media.*, 38(1-2), 57-77, 2000.

Powers, S. E., L. M. Abriola, and W. J. Weber, An experimental investigation of nonaqueous phae liquid dissolution in saturated subsurface systems-steady state mass transfer rates, *Water Resour. Res.*, 28(10), 2691-2705, 1992.

Powers, S. E., L. M. Abriola, and W. J. Weber, an experimental investigation of non-aqueous phae liquid dissolution in saturated subsurface systems-transient state mass transfer rates, *Water Resour. Res.*, 30(2), 321-332, 1994.

Powers, S. E., I. M. Nambi, and G. W. Curry Jr., Non-aqueous phase liquid dissolution in heterogeneous systems: Mechanisms and a local equilibrium modeling approach, *Water Resour. Res.*, 34(12), 3293–3302, 1998.

Press, W. H., S. A. Teukolsky, W. T. Vetterling, and B. P. Flannery, Numerical Recipes in Fortran 90: The Art of Parallel Scientific Computing, 2nd ed., New York, Cambridge University Press, 1996.

Preston, J. M. and W. S. Johnson, Acoustic enhancement of the rate of heat transfer over a flat plate–an experimental investigation, *J. Energy Resour. Technol.*, 119, 257-264, 1997.

Qian, Z. W., Dynamic viscosity in porous media, *J. Sound Vibrat.*, 211(5), 791–799, 1998.

Rao, P. S. C., M. D. Annable, R. K. Sillan, D. P. Dai, K. Hatfield, W. d. Graham, A. L. Wood, and C. G. Enfield, Field-scale evaluation of in-situ cosolvent flushing for remediation of a shallow unconfined aquifer contaminated with residual LNAPL, *Water Resour. Res.*, 33(12), 2673-2686, 1997.

Reddi, L. N., and H. Wu, Mechanisms involved in vibratory destabilization of NAPL ganglia in sands, *J. Environ. Eng.*, 122(12), 1115-1119, 1996.

Reddi, L. N., and S. Challa, Vibratory mobillization of immiscible liquid ganglia in sands, *J. Environ. Eng.*, 120(5), 1170-1190, 1994.

Reddi, L. N., S. Menon, and A. Plant, Pore-scale investigations on vibratory mobilization of LNAPL ganglia, *J. Hazardous Materials*, 62, 211-230, 1998.

Richardson, P. D., Local effects of horizontal and vertical sound fields on natural convection from a horizontal cylinder, *J. Sound Vibration* 10(1), 32-41, 1969.

Rigord, P., Y. Caristan, and J. P. Hulin, Analysis of porous media heterogeneities using the diffusion of pressure waves, *J. Geophys. Res.*, 98(B6), 9781-9791, 1993.

Roy, J. W., J. E. Smith, R. W. Gillham, Natural remobilization of multicomponent DNAPL pools due to dissolution. *J. Contam. Hydrol.*, 59, 163-186, 2002.

Santos, J. E., J. Douglas, Jr., J. Corbero, and O. M. Lovera, A model for wave propagation in a porous medium saturated by a two-phase fluid, *J. Acoust. Soc. Am.*, 87(4), 1439–1448, 1990.

Scheidegger, A. E., *The Physics of Flow Through Porous Media*, Macmillan Co., NY, 1960.

Schwarzenbach, R. P., P. M. Gschwend, D. M. Imboden, *Environmental Organic Chemistry*, Wiley: New York, 1993.

Seagren, E. A., B. E. Rittmann, and A. J. Valocchi, Quantitative evaluation of the enhancement of NAPL–pool dissolution by flushing and biodegradation, *Environ. Sci. Technol.*, 28(5), 833-839, 1994.

Sitar, N., J. R. Hunt, and K. S. Udell, Movement of nonaqueous liquids in groundwater, *Proc., Geotech. Practice for Waste Disposal*, Geotechnical Division of ASCE, New York, N. Y., 205-223, 1987.

Skjold-Jørgensen, S., B. Kolbe, J. Gmehling, P. Rasmussen, Vapor-liquid equilibria by UNIFAC group contribution: Revision and extension. *Ind. Eng. Chem. Process Des. Dev.*, 18, 714-722, 1979.

Sniekers, R. W., D. M. Smoulders, M. E. Van Dongen, and H. Van der Kogel, Pressure wave propagation in a partially water-saturated porous medium, *J. Appl. Phys.*, 66(9), 4522-4524, 1989.

Sorens, T. S., D. A. Sabatini, and J. H. Harwell, Effects of flow bypassing and nonuniform NAPL distribution on the mass transfer characteristics of NAPL dissolution, *Water Resour. Res.*, 34(7), 1657-1673, 1998.

Tabor, J. J., Dynamic and static forces required to remove a discontinuous oil phase from porous media containing both oil and water, *Soc. Pet. Engrg. J.*, 9, 3-12, 1969.

Tatalovich, M. E., K. Y. Lee, and C. V. Chrysikopoulos, Modeling the transport of contaminants originating from the dissolution of DNAPL pools in aquifers in the presence of dissolved humic substances, *Transp. Porous Media*, 38, 93–115, 2000.

Tiegs, D., J. Gmehling, P. Rasmussen, A. Fredenslund, Vapor-liquid equilibria by UNIFAC group contribution, 4, Revision and extension, *Ind. Eng. Chem. Process Des. Dev.*, 26, 159-161, 1987.

Vainshtein, P., M. Fichman, and C. Gutfinger, Acoustic enhancement of heat transfer between two parallel plates, *Int. J. Heat mass Transfer*, 38(10), 1893-1899, 1995.

Valocchi, A. J., Spatial moment analysis of the transport of kinetically adsorbing solutes through stratified aquifers, *Water Resour. Res.*, 25(2), 273–279, 1989.

Van Der Grinten, J. G. M., M. E. H. Van Dongen, and H. Van der Kogel, A shock tube technique for studying pore-pressure propagation in a dry and water-saturated porous medium, *J. Appl. Phys.*, 58(8), 2937-2942, 1985.

Van Der Grinten, J. G. M., M. E. H. Van Dongen, and H. Van der Kogel, Strain and pore-pressure propagation in a water-saturated porous medium, *J. Appl. Phys.*, 62(12), 4682-4687, 1987.

Vogler, E. T., and C. V. Chrysikopoulos, Dissolution on nonaqueous phase liquid pools in anisotropic aquifers, *Stochastic Environ. Res. Risk Assess.*, 15, 33-46, 2001.

Vogler, E. T., and C. V. Chrysikopoulos, Experimental investigation of acoustically enhanced solute transport in porous media, *Geophysical Res. Letters*, 29(15), doi: 10.1029/2002GL01534, 2002.

Voudrias, E. A. and M. F. Yeh, dissolution of a toluene pool under constant and variable hydraulic gradients with implications for aquifer remediation, *Ground Water*, 32(2), 305-311, 1994.

Watson, E. J., Diffusion in oscillatory pipe flow, *J. Fluid Mech.*, 133, 233–244, 1983.

Wilson, J. L., and S. H. Conrad, "Is physical displacement of residual hydrocarbons a realistic possibility in aquifer restoration?", in proceedings of *Petroleum Hydrocarbons and Organic Chemicals in Ground Water*, NWWA, Houston, TX, 274-298, 1984.

Wilson, J. L., S. H. Conrad, W. R. Mason, and W. Peplinski, Laboratory investigation of residual liquid organics from spills, leaks, and the disposal of hazardous wastes in groundwater, *EPA/600/6-0/004*, U. S. EPA, Narraganset, R.I., 1990.

Woods, B. G., Sonically enhanced heat transfer from a cylinder in cross flow and its impact on process poer consumption, *Int. J. Heat and Mass Transfer*, 35(10), 2367-2376, 1992.

Zhou, D., L. A. Dillard, and M. J. Blunt, A physically based model of dissolution of nonaqueous phase liquids in the saturated zone, *Transp. Porous Media*, 39, 227–255, 2000.

Zhou, M. Y. and P. Sheng, First-principles calculations of dynamic permeability in porous media, *Phys. Rev. B*, 39(16), 12 027–12 039, 1989.

Zhu, J., F. Feng, M. L. Laucks, and E. J. Davis, Mass transfer from an oscillating microsphere, *J. Colloid Interface Sci.*, 249, 351-358, 2002.